JELS

ISSN 2087-2852

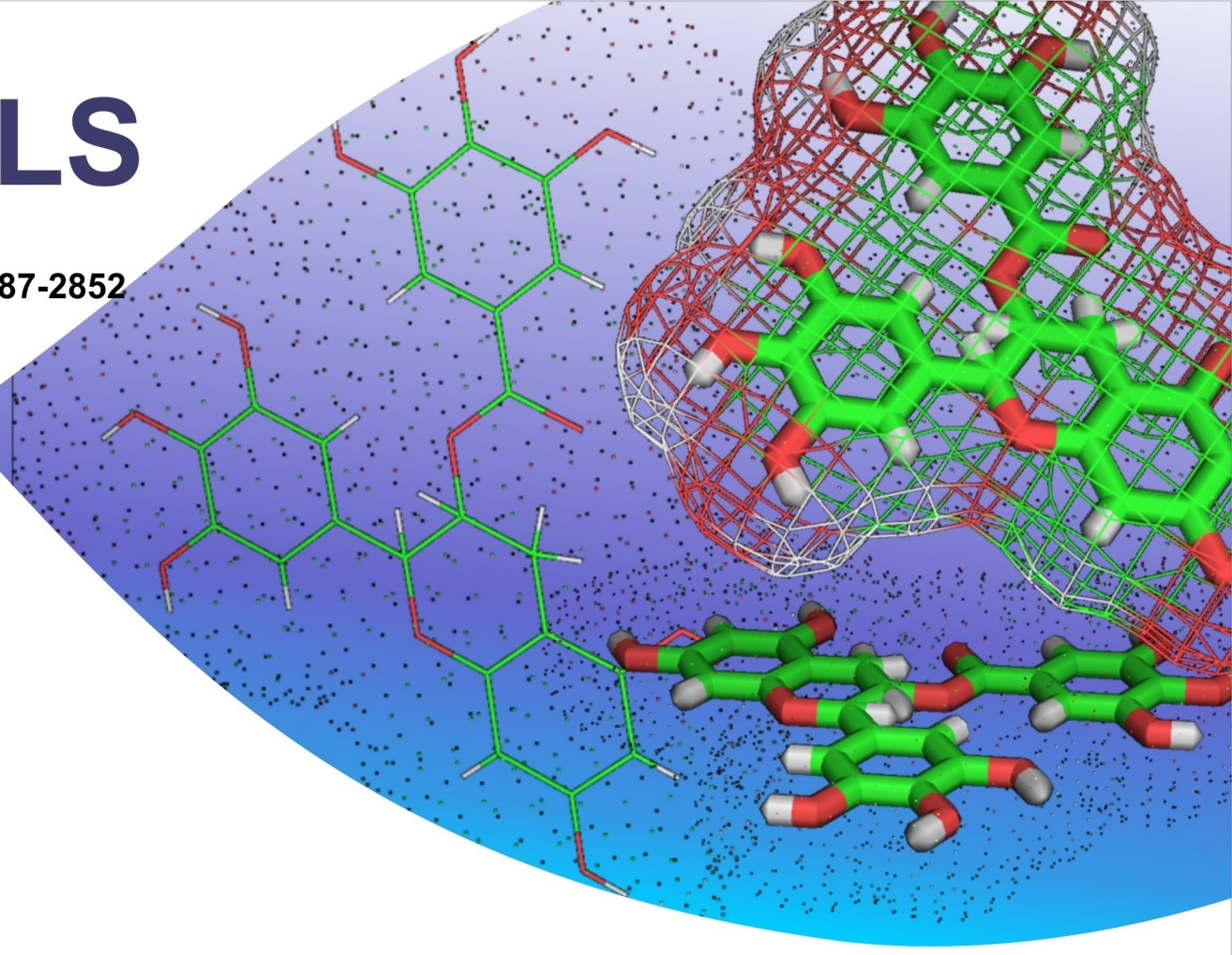

The Journal of EXPERIMENTAL LIFE SCIENCE

J.Exp. Life Sci.	Vol. 13	No. 3	pages. 138 - 188	October 2023

Published by :
Graduate Program, Universitas Brawijaya

jels.ub.ac.id

ISSN. 2087-2852
E-ISSN. 2338-1655

The Journal of Experimental Life Science

Discovering Living System Concept through Nano, Molecular and Cellular Biology

Editorial Board

Address

The Journal of Experimental Life Science
Building B, 1st Floor, Postgraduate School, University of Brawijaya
Jl. Mayor Jenderal Haryono 169, Malang, 65145
Telp: (0341) 571260 ; Fax: (0341) 580801
Email: jels@ub.ac.id
Web: http://www.jels.ub.ac.id

ISSN. 2087-2852
E-ISSN. 2338-1655

Table of Content

Particle Swarm Optimization – Extreme Learning Machine with Decreasing Inertia Weight for COVID-19 Prediction in Surabaya

Mohamad Handri Tuloli[1*], Syaiful Anam[2], Nur shofianah[2]

[1]Master Program of Mathematics, Faculty of Mathematics and Natural Sciences, University of Brawijaya, Malang, Indonesia

[2]Department of Mathematics, Faculty of Mathematics and Natural Sciences, University of Brawijaya, Malang, Indonesia

Abstract

COVID-19 has spread all throughout the world, even to Indonesia. Surabaya becomes one of Indonesia's major cities where COVID-19 is fast spreading, culminating in a large number of positive cases and over 1000 deaths from the disease by November 2020. The number of positive COVID-19 cases predicted can be utilized to limit hospital facility availability and develop plans and policies for tackling the illness outbreak. One of the many prediction systems identified is the Extreme Learning Machine (ELM). ELM has a quick and precise training speed. However, the performance of ELM depends on the number of neurons. When the number of neurons is not precisely specified, prediction accuracy suffers. Particle Swarm Optimization (PSO) has the ability to optimize the number of node ELM neurons so the ELM can achieve better results. The number of neurons is determined using Particle Swarm Optimization (PSO) with decreased inertia weight. As a result, this research proposes predicting COVID-19 instances in Surabaya using a hybrid of PSO and ELM (PSO-ELM) with decreased inertia weight. The studies reveal that the offered techniques with different activation functions work comparably well in predicting COVID-19 instances in Surabaya. The best MAPE is achieved using the sigmoid activation function with the number of hidden layer nodes around $L = 25$.

Keywords: Covid-19, Optimization, Prediction, PSO-ELM.

INTRODUCTION

The new coronavirus (COVID-19) that emerged in 2019 has an impact on the respiratory tract, especially the lungs. In late 2019, people in Wuhan, China, were first infected with COVID-19. COVID-19 can be transmitted through the air, so the virus can be transmitted from an infected person to a healthy person through coughing or sneezing, which causes droplets. People infected with this virus can experience different symptoms. However, the most common symptoms are loss of the ability to smell and taste food, weakness, fever, difficulty breathing, and even mental infections can occur [1]. However, many infected people are asymptomatic, which is called asymptomatic. According to data, Surabaya City has the highest number of COVID-19 cases in Indonesia. Surabaya has more than 15,000 positive cases and more than 1,000 deaths due to COVID-19 in November 2020 [2].

COVID-19 cases can be controlled through social distancing, wearing masks, and other measures. One of the researchers' contributions is to analyze COVID-19 behavior by predicting the number of COVID-19 cases. Predicting the number of COVID-19 cases is very important so that we can know the situation going forward and determine the best steps to deal with the outbreak and mitigate the impact of the outbreak. Prediction methods that exist to date are very different. One of them is an artificial neural network (ANN) inspired by the human nervous system. Extreme Learning Machine (ELM) is a type of ANN method with much simpler speed and accuracy compared to several other types of ANN [3]. Several machine learning studies have been conducted. Yadav *et al.* [4] used machine learning methods to analyze the novel coronavirus, Liu *et al.* [5] studied dynamic kernel-based ELM to predict water treatment processes in paper manufacturing, and ELM has even been used in the classification of tumor diseases [6] and the diagnosis of COVID-19 [7].

The ELM method is based on many neurons. Therefore, if the hidden layer nodes are not precisely defined, an insufficient or excessive configuration may occur, which may lead to poor estimates. Defining the hidden nodes and initializing the $\boldsymbol{w}$-weights and $\boldsymbol{b}$-bias, which makes ELM performance more optimal, is very important. Various optimization methods, including swarm-based methods, can improve ELM performance. Particle Swarm Optimization (PSO) is a swarm-based optimization method discovered by Kennedy and Eberhart, inspired by the behavior of flocks of birds [8]. PSO is a search algorithm that can balance the exploration and exploitation processes. Therefore, PSO is proven to maximize ELM's performance in predicting [9]. However, Bansal et al. tried in their study to compare the performance of PSO with several types of dynamic inertial weights and found that iteration-based decreased inertial weights performed the best [10].

This study aims to use PSO with decreasing inertial weight by optimizing hidden nodes in the ELM hidden layer, which is then called PSO-ELM, to predict cumulative cases of COVID-19. Experiments were conducted by comparing several activation functions to find an activation function that optimizes PSO-ELM performance. The optimal PSO-ELM is then compared with the standard ELM.

MATERIAL AND METHOD

Particle Swarm Optimization (PSO)

The positions of particle i at iteration of t time are written: $\boldsymbol{x_i}\ (t)$ with the initial position in Eq. (1),

$$\boldsymbol{x_i}(0) = \mathbf{1}.x_{i,min} + \left(x_{i,min} - x_{i,max}\right).\boldsymbol{r_i} \in \mathbb{R}^N, \quad (1)$$

where $\mathbf{1}$, $x_{i,min}, x_{i,max}$, $\boldsymbol{r_i}$, and N are respectively the vector which all the elements are 1, minimum value of component $\boldsymbol{x_i}$, the maximum value of component $\boldsymbol{x_i}$, the vector of random elements between 0 and 1 for particle i, and the dimension of vector $\boldsymbol{x_i}$. The value of the objective function for each particle i at iteration time t is

$$f\left(\boldsymbol{x_i}(t)\right) \quad (\mathbf{2})$$

and

$$pbest_i(t) = optimum\left(f\left(\boldsymbol{x_i}(t)\right)\right), \quad (3)$$

as the best objective function value for particle i. The global best function value is calculated by Eq. (4).

$$gbest(t) = optimum\left(pbest_i(t)\right). \quad (4)$$

For all particle i and iteration t, the best position of particle i and best global position are $\boldsymbol{pb_i}(t)$ and $\boldsymbol{gb}(t)$ respectively. Particle velocities are updated using the formula

$$\begin{aligned}\boldsymbol{v_i}(t+1) = {} & \omega(t).\boldsymbol{v_i}(t) \\ & +\varphi_1 c_1\left(\boldsymbol{pb_i}(t) - \boldsymbol{x_i}(t)\right) \\ & +\varphi_2 c_2\left(\boldsymbol{gb}(t) - \boldsymbol{x_i}(t)\right),\end{aligned} \quad (5)$$

$$\omega(t) = \omega_{max} - \frac{(\omega_{max} - \omega_{min})}{t_{max}}.t, \quad (6)$$

where $\boldsymbol{v_i}(t)$ is the velocity of particle i at iteration t, $\omega(t)$ is the inertia weight at iteration t, c_1 and c_2 are random numbers between 0 and 1, and φ_1 and φ_2 are the particle's learning coefficient weights. Eq. (6) describe the decreased inertia weight $\omega(t)$ related to t iteration. The performance of PSO with several types of dynamic inertial weights found that iteration-based decreased inertial weights performed the best. The position of each particle for each iteration is calculated by Eq. (7)

$$\boldsymbol{x_i}(t+1) = \boldsymbol{x_i}(t) + \boldsymbol{v_i}(t). \quad (7)$$

However, if the particle's position exceeds the specified minimum or maximum values, the particle's position falls within the element bounds $x_{i,min}$ and $x_{i,\max}$. The PSO algorithm procedure aimed at minimizing the objective function consists of the following steps:

1. Initialize t_{max} (maximum iteration), $\omega(t), \varphi_1, \varphi_2, S$ (population size), $x_{i,\min}$ and $x_{i,\max}$.
2. Initialize the initial position of each i particle with Eq. (1) and the initial velocity $\boldsymbol{v_i}(0) = \mathbf{0}$.
3. Compute the value of the objective function for each i particle at $f\left(\boldsymbol{x_i}(t)\right)$.
4. Calculate the best fitness function value for each particle and the global best fitness using Eq. (3) and (4).
5. Update the particle velocity vector using Eq. (5) and (6).
6. Update the particle positions using Eq. (7).
7. Update the objective function value for particle $f\left(\boldsymbol{x_{i+1}}(t)\right)$.
8. Update the particle positions and optimal values using the Eqs. (8) and (9) respectively

$$\boldsymbol{pb_i}(t+1) = \begin{cases}\boldsymbol{x_i}(t+1), & f\left(\boldsymbol{x_i}(t+1)\right) < pbest_i(t) \\ \boldsymbol{pb_i}(t), & others.\end{cases} \quad (8)$$

$$pbest_i(t+1) = \begin{cases}f\left(\boldsymbol{x_i}(t+1)\right), & f\left(\boldsymbol{x_i}(t+1)\right) < pbest_i(t) \\ pbest_i(t), & others.\end{cases} \quad (9)$$

9. Update the best global positions and value using the Eqs. (10) and (11) respectively

$$\boldsymbol{gb}(t+1) = argmin\left\{f\left(\boldsymbol{pb_i}(t+1)\right)\right\}, \quad (10)$$

$$gbest(t+1) = min\{pbest_i(t+1)\}. \quad (11)$$

10. check stop criteria. If $t < t_{max}$, $t = t+1$ and go back to step 5. Otherwise, the algorithm is terminated.

Extreme Learning Machine (ELM)

Extreme Learning Machine (ELM) was introduced by Huang in 2004. The training data set is $D = \left\{\left(\boldsymbol{d_p}, \boldsymbol{y_p}\right)\right\}$, where $\boldsymbol{d_p} =$

ISSN. 2087-2852
E-ISSN. 2338-1655

$(d_{p1}, d_{p2}, \dots, d_{pq}) \in \mathbb{R}^q$ are input values and $\boldsymbol{y_p} = (y_{p1}, y_{p2}, \dots, y_{pm}) \in \mathbb{R}^m$ are target values. The output $\boldsymbol{o}$ of an ELM with L hidden nodes can be expressed as

$$\sum_{i=1}^{L} \boldsymbol{\beta_i} h(\boldsymbol{w_i d_j} + b_i) = \boldsymbol{o_j}, \quad j = 1,2, \dots, N, \tag{12}$$

where $h(u)$ is the hidden layer activation function. In ELM, the activation function used is a nonlinear function that provides a nonlinear mapping to the system. Here are some of the activation functions that can be used (Table 1).

Table 1. Activation Function

Activation function	Equation
Sigmoid function	$h(u) = \frac{1}{1+e^{-u}}$
Hyperbolic tangent function	$h(u) = \frac{1-e^{-u}}{1+e^{-u}}$
Radial basis function	$h(u) = e^{-\lvert u-1 \rvert}$
Multi-Quadratic function	$h(u) = \left(\sqrt{\lvert u-1 \rvert}\right)^{\frac{1}{2}}$
Cosine function	$h(u) = \cos u$

The goal of the training process is to minimize the error between the target values and the output of the ELM. The objective function commonly used to compute the error is the mean squared error (MSE) between $\boldsymbol{o}$ and $\boldsymbol{y}$. So, there must exist a set $\boldsymbol{w}, b_i, \boldsymbol{\beta_i}$ satisfying

$$\sum_{i=1}^{L} \boldsymbol{\beta_i} h(\boldsymbol{w_i d_j} + b_i) = \boldsymbol{y_j}, \quad j = 1,2, \dots, N \tag{13}$$

Eq. (13) can be omitted with the following formula:

$$H\boldsymbol{\beta} = \boldsymbol{Y} \tag{14}$$

where β_i is the vector connecting i hidden node to the output, $\boldsymbol{Y}$ is the target, and H is the output of the hidden layer. Therefore, ELM also aims to obtain the best values of weight $\boldsymbol{w_i}$, bias b_i, and β_i [10]. Standard ELM uses the least-norm least-squares method.

$$\boldsymbol{\beta} = H^{\psi}\boldsymbol{Y} \tag{15}$$

and

$$H^{\psi} = \begin{cases} (H^T H)^{-1} H^T, & H^T H \text{ is singular} \\ H^T (H H^T)^{-1}, & H H^T \text{ is singular} \end{cases} \tag{16}$$

is a generalization of the inverse H matrix introduced by Moore-Penrose [11]. The ELM algorithm procedure consists of the following steps

1. Input training data $(\boldsymbol{d_p}, \boldsymbol{y_p}) \in \mathbb{R}^q \times \mathbb{R}^m$ activation function $h(u)$.
2. Randomly generate $\boldsymbol{w}$, $\boldsymbol{b}$, and choose number of hidden nodes $L \in N$.
3. Compute H^{ψ} using Eq. (16).
4. Compute $\boldsymbol{\beta}$ using Eq. (15).

Mean Absolute Percentage Error (MAPE)

According to Hsu and Wang [12], one of the most prominent forecast measuring methodologies is Mean Absolute Percentage Error (MAPE). The average percentage error in absolute terms is denoted by MAPE. For example, if $\boldsymbol{y_i}$ and $\boldsymbol{o_i}$ represent the actual and estimated values at data point i, then MAPE is defined as:

$$\text{MAPE} = \frac{1}{N}\sum_{i=1}^{N} \left| \frac{\boldsymbol{o_i} - \boldsymbol{y_i}}{\boldsymbol{y_i}} \right| \times 100\%, \tag{17}$$

N denotes the number of data points. The lower the percentage of MAPE, the better the forecast outcomes. Table 2 shows the MAPE criteria for evaluating models.

Table 2. MAPE Criteria

MAPE	Prediction Power
< 10%	Highly accurate forecasting
10% - 20%	Good forecasting
20% - 50%	Reasonable forecasting
> 50%	Weak and inaccurate forecasting

Hybrid PSO-ELM

Number of the ELM hidden nodes L are natural numbers. Therefore, the position of particle i in t time iterations acting as a surrogate for L in the optimization process needs to be determined Eq. (18)

$$x_i(t) \in \mathbb{N}, \tag{18}$$

and initial position is calculated by Eq. (19)

$$x_i(0) = x_{i,min} + (x_{i,min} - x_{i,max}).r_i \in \mathbb{N}, \tag{19}$$

where $x_{i,min} \in \mathbb{N}$, $x_{i,max} \in \mathbb{N}$, and r_i are the minimum value of the x_i, the maximum value of the x_i component, and the random elements from 0 to 1 of particle i. Therefore, the particle position notations such as $x_i(t)$, $pb_i(t)$, and $gb(t)$ in the iterations of the algorithm should be rounded up to

ISSN. 2087-2852
E-ISSN. 2338-1655

the nearest natural number if they deviate from the natural number. The value of the objective function for each particle i in iterations at t iteration is the MAPE value of the test data expressed as

$$f(\boldsymbol{x_i}(t)) = \frac{1}{N}\sum_{i=1}^{N}\left|\frac{\boldsymbol{o_i} - \boldsymbol{y_i}}{\boldsymbol{y_i}}\right| \times 100\%, \qquad (20)$$

where $\boldsymbol{o_i}$ is the predicted output for test data i using MPSO-ELM, $\boldsymbol{y_i}$ is the actual data i, and N is the number of predicted data.

Hybrid PSO-ELM algorithm method that optimizes many hidden nodes L. PSO-ELM method aimed at minimizing the MAPE of the test data and optimizing for many hidden nodes L involves the following steps:

1. Input training data $(\boldsymbol{d_p}, \boldsymbol{y_p}) \in \mathbb{R}^q \times \mathbb{R}^m$, test data $(\boldsymbol{d_{pr}}, \boldsymbol{y_{pr}}) \in \mathbb{R}^q \times \mathbb{R}^m$, and activation function $h(u)$.
2. Initialize If t_{max} (maximum number of iterations), ω_{min}, ω_{max}, φ_1, φ_2, S, (population size), $x_{i,min}$ and $x_{i,max}$.
3. Initialize the initial position of each i particle with initial velocity $v_i(0) = 0$ using equations (18) and (19).
4. Compute the value of the objective function for each particle i using $L_i = x_i(t)$, which is the number of ELM hidden nodes for i particle.
   a. Randomly generate $\boldsymbol{w}$ and $\boldsymbol{b}$ for each particle i.
   b. Compute H^{ψ} using equation (16).
   c. Compute the output weight $\boldsymbol{\beta}$ using equation (15) for each particle i.
   d. Implement the $\boldsymbol{\beta}$ weight for each particle i in the testing data using equation
   $$\boldsymbol{o} = H\boldsymbol{\beta} \qquad (21)$$
   e. Compute the value of the objective function for each particle i using equation (20).
5. Use Eq. (8)-(11) to determine the best function value for each particle and the objective function of global position.
6. Update the particle velocity using Eqs. (5) and (6).
7. Update the particle positions based on the criteria in Eqs. (7) and (18).
8. Compute the objective function value for particle i using step 4.
9. Update the best i particle positions and the fitness values using Eqs. (8) and (9).
10. Update global best position and the objective function of global position using Eqs. (10) and (11).

We checked the stopping criteria if $t < t_{max}$, $t = t + 1$ and got back to step 4. Otherwise, the algorithm is terminated.

Data Collection

The COVID-19 data in Surabaya City is divided into two parts from March 20, 2020, to December 31, 2022. A total of 90% of the initial COVID-19 data was chosen for training (903 rows of data), while the remaining 10% was used for testing (100 rows of data). Cumulative confirmed positive, cumulative death, and cumulative cure COVID-19 data are used. The starting weights and other parameters of the Hybrid ELM-PSO are created at random. In addition, Hybrid PSO-ELM will perform training steps on the training data. In this stage, the number of hidden layer nodes is modified to create the best value by reducing the difference between the Hybrid PSO-ELM output and the goal value. The training data will be used to apply the final findings of the number of hidden layer nodes. The testing data becomes input data in the prediction test stage, and the output data reflects the cumulative predictive representation of the confirmed COVID-19 cases.

The variables that have an impact on the cumulative positive cases of COVID-19, namely the cumulative positive confirmed cases over the last two weeks, the cumulative deaths, and the cumulative cures, will have an impact on confirmed cases the next day in this paper. As a result, these variables serve as input data. The ANN architecture was built with 16 factors that affect confirmed COVID-19 instances. The variables $\boldsymbol{d_1}, \boldsymbol{d_2}, \ldots, \boldsymbol{d_{14}}$ represent the cumulative cases of confirmed COVID-19 from two weeks to the day prior, $\boldsymbol{d_{15}}$ represents the death cumulative, and $\boldsymbol{d_{16}}$ represents the recovery cumulative. Figure 1 depicts a visualization of the Hybrid PSO-ELM architecture.

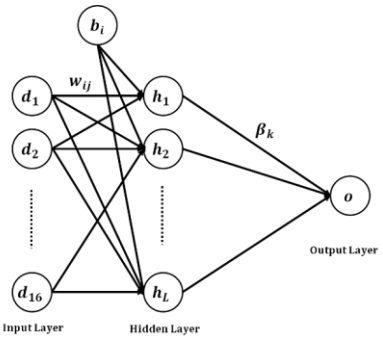

Figure 1. PSO-ELM Architecture

ISSN. 2087-2852
E-ISSN. 2338-1655

RESULTS AND DISCUSSION

The experiment is powered by a Core i7 processor running at 3.4 GHz, Windows 10, and Pycharm software. The population size is 20, and the maximum number of iterations is 100. The weighting of inertia (ω_{min} and ω_{max}), self-learning factor (φ_1), and other particles learning factors (φ_2) have minimum and maximum values of 0.4, 0.9, 2, and 2, respectively. The number of hidden layer nodes ranges from 1 to 50. Every activation function scenario is simulated 30 times.

Table 3 demonstrates a comparison of PSO-ELM with decreased inertia weight performance with various activation functions. According to Table 3, the accuracy provided by the PSO-ELM with decreased inertia weight using the sigmoid function is better than that obtained by other activation functions with 0.022426% MAPE mean in 30 times simulations. Even though the Hyperbolic Tangent function achieves the best MAPE, which is 0.0196387%, the MAPE in 30 times simulations was less consistent compared to the Sigmoid function. The number of hidden layer nodes (L) based on Table 3, the ideal number of hidden layer nodes for PSO-ELM is around 23-25 nodes.

Based on Figure 2, PSO-ELM using sigmoid function prediction testing data fits more into the actual testing data than the other activation functions. MAPE value progress based on Figure 3, PSO-ELM using sigmoid function achieves best MAPE value.

Table 3. Simulation Results

MAPE and L Value		Mean	Standard Deviation	Best Value
Sigmoid	**MAPE (%)**	0.02242600333	0.003234530972	0.02019424
	L	25	8	23
Hyperbolic Tangent	**MAPE (%)**	0.02385335833	0.004757438134	0.01963487
	L	30	11	24
Radial Basis	**MAPE (%)**	0.03036940733	0.006379166335	0.022662
	L	33	10	31
Multi-Quadratic	**MAPE (%)**	0.02533505867	0.002349999899	0.02138656
	L	25	6	27
Cosine	**MAPE (%)**	0.03726241767	0.003186058715	0.02998423
	L	48	6	50

Notes: L = The number of hidden layer nodes

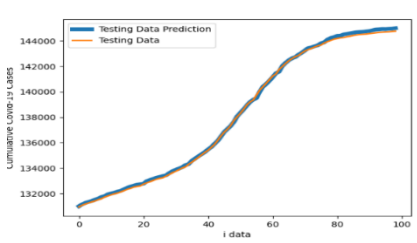

a) Sigmoid

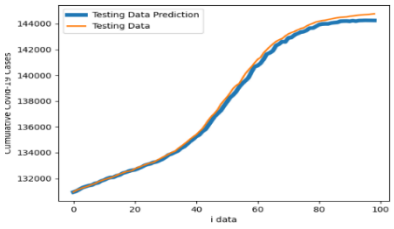

b) Hyperbolic Tangent

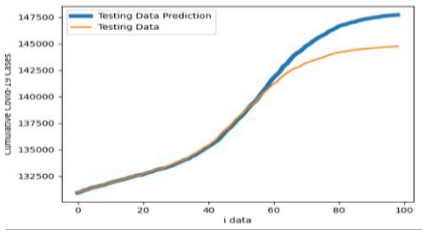

c) Radial Basis

d) Multi-Quadratic

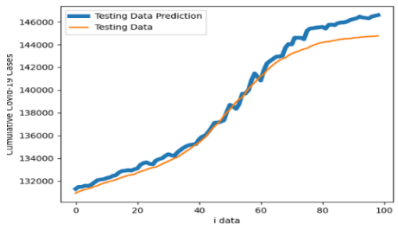

e) Cosine

Figure 2. Testing Data and Testing Data Prediction Plot

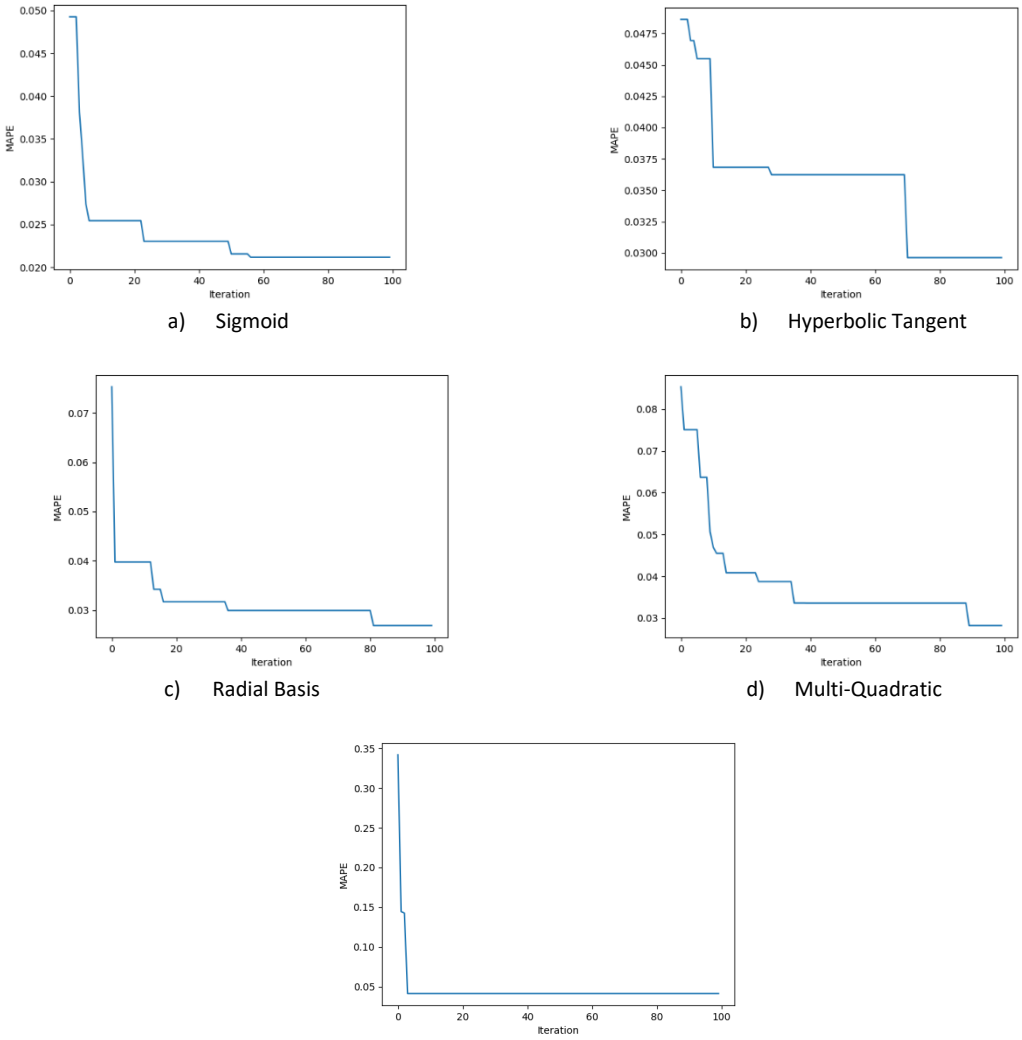

a) Sigmoid

b) Hyperbolic Tangent

c) Radial Basis

d) Multi-Quadratic

e) Cosine

Figure 3. MAPE Prediction Results Plot

CONCLUSION

According to the experimental results, the number of hidden layer nodes and activation affect PSO-ELM performance. The number of hidden layer nodes should be manageable in general and in this case. All of the activation functions achieve high accuracy based on the MAPE criteria. However, the PSO-ELM with decreased inertia using the sigmoid activation function outperforms the other in predicting the cumulative cases of COVID-19.

REFERENCES

[1] World Health Organization. 2023. COVID-19. Available at: https://www.who.int/. World Health Organization. Geneva.

[2] Government of Surabaya. 2023. Surabaya Lawan COVID-19. Available at: https://lawanCovid-19.surabaya.go.id/visualisasi/graph. Government of Surabaya. Surabaya.

[3] Huang, G.B., Q.Y. Zhu, C.K. Siew. 2006. Extreme learning machine: Theory and applications. *Neurocomputing*. 70(1-3). 489-501. DOI: 10.1016/j.neucom.2005.12.126.

[4] Yadav, M., M. Perumal, M. Srinivas. 2020. Analysis on novel coronavirus (COVID-19) using machine learning methods. *Chaos Solitons Fractals*. 139. 110050. DOI: 10.1016/j.chaos.2020.110050.

[5] Liu, H., Y. Zhang, H. Zhang. 2020. Prediction of effluent quality in papermaking wastewater treatment processes using dynamic kernel-based extreme learning machine. *Process Biochem.* 97. 72-79. DOI: 10.1016/j.procbio.2020.06.020.

[6] Ren, L.R., Y.L. Gao, J.X. Liu, R. Zhu, X.Z. Kong. 2020. L2,1-Extreme learning machine: An efficient robust classifier for tumor

classification. *Comput. Biol. Chem.* 89. DOI: 10.1016/j.compbiolchem.2020.107368.
[7] Pi, P., D. Lima. 2021. Gray level co-occurrence matrix and extreme learning machine for COVID-19 diagnosis. Int. J. Cogn. Comput. Eng. 2. 93-103. DOI: 10.1016/j.ijcce.2021.05.001.
[8] Yang, X.S. 2021. Nature-Inspired Optimization Algorithms, 2nd Ed. Academic Press, Elsevier Inc. DOI: 10.1016/C2019-0-03762-4.
[9] Sukma, T.D., I. Cholissodin, E. Santoso. 2021. Penerapan metode Extreme Learning Machine (ELM) dengan Optimasi Particle Swarm Optimization (PSO) untuk memprediksi harga cabai keriting di Kota Malang. 5(9). 3950-3958.
[10] Bansal, J.C., P.K. Singh, M. Saraswat, A. Verma, S.S. Jadon, A. Abraham. 2011. Inertia Weight strategies in Particle Swarm Optimization. Third World Congress on Nature and Biologically Inspired Computing. 633-640.
[11] Wang, J., S. Lu, S.H. Wang, Y.D. Zhang. 2021. A review on extreme learning machine. *Multimed. Tools Appl.* 81. 41611-41660.
[12] Hsu, L.C., C.H. Wang. 2008. Applied multivariate forecasting model to tourism industry. *Tourism.* 56(2). 159-172.

Phylogenetic Inference on *Limnonectes kuhlii* Complex in Java and Sumatra Reveals Significant Novel Diversity

Muhamad Fahmi[1*], Ahmad Muammar Kadafi[2], Bagus Priambodo[3,4], Muhammad Alif Fauzi[1], Amir Hamidy[5], Anggun Sausan Firdaus[6], Eric Nelson Smith[7], Nia Kurniawan[1]

[1]Department of Biology, University of Brawijaya, Malang, Indonesia
[2]Department of Biology, Universitas Palangka Raya, Palangka Raya, Indonesia
[3]Department of Biology, Universitas Negeri Malang, Malang, Indonesia
[4]Amphibian Research Center, Hiroshima University, Hiroshima, Japan
[5]Laboratory of Herpetology, Museum Zoologicum Bogoriense, Research Centre for Biosystematics and Evolution, National Research and Innovation Agency (BRIN), Bogor, Indonesia
[6]Department of Life Sciences, National Central University, Taoyuan City, Taiwan
[7]Department of Biology, University of Texas Arlington, Texas, USA

Abstract

The fanged frog, *Limnonectes kuhlii*, exemplifies the complexity of cryptic species. Though originally described from Java, subsequent studies indicate that *L. kuhlii* encompasses multiple lineages, suggesting the presence of several undescribed species. Suspecting the existence of multiple undescribed species within the *L. kuhlii* complex in Sumatra, we collected 17 specimens from Java and Sumatra. We extracted the 12S, tRNAval, and 16S mitochondrial DNA from these specimens for phylogenetic analysis using Maximum Likelihood and Bayesian Inference methods and for estimating time divergence. Our findings uncovered two novel diversity within the *L. kuhlii* complex both in Sumatra and Java. Furthermore, our estimation of time divergence suggests that the diversification of *L. kuhlii* in Java and Sumatra was influenced by geological and climatic events, including landmass emergence and sea-level fluctuations. In conclusion, our research provides critical insights into the evolutionary complexity and diversity of the *L. kuhlii* complex in Sumatra and Java. While our molecular evidence suggests novel diversity, further comprehensive morphological studies are imperative to confirm and describe these potential new species. Furthermore, additional sampling across its range and deeper investigations integrating both molecular and morphological data are crucial.

Keywords: fanged frogs, *Limnonectes kuhlii*, *Limnonectes sisikdagu*, phylogenetics.

INTRODUCTION

Amphibian populations are globally suffering from numerous threats, including habitat loss, climate change, pathogens and diseases, wildlife harvesting, and competition with invasive species [1]. Currently, 41% of identified species of amphibians are classified as threatened (CR, EN, or VU) [2]. Increased attention must be given to this group to preserve its diversity, and taxonomic uncertainties within this group urgently need to be resolved. Mostly, taxonomically unresolved species are cryptic, a group of closely related organisms that are morphologically similar but genetically distinct; this group commonly includes several species that are classified within a single taxon. Moreover, the cryptic species is likely considered a least concern species because of its abundance, widespread distribution, and tolerance to disturbance as a result of the combined fitness of numerous species classified within a single taxon.

*Correspondence address:
Muhamad Fahmi
Email : muhammadfahmibio@gmail.com
Address : Dept. Biology, University of Brawijaya, Veteran Malang 65145, Indonesia.

Limnonectes kuhlii is one of the well-known examples of cryptic species cases in amphibians. This species is a wide-headed, robust frog with a fang-like projection at the tip of the lower jaw in males; it can be distinguished from its congeners by the hidden tympanum and fully webbed toes [3]. Although the species was originally described from Java, *L. kuhlii* was recorded as a wide-ranging frog distributed from northeastern India through Taiwan, southern China, and Southeast Asia [3,4]. Later, several molecular data studies elucidated that *L. kuhlii* from different populations showed distinct evolutionary relationships [4–6]. Furthermore, a recent study indicated using mitochondrial DNA (mtDNA) sequences that *L. kuhlii* from approximately 63 populations across its known distribution is a complex species of more than 22 lineages (viz., species) [7]. Additionally, another study reported 17 lineages of the *L. kuhlii* complex in addition to the already described *L. hikidai*, *L. cintalubang*, and *L. asperatus* in Borneo using mtDNA and nuclear sequences, and those lineages are genetically distinct from Javan *L. Kuhlii* [3].

Java, as the origin of *L. kuhlii*, shares the greatest similarity of herpetofauna diversity with

Sumatra due to the proximity between these two islands and the narrowness of the Sunda Strait separating them. Most of the nonendemic Javan frogs are known to have originated from Sumatra, which may represent a faunal exchange with Sumatra that was possible during the Pleistocene or at an earlier period [8]. Although Java was connected with Borneo in the Pleistocene and shares sixteen species of amphibia, the evidence of direct faunal exchange between these two lands is few compared between Java and Sumatra. In contrast, comparing the genetic distance of Javan, Sumatran, and Borneo species could explain the historical biogeography relation among these areas [8]. The diversity of Sumatran frogs is much poorer than that of both Borneo and the Malay Peninsula regarding area size [8], and it was suggested that the herpetofauna needed to be better explored [9].

Limnonectes sisikdagu, a newly identified species from western Sumatra, is a species that was identified from the *L. kuhlii* complex lineage and currently is the most closely related species to the Javan *L. kuhlii* [7]. *L. sisikdagu* is distinct from the true *L. kuhlii* (from Java) by the presence of a spinule-covered mental patch on the ventral surface of the anterior chin in males; this is also a character that distinguishes *L. sisikdagu* from all other members of the *Limnonectes* genus [10]. In addition to *L. sisikdagu*, it was suggested that there may be multiple species of the *L. kuhlii* complex in Sumatra [10]. To explore this issue, we conducted a comprehensive assessment of *L. kuhlii* complex diversity within Java and Sumatra.

MATERIAL AND METHOD

Sample collection and DNA extraction

Sampling was conducted in Sumatra and Java, Indonesia, from 2014 to 2015. We collected 17 individuals identified as members of the *L. kuhlii* complex from their natural habitats (Table 1). Total genomic DNA was extracted from tissue samples using DNA suisui-F (RIZO) following the manufacturer's instructions. F51 (5'-CCC GCC TGT TTA CCA AAA ACA T-3'), R51 (5'-GGT CTG AAC TCA GAT CAC GTA-3') and F51Rev (5'-GGC GAT GTT TTT GGT AAA CAG GC-3') were used for amplification and sequencing of 16S rRNA [11]. The genes were amplified by denaturation for 4 min at 95°C, followed by 35 cycles of amplification consisting of denaturation for 40 s at 95°C, annealing for 45 s at 55°C, and extension for 90 s at 72°C for each cycle, and a final extension for 7 min at 72°C. The PCR products were purified using polyethylene glycol precipitation. The sequencing procedure for PCR products was conducted using an ABI3130 sequencer. The tRNAval, 16S rRNA, and a few portions of 12S rRNA sequences of 17 samples were deposited in GenBank (Table 1).

Table 1. Specimens of the *L. kuhlii* complex collected in this study.

No	Species	Locality	GenBank
1	*L. sisikdagu*	North Sumatra, Bandar Baru	KY132183
2	*L. sisikdagu*	North Sumatra, Toba Samosir	KY132184
3	*L. sisikdagu*	North Sumatra, Labuhan Batu	KY132181
4	*L.sisikdagu*	Aceh, Bener Merah	KY228866
5	*L.sisikdagu*	Aceh, Bener Merah	KY228868
6	*L. sisikdagu*	North Sumatra, Rau Batang Gadis	KY228867
7	*L. sisikdagu*	North Sumatra, Rumbung Baru	KY132180
8	*L. sisikdagu*	West Sumatra, Solok	KY132182
9	*L. cf. sisikdagu*	West Sumatra, Tapan	KY132179
10	*L.cf. sisikdagu*	Lampung, Tanggamus	KY228870
11	*L.cf. sisikdagu*	Lampung, Mt. Pesawaran	KY228869
12	*L.cf. sisikdagu*	Lampung, Tanggamus	KY228871
13	*L.cf. sisikdagu*	Lampung, Western Lampung	KY228872
14	*L. kuhlii*	West Java, BRIN Botani Garden	KY228864
15	*L. kuhlii*	Lampung, Tanggamus	KY228862
16	*L. kuhlii*	Banten, Pulosari	KY228863
17	*L. kuhlii*	West Java, Bandung	KY228865

Phylogenetic analysis

We collected numerous sequences of the *L. kuhlii* complex from NCBI as references (Table 2). Sequences of *Fejervarya limnocharis* (AY158705) and *Occidozyga lima* (DQ283224) were also collected for the outgroup in phylogenetic analysis following a previous similar analysis on *Limnonectes* [4–6,12–14]. Sequences of the collected samples and references were aligned using MEGA 7 with the Clustal W option [15], and the alignment result was used for genetic distance analysis, constructing phylogenetic trees, and estimating time divergence. Genetic distances were calculated as uncorrected pairwise sequence divergence using MEGA 7 [15].

ISSN. 2087-2852
E-ISSN. 2338-1655

Phylogenetic trees were constructed using maximum likelihood (ML) and Bayesian inference (BI). Transition model 2 (TIM2) and a gamma-shape parameter (G) were selected as the best-fit nucleotide substitution model for the dataset under Akaike Information Criterion by Modeltest-NG [16]. ML trees were constructed using RAxML-NG in the CIPRES Science Gateway with an automatic bootstrapping option and the TIM2+G model [17,18]. BI trees were constructed using MrBayes 3.2.6 in the CIPRES Science Gateway with the general time reversible (GTR) + G model replacing the selected best-fit model TIM2 + G since TIM2 is unavailable in MrBayes and GTR is considered the most closely related model [19]. We used 5,000,000 generations with a sampling frequency of 1,000 for four simultaneous metropolis-coupled Markov chain Monte Carlo (MCMC) algorithm runs. We discarded the first 25% of the estimated trees for the selection of consensus topology trees in BI.

Table 2. Collected reference species for phylogenetic analysis and estimation of time divergence.

Species	GenBank	Reference
L. fujianensis	AB526311	[22]
L. fujianensis	HM067240	[7]
L. fragilis	AB526315	[22]
L. taylori	AB558929	[23]
L. jarujini	AB558940	[23]
L. megastomias	AB558953	[23]
L. cf. kuhlii 'lineage 2'	HM067245	[7]
L. cf. kuhlii 'lineage 2'	HM067244	[7]
L. sisikdagu	JF836873	[10]
L. sisikdagu	JF836880	[10]
L. sisikdagu	JF836881	[10]
L. kiziriani	MT459153	[24]
L. utara	AB981375	[25]
L. utara	AB981376	[25]
L. selatan	AB981388	[25]
L. selatan	AB981385	[25]
L. selatan	AB981382	[25]
L. kuhlii	AB526316	[22]

Estimation of time divergence

Time divergence was estimated using BEAST under the Hasegawa-Kishino-Yano model evolution with a relaxed log normal clock model [20,21]. The prior distribution of the calibration point was specified following the previous study [3]. These include the divergence time between Dicroglossinae and Occidozyginae at 82.7 million years ago (Mya) (95% credibility interval [CI] 55-118 Mya), *L. bannaensis* and *L. fujianensis* at 24 Mya (CI 14-46 Mya) [3,6], and *L. fujianensis* from Taiwan and continental China at 1.25 Mya (CI 1.05-1.45 Mya) as internal calibration points. We sampled the MCMC chain every 1000 generations for 10,000,000 generations. The convergence was assessed in Tracer version v.1.5, and a maximum clade credibility tree was constructed using TreeAnnotator v.1.10.4 with a burn-in percentage of 20%.

RESULT AND DISCUSSION

We evaluated the diversity of the *L. kuhlii* complex in Java and Sumatra following the hypothesis of unidentified *L. kuhlii* complex diversity in Sumatra. We collected 17 samples of *L. kuhlii*-like fanged frogs in Java and Sumatra and conducted phylogenetic analyses on these samples against related references from GenBank. Two distinct methods of phylogenetic analyses produced consistent topologies. Here, we combined the branching reliability scores of each tree onto the ML tree to minimize redundancy (Fig. 1). Samples of the *Limnonectes* genus formed a monophyletic clade from *Fejervarya* and *Occidozyga* as the outgroup with unequivocal support from both ML bootstrap and BI posterior probability. The Javan and Sumatran *L. kuhlii* complex formed a clade separated from the *L. kuhlii* complex from mainland Southeast Asia, China, and Taiwan. The group of Javan and Sumatran *L. kuhlii* complexes branched into two Subclades with unequivocal support; named Subclade A and B. Subclade A contained samples from Sumatra, while Subclade B consisted of four samples from Java and one sample from Sumatra. These Subclades were separated by a genetic distance of 9-13% (Table 3).

Novel diversity of the *Limnonectes kuhlii* complex in Sumatra and Java

Currently, *L. sisikdagu* is the sole species in Sumatra that was described from the *L. kuhlii* complex. The study that described *L. sisikdagu* demonstrated the occurrence of three lineages in the Sumatran *L. kuhlii* complex clade: (1) a lineage that contained *L. sisikdagu* paratype samples from west Sumatra; (2) a lineage that contained samples from Batu Layang, Bengkulu, which was previously identified as *L. cf. kuhlii* 'lineage 2' [7]; this lineage had 5.3-7% genetic divergence from the holotype lineage; and (3) a lineage that contained two samples from west Sumatra with voucher id FMNH 266612 and FMNH 266617; this lineage had high genetic divergence of approximately 8.6 – 9.3% from the paratype lineage [10]. Even though *L. cf. kuhlii* 'lineages 2' had moderate genetic distance to the lineage that contains the *L. sisikdagu* paratype, the samples were assigned as *L. sisikdagu* due to the unavailable voucher for examination [10].

ISSN. 2087-2852
E-ISSN. 2338-1655

Table 3. Pairwise genetic distance among lineages identified from maximum likelihood and bayesian inference.

	Lineage 1	Lineage 2	Lineage 3	Lineage 4	Lineage 5
Lineage 1					
Lineage 2	5-6%				
Lineage 3	7-10%	7-9%			
Lineage 4	8-10%	9-10%	11-12%		
Lineage 5	10-11%	9-10%	11-12%	12-13%	
Lineage 6	10%	10%	10-12%	11-13%	7%

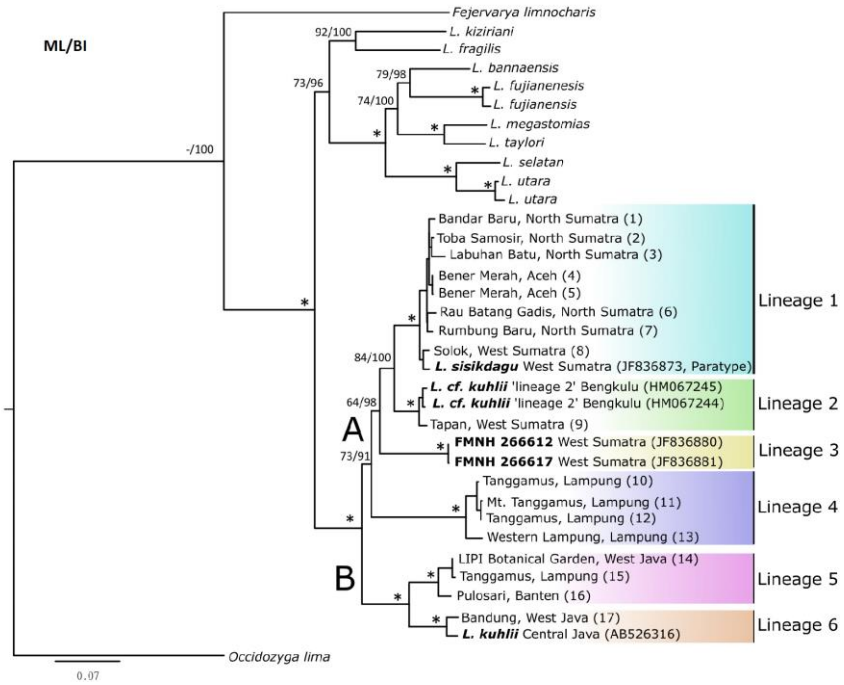

Figure 1. Combined maximum likelihood (ML) and Bayesian inference (BI) tree of fragment of 12S rRNA, tRNAval and 16S rRNA of *Limnonectes kuhlii* complex in Java, Sumatra, mainland Asia and Taiwan. Numbers within the bracket at the end of several tip labels represent the specimen number based on Table 1. Numbers near branches represent bootstrap supports of ML bootstrap (on the left part) and BI posterior probability (on the right part). Asterisk symbol represents a fully support of the two reliability scores. The alphabetical symbol 'A' represents Subclade A, comprising lineages 1 to 4, while 'B' represents Subclade B with lineages 5 and 6.

However, McLeod *et al*. [10] argued that *L. cf. kuhlii* 'lineages 2' may represent a unique species to *L. sisikdagu*. Additionally, the samples with voucher id FMNH 266612 and FMNH 266617 had a further genetic distance to the *L. sisikdagu* paratype compared with *L. cf. kuhlii* 'lineage 2' to the *L. sisikdagu* paratype [10]. However, the taxonomic position of these samples was not discussed. In this study, eight of our samples were clustered together with the *L. sisikdagu* paratype (JF836873) in Lineage 1 with a slight difference in genetic distance; hence, our samples in Lineage 1 can be described as *L. sisikdagu*.

Our results expand the distribution of *L. sisikdagu* to North Sumatra and Aceh, the northernmost province in Sumatra (Fig. 2). *Lineage 2* contained two reference samples of *L. cf. kuhlii* 'lineages 2' from Bengkulu and our sample from Tapan, West Sumatra, with unequivocal support. This result expands the distribution of this diversity to West Sumatra. Additionally, our sample can be used as a reference to investigate the taxonomic position of *L. cf. kuhlii* 'lineages 2'. Unfortunately, we did not find a sample that is closely related to FMNH 266612 and FMNH 266617.

We found a novel diversity of the *L. kuhlii* complex in Sumatra. The samples were clustered in Lineage 4 and specifically distributed in Lampung, the southernmost province in Sumatra. Lineage 4 has high genetic distance of approximately 8-10%, 9-10%, and 11-12% to Lineages 1-3 in Subclade A, respectively, and 12-

ISSN. 2087-2852
E-ISSN. 2338-1655

13% and 11-13% to Lineages 5 and 6 in Subclade B, respectively. Hence, it is likely that this lineage is unique to both *L. kuhlii* and *L. sisikdagu*. Further investigation using molecular and morphological datasets is needed to ensure the taxonomical position of this lineage since the sole molecular analysis in this study is not prudent to describe a novel species.

Subclade B contained two lineages, 5 and 6, with fully supported values from ML bootstrap and BI posterior probability, and the genetic distance between these lineages was 7%. Lineage 5 contained two samples from the western part of Java (Banten and BRIN Botanical Garden, Bogor) and one from Tanggamus, Lampung. Interestingly, the sample from BRIN Botanical Garden, Bogor, was more closely related to the sample from Sumatra, with 0% genetic distance, than to the Javan sample counterpart from Banten, which had 2% genetic distance. Additionally, the Sumatran sample within lineage 5 was syntopy with a sample from Lineage 4 of Subclade A (KY228871). The fact that they are not sister lineages concurs with Stuart *et al*. [26] and Inger *et al*. [27], who assert that sympatric lineages of cryptic species are frequently not sister lineages of one another. Sympatry/syntopy occurrence is commonly found for the *L. kuhlii* complex. Previously, McLeod found syntopic lineages in Ha Giang Province, Vietnam, between *L. bannaensis* and a novel *L. kuhlii* diversity complex that was later described as *L. Nguyenorum* [28]. McLeod also found a similar phenomenon in Phongsaly Province, Lao PDR, between *L. bannaensis* and a novel *L. kuhlii* diversity complex that was later described as *L. Taylori* [23]. Moreover, Matsui *et al.* [3] reported numerous lineages of the *L. kuhlii* complex in Borneo that occur syntopically.

Lineage 6 contained samples from West Java and Central Java that had a 2% genetic distance. The sample from Central Java was a reference sample of *L. kuhlii* [22]. This result in Subclade B opens the possibility of multiple species occurrences of the *L. kuhlii* complex in Java. Java itself is assigned as the original place of *L. kuhlii* - type material, but its specific locality is unknown. We suggest further study to comprehensively assess *L. kuhlii* complex diversity in Java using both morphological and molecular data to determine the 'true' *L. kuhlii* and *L. kuhlii* complex diversity.

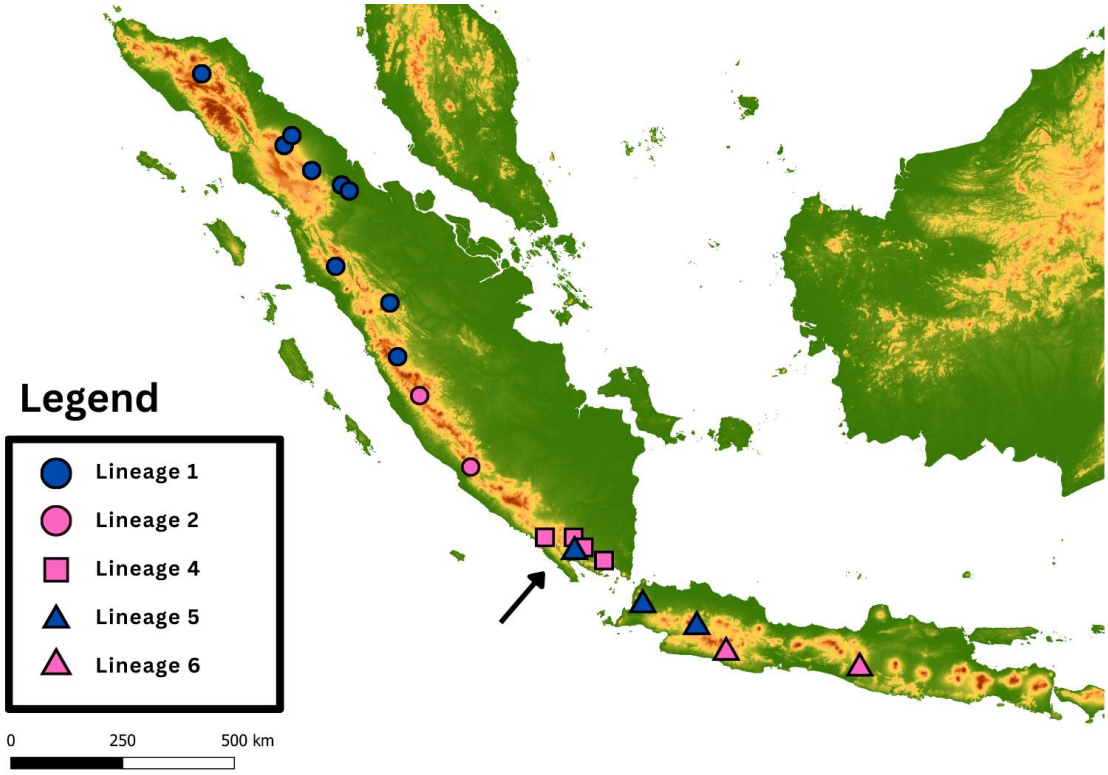

Figure 2. Distribution of Specimens from Lineages 1,2,4,5, and 6 of this study. Arrow indicates the presence of syntopy between Lineages 4 and 5.

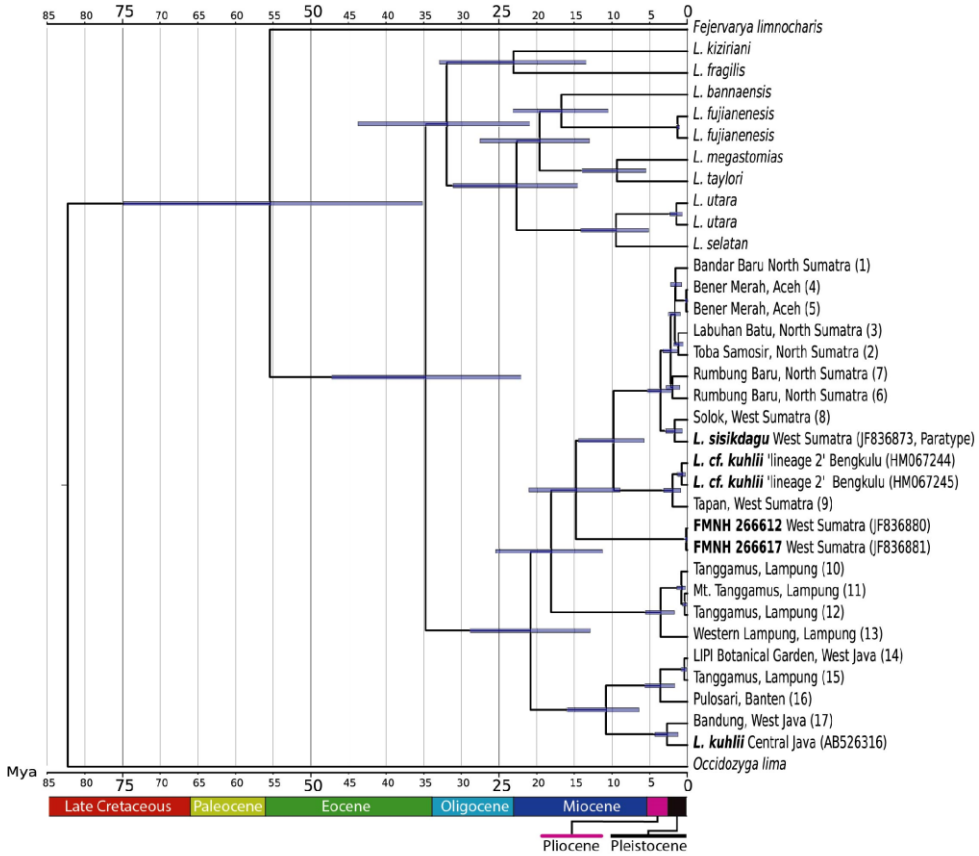

Figure 3. Estimation of time divergence of fragment of 12S rRNA, tRNAval and 16S rRNA of *Limnonectes kuhlii* Complex in Java, Sumatra, mainland Asia, and Taiwan. Numbers at the X axis represent million years (Mya) before present.

Geological evolution and divergence patterns of the *Limnonectes kuhlii* complex in Sumatra and Java

We estimated that the time divergence for the most common ancestor (MRCA) of Sumatran and the Javan *L. kuhlii* complex occurred in the early Miocene at approximately 20.8 Mya (CI: 12.8-28.8 Mya), which is a subepoch when much of Sumatra and Java were inundated by shallow seas (Fig. 3); the divergence resulted in Subclades A (Sumatran *L. kuhlii* complex) and B (mostly Javan and one Sumatran *L. kuhlii* complex) in this study. Portions of Sumatra and Java were part of the Southeast Asian land mass from the early Eocene (c. 50 Mya) to the late Oligocene (c. 25 Mya) [8].

Subsequently, sea levels began to rise gradually until the middle Miocene (c. 15 Mya), isolating small areas of volcanoes and high elevation into small multiple islands [8,29]. During this interval, the local genetic differentiation of terrestrial vertebrates is suggested to increase due to geographic barriers [8]. Lineages 4 and 3 of Subclade A are estimated to have diverged during this interval, specifically at approximately 18 Mya (CI: 11.3-25.4 Mya) and 14.7 Mya (CI: 8.9-21 Ma), respectively (Fig. 3). Additionally, Lineages 1 and 2 of Subclade A are estimated to diverge during the late Miocene at approximately 9.8 Mya (CI: 5.7-14.4 Mya) when sea levels receded, connecting some isolated volcanic islands of Sumatra [30]. Despite the occurrence of complex land separation and connection events during the early Miocene to the middle Pliocene, it was hypothesized that there are two persistent transverse inland seaways on Sumatra, currently located at Padang Sidempuan Valley and Pagar Alam Valley, which divided the island into at least three large islands for much of its geologic history [31].

In the early late Miocene (around 10 Mya), Java only had a prominent landmass in its western region [29]. Consistent with this, our estimations suggest that the MRCA of Lineages 5 and 6 emerged during this time. Moreover, our data indicates that these two lineages arose during the middle Pliocene. It was in this epoch that parts of east Java rose in the form of several

ISSN. 2087-2852
E-ISSN. 2338-1655

volcanic clusters, causing Java to exist as three main islands separated by the sea [29]. By the Late Pliocene, the emergence of highlands in central Java eventually led to the unification of these three previously isolated islands [29]. This geological evolution may have fostered the presence of two distinct lineages within the *L. kuhlii* complex in Java. Additionally, the recent glacial maximum approximately 17,000 years ago caused sea levels to recede by 120 m below current levels, bridging Java and Sumatra [8]. We hypothesize that a population from Lineage 5 migrated from Java to Sumatra, which would explain the presence of a specimen belonging to Lineage 5 found in Sumatra.

CONCLUSION

Our phylogenetic analysis of the *L. kuhlii* complex, using samples from Java and Sumatra, has illuminated previously unidentified diversity in Sumatra. We revealed the distinct evolutionary branches of this complex, including the potential presence of new species unique to specific localities in Java and Sumatra. Geological and climatic events, such as the emergence of land masses and changes in sea levels, have played pivotal roles in shaping the genetic landscape of this complex.

ACKNOWLEDGEMENT

This research was supported by the Partnerships for Enhanced Engagement in Research (Peer) Science. The authors would like to thank NK research members for their thorough comments and suggestions on this study.

REFERENCES

[1] Collins, J.P., A. Storfer. 2003. Global amphibian declines: Sorting the hypotheses. *Divers. Distrib.* 9(2). 89–98.

[2] International Union for Conservation of Nature (IUCN). 2017. The IUCN Red List of Threatened Species. Available at: https://www.iucnredlist.org/.

[3] Matsui, M., N. Kuraishi, K. Eto, A. Hamidy, K. Nishikawa, T. Shimada, P. Yambun, C.S. Vairappan, M.Y.B. Hossman. 2016. Unusually high genetic diversity in the Bornean Limnonectes kuhlii-like fanged frogs (Anura: Dicroglossidae). *Mol. Phylogenet*. *Evol*. 102. 305–319. DOI: 10.1016/j.ympev.2016.06.009.

[4] Emerson, S.B., R.F. Inger, D. Iskandar. 2000. Molecular systematics and biogeography of the fanged frogs of Southeast Asia. *Mol. Phylogenet*. 16(1). 131–142. DOI: 10.1006/mpev.2000.0778.

[5] Evans, B.J., R.M. Brown, J.A. McGuire, J. Supriatna, N. Andayani, A. Diesmos, *et al*. 2003. Phylogenetics of fanged frogs: Testing biogeographical hypotheses at the interface of the Asian and Australian faunal zones. *Syst. Biol.* 52(6). 794–819. DOI: 10.1093/sysbio/52.6.794.

[6] Jifeng, Z., N. Liuwang, P. Qiaoling, G. Yadong, W. Yang, X. Jingcheng, *et al*. 2005. Relationships among the Chinese group of *Limnonectes* based on mitochondrial 12S and 16S rRNA sequences. *Acta Zool. Sin.* 51(2). 354–359.

[7] McLeod, D.S. 2010. Of least concern? Systematics of a cryptic species complex: *Limnonectes kuhlii* (Amphibia: Anura: Dicroglossidae). *Mol. Phylogenet*. *Evol*. 56(3). 991–1000. DOI: 10.1016/j.ympev.2010.04.004.

[8] Inger R.F., H.K. Voris. 2001. The biogeographical relations of the frogs and snakes of Sundaland. *J. Biogeogr.* 28(7). 863–891. DOI: 10.1046/j.1365-2699.2001.00580.x.

[9] Iskandar, D.T., K.N. Tjan. 1996. The amphibians and reptiles of Sulawesi, with notes on the distribution and chromosomal number of frogs. In: Proceedings of the First International Conference on Eastern Indonesian-Australian Vertebrate Fauna Manado, Indonesia. 39–46.

[10] McLeod, D.S., S.J. Horner, C. Husted, A. Barley, D. Iskandar. 2011. Same-same, but different: an unusual new species of the *Limnonectes kuhlii* complex from West Sumatra (Anura: Dicroglossidae). *Zootaxa.* 2883. 52-64. DOI: 10.11646/ZOOTAXA.2883.1.4.

[11] Sumida, M., Y. Kondo, Y. Kanamori, M. Nishioka. 2002. Inter- and intraspecific evolutionary relationships of the rice frog *Rana limnocharis* and the allied species *R. cancrivora* inferred from crossing experiments and mitochondrial DNA sequences of the 12S and 16S rRNA genes. *Mol. Phylogenet. Evol.* 25(2). 293–305. DOI: 10.1016/S1055-7903(02)00243-9.

[12] Che, J., J. Pang, H. Zhao, G. Wu, E. Zhao, Y. Zhang. 2007. Molecular phylogeny of the Chinese ranids inferred from nuclear and mitochondrial DNA sequences. *Biochem. Syst. Ecol.* 35(1). 29–39. DOI: 10.1016/j.bse.2006.09.003.

[13] Frost, D.R., T. Grant, J. Faivovich, R.H. Bain, A. Haas, C.F.B. Haddad, *et al*. 2006. The amphibian tree of life. *Bull. Am. Mus. Nat. Hist.* 297. 1–291.

[14] Liu, Z.Q., Y.Q. Wang, B. Su. 2005. The mitochondrial genome organization of the rice frog, *Fejervarya limnocharis* (Amphibia: Anura): a new gene order in the vertebrate mtDNA. *Gene.* 346. 145–151. DOI: 10.1016/ j.gene.2004.10.013.

[15] Kumar, S., G. Stecher, K. Tamura. 2016. MEGA7: Molecular Evolutionary Genetics Analysis version 7.0 for bigger datasets. *Mol. Biol. Evol.* 33(7). 1870-1874. DOI: 10.1093/molbev/msw054.

[16] Darriba, D., D. Posada, A.M. Kozlov, A. Stamatakis, B. Morel, T. Flouri. 2020. ModelTest-NG: A new and scalable tool for the selection of DNA and protein evolutionary models. *Mol. Biol. Evol.* 37(1). 291–294. DOI: 10.1093/molbev/msz189.

[17] Kozlov, A.M., D. Darriba, T. Flouri, B. Morel, A. Stamatakis. 2019. RAxML-NG: a fast, scalable and user-friendly tool for maximum likelihood phylogenetic inference. *Bioinformatics.* 35(21). 4453–4455. DOI: 10.1093/bioinformatics/btz305.

[18] Miller, M.A., W. Pfeiffer, T. Schwartz. 2010. Creating the CIPRES Science Gateway for inference of large phylogenetic trees. In: 2010 Gateway Computing Environments Workshop. 1-8.

[19] Huelsenbeck, J.P., F. Ronquist. 2001. MrBayes: Bayesian inference of phylogenetic trees. *Bioinformatics.* 17(8). 754–755.

[20] Drummond, A.J., S.Y.W. Ho, M.J. Phillips, A. Rambaut. 2006. Relaxed phylogenetics and dating with confidence. *PLOS Biol.* 4(5). 699–710.

[21] Drummond, A.J., A. Rambaut. 2007. BEAST: Bayesian evolutionary analysis by sampling trees. *BMC ecol. evol.* 7(1). 214. DOI: 10.1186/1471-2148-7-214.

[22] Matsui, M., N. Kuraishi, J-P. Jiang, H. Ota, A. Hamidy, N.L. Orlov, et al. 2010. Systematic reassessments of fanged frogs from China and adjacent regions (Anura: Dicroglossidae). *Zootaxa.* 2345(1). 33–42.

[23] Matsui, M., S. Panha, W. Khonsue, N. Kuraishi. 2010. Two new species of the "kuhlii" complex of the genus *Limnonectes* from Thailand (Anura: Dicroglossidae). *Zootaxa.* 2615(1). 1–22.

[24] Stuart, B.L., S.N. Schoen, E.E.M. Nelson, H. Maher, T. Neang, J.J.L. Rowley, *et al.* 2020. A new fanged frog in the *Limnonectes kuhlii* complex (Anura: Dicroglossidae) from northeastern Cambodia. *Zootaxa.* 4894(3). DOI: 10.11646/ZOOTAXA.4894.3.11.

[25] Matsui, M, D.M. Belabut, N. Ahmad. 2014. Two new species of fanged frogs from Peninsular Malaysia (Anura:Dicroglossidae). *Zootaxa.* 3881(1). 75–93.

[26] Stuart, B.L., R.F. Inger, H.K. Voris. 2006. High level of cryptic species diversity revealed by sympatric lineages of Southeast Asian forest frogs. *Biol. Lett.* 2. 470–474. DOI: 10.1098/rsbl.2006.0505.

[27] Inger, R.F., B.L. Stuart, D.T. Iskandar. 2009. Systematics of widespread Southeast Asian frog, *Rana chalconota* (Amphibia: Anura: Ranidae). *Zool. J. Linn. Soc*. 155. 123–147. DOI: 10.1111/j.1096-3642.2008.00440.x.

[28] McLeod, D.S., S. Kurlbaum, N.V. Hoang. 2015. More of the same: a diminutive new species of the *Limnonectes kuhlii* complex from northern Vietnam (Anura: Dicroglossidae). *Zootaxa.* 3947(2). 201–214. DOI: 10.11646/zootaxa.3947.2.4.

[29] Barber, A.J., M.J. Crow. 2009. Structure of Sumatra and its implications for the tectonic assembly of Southeast Asia and the destruction of Paleotethys. *Island Arc.* 18(1). 3–20.

[30] Haq, B.U., J. Hardenbol, P.R. Vail. 1987. Chronology of Fluctuating Sea Levels Since the Triassic. *Science.* 235(4793). 1156–1167.

[31] O'Connell, K.A., A. Hamidy, N. Kurniawan, E.N. Smith, M.K. Fujita. 2018. Synchronous diversification of parachuting frogs (Genus *Rhacophorus*) on Sumatra and Java. *Mol. Biol. Evol.* 123. 101–112. DOI: 10.1016/ j.ympev.2018.02.003.

ISSN. 2087-2852
E-ISSN. 2338-1655

Effectiveness of Extract Supplements (*Apium graveolens* L.) to Estrogen Receptors Expression and Oocyte Diameter at Nucleolar Chromatin and Perinucleolar Stages in Female of Nile tilapia (*Oreochromis niloticus* L.)

Novy Kurnia Rikardo[1*], Agung Pramana Warih Marhendra[2], Nia Kurniawan[2], Wibi Riawan[3], Sri Rahayu[2]

[1]Master Program of Biology, Department of Biology, Faculty of Mathematics and Natural Sciences, University of Brawijaya, Malang, Indonesia
[2]Department of Biology, Faculty of Mathematics and Natural Sciences, University of Brawijaya, Malang, Indonesia
[3]Laboratory of Physiology, Faculty of Medicine, University of Brawijaya, Malang, Indonesia

Abstract

The study of the use of celery (*Apium graveolens* L.) in the health sector has been widely discussed. The analysis of the use of celery in the process of oocyte development still needs to be addressed. This study was conducted to see the effect of celery extract on the expression of estrogen receptors on the gonads and oocyte diameter in tilapia for the first time. Fish are divided into four groups: P_0 = Control treatment, feed without mixture; P_1 = Treatment with celery extract concentration of 2,000 mg.kg^{-1} of feed; P_2 = Treatment with celery extract concentration of 4,000 mg.kg^{-1} of feed; P_3 = Treatment with celery extract concentration of 6,000 mg.kg^{-1} of feed. The results showed celery extracts expressed estrogen receptors on the gonads. The expressed estrogen receptor is the estrogen receptor β, whereas the estrogen receptor α is not detected in the gonad. Group statistical tests ANOVA showed no significant results in the development of oocytes. On the other hand, celery extract also impacted the development of oocytes at the nucleolar stage of chromatin, with a markedly greater oocyte diameter. Meanwhile, in the perinucleolar stage, celery extract reduces the oocyte diameter.

Keywords: *Apium graveolens* L, *ERα*, *ERβ*, nucleolar chromatin, perinucleolar.

INTRODUCTION

Nile tilapia (*Oreochromis niloticus*) is a type of fish that is easy to cultivate. However, in some cases, there is a problem with fish health and reproduction because of environmental factors; for example, exposure to radiation and environmental chemicals can decrease spawning frequency and egg production [1,2]. It can disturb growth and development, especially in reproduction. The acceleration of fish cultivation can be further increased by adding natural supplements to the feed, such as celery (*Apium graveolens*). The content of antioxidant compounds found in celery is also very strong [3]. Apigenin is one of the antioxidant compounds with high levels in celery [4].

Apigenin belongs to the group of phytoestrogens, resembling natural estrogen-like structures secreted by the human body and animals [5]. Because of its estrogen-like structure, phytoestrogens can interact with estrogen receptors to cause various cellular responses [6]. In fish, cellular responses from active estrogen receptors, such as the mitotic division of oogonia and vitellogenesis [7].

Among the types of estrogen receptors that are known in fish are estrogen α (ERα) receptors and estrogen receptors β (ERβ) [8]. The administration of celery extract with high apigenin content is expected to trigger further the development of gonads of tilapia (*O. niloticus*) with activation parameters from both estrogen receptors. Before the oocyte enters the vitellogenesis stage, it is preceded by the nucleolar stage of chromatin and perinucleolar. The nucleolar stages of chromatin and perinucleolar include primary growth forms from oogenesis [9]. The effect of giving plant extracts to both stages of oocyte growth has not been specifically discussed. We predict that the supplement of *A. Graveolens* L. can have a biological effect on the early oogenesis process.

MATERIAL AND METHOD

Experiments used female tilapia from the Punten Fish Seed Hall. The fish used is 2.5 months old with an average mass of 5.13 grams. The tilapia is acclimatized for three days in the aquarium before being treated. The chosen sample is 2.5-month-old fish because, at that age, we can distinguish the fish morphologically as male or female. We use only female fish for the treatment.

*Correspondence address:
Novy Kurnia Rikardo
Email : novy.kurnia.r@gmail.com
Address : Dept. Biology, University of Brawijaya, Veteran Malang, 65145.

The container used for treatment is an aquarium with a size of 49.5 × 34.5 × 25.7 cm. The total aquarium used is four units, and all are equipped with aerators. Once a day, in the afternoon, aquarium water is used to clean the dirt and the remaining fish food, with ten fish per aquarium—all populations in one group to make the slide. The observation was repeated, and we used each individual to replicate the slides five times. The slide runs from left to right, anterior to posterior. Fish are divided into four groups, namely: P_0 = Control treatment, feed without mixture; P_1 = treatment with celery extract concentration of 2,000 mg.kg^{-1} of feed; P_2 = treatment with celery extract concentration of 4,000 mg.kg^{-1} of feed; P^3 = treatment with celery extract concentration of 6,000 mg.kg^{-1} of feed. The control and treatment fish were fed daily in standard feed (pellets), which was 3-5% of the total body weight [10]. Each fish has an average weight of 5.1345 grams. The feed is given twice daily in the morning and evening with a dose of 0.2567 g.fish^{-1} per day. Fish weight is weighed ten days to determine the new feeding dose.

Detection of Estrogen Receptors α and β with the Immunohistochemistry Method

The tissue block was attached to the holder and cut with a thickness of 4.5 µm with a rotary microtome. It was followed by the attachment process on glass objects with 5% gelatin. The slides from the gonad cutting are put in an oven at an incubator temperature of 60°C for three days before deparaffinization. The slide is dipped in the first xylol for 8 minutes. Then, the slide was rinsed by dipping it into the second xylol for 8 minutes. The slides are rinsed with xylol for the last 8 minutes. Xylol on the slide was rinsed with immersion in absolute ethanol for 8 minutes. The slide was dipped in 80% ethanol for 8 minutes. The slide was dipped in 70% ethanol for 8 minutes. Slides are stored at 4°C overnight so the alcohol evaporates. Slides are rinsed with distilled water thrice, each for 5 minutes [11].

The slides were rinsed with PBS three times, each for 5 minutes. The slides were incubated using Peroxidase Blocking for Image Analysis for 40 minutes at room temperature. The slides are rinsed again with PBS three times, each for 5 minutes. Slides were incubated with SuperBlock overnight at 4°C. The slides were rinsed with PBS three times, each for 5 minutes. Slides were incubated with Primary Antibodies, diluted in blocking 1:50 overnight at 4°C. The slides were rinsed with PBS three times, each for 5 minutes. The slides were incubated on (diaminobenzidine) DAB Chromogen in the DAB substrate for 40 minutes. Slides are rinsed with distilled water until the substrate is clean. Mayer's Hematoxylin Counter Stain is given on the slide for 5 minutes. The slide was rinsed with water three times. The slides are dried in an incubator at 40°C. Mounting slides are done with entanglement and covered with a glass cover. Then, we observed with a light microscope with 400x and 1000x magnification. If there are expressions of ERα and ERβ, then the presence of brown in oocytes, theca cells, granulosa cells, and tissue stromal cells in the gonads of tilapia is shown [11].

Measurement of Oocyte Diameter

Oocyte diameter measurements were carried out with the CX21FS1 Olympus CX21 Model Binocular Microscope with 100x magnification. The microscope is equipped with a micrometer (Olympus-Japan). The oocytes observed were the nucleolar chromatin and perinucleolar stages, with reference to the stages of oocyte development described by Srijunngam and Wattanasirmkit [12]. Oocytes from the nucleolar chromatin stage were treated for ten oocytes to measure their diameter, while the perinucleolar stage was taken from five oocytes. Data acquisition is obtained in a ratio (scale): length and diameter. Data are tabulated according to the group. The data were tested for normality and homogeneity. Then, an ANOVA test was used.

RESULT AND DISCUSSION

Oocyte Diameter After Giving Celery Extract

Nucleolar chromatin is the first stage of oocyte development in small oocyte fish. The nucleus contains nucleoli, which, together with chromatin, the cytoplasm is thin, follicular cells are challenging to see, and oocytes are in the middle of the follicle (Fig. 1A). The next stage of development after nucleolar chromatin is perinucleolar, which is characterized by the nucleus containing the nucleoli at the edge.

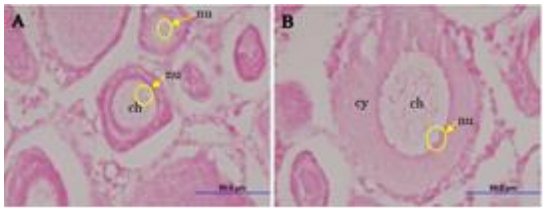

Figure 1. The oocyte structure of tilapia is at the nucleolar stage of chromatin (A) and perinucleolar stage (B). ch: chromatin, nu: nucleoli, cy: cytoplasm

ISSN. 2087-2852
E-ISSN. 2338-1655

The nucleoli are separated by chromatin, and the cytoplasm is thicker than the nucleolar chromatin stage (Fig. 1B). After the nucleolar chromatin and perinucleolar stages are complete, the oocytes enter the cortical alveoli formation stages, vitellogenin (yolk), and mature (adult).

This study looked at the pattern of oocyte development after receiving various doses of celery extract. It appears that, with Hematoxylin-Eosin staining, the nucleolar chromatin stage in the control group, the extract treatment of 2,000 mg.kg^{-1} of feed, and the treatment of 4,000 mg.kg^{-1} showed results of 33 µm, 33 µm, and 38 µm respectively. Moreover, with a statistical test, the treatment groups of 2,000 mg.kg^{-1} and 4,000 mg.kg^{-1} had no significant effect (P> 0.05). However, the 4,000 mg.kg^{-1} exposure group of feed affected oocyte diameter, which tended to be greater than the control treatment (without celery extract). At the same time, the celery extract treatment of 2,000 mg.kg^{-1} of feed gave the effect of the oocyte diameter equal to the control (Table 1).

Table 1. Average Oocyte Diameter of Nucleolar Chromatin Stage

No	Treatment of Celery Extract	Average Oocyte Diameter (µm)
1	0 mg.kg^{-1} of feed (control)	33±10.6 a
2	2,000 mg.kg^{-1} of feed	33±6.7 a
3	4,000 mg.kg^{-1} of feed	38±7.9 a

A large oocyte diameter is observed at a high extract concentration under a light microscope. At the nucleolar chromatin stage, the oocyte undergoes meiosis in the prophase I phase [13,14]. Prophase I includes the longest and relatively complicated phase compared to other meiotic stages. This is because there is an exchange process. The chromosome pairs go through four stages, namely leptotene, zygotene, pachytene, and diplotene [15], so that oocyte cells require a sufficiently large volume of space when they are in prophase I phase so that the process takes place correctly.

The provision of celery extract with a concentration of 4,000 mg.kg^{-1} of feed proved to cause the oocyte diameter in the nucleolar chromatin stage to be larger. Previous studies on tilapia oocyte size explained that a decrease in oocyte diameter decreased the gonadal period and gonadal somatic index (GSI) [16]. The low gonadal period indicates low reproductive success in fish, and vice versa if the high gonadal period shows a high level of reproductive success. The concentration of celery extract used in this study can increase the oocyte diameter, potentially supporting the successful reproduction of fish.

At the beginning of the egg formation process, germinative primordial cells turn into oogonia. Oogonia then multiplies the amount through mitotic division [9]. Oogonia is a diploid cell [13]. When mitosis is in the interphase stage, there is also duplication of chromosomes and production of cytoplasmic organelles and proteins. Then, proceed with the mitosis prophase stage, which begins spindle thread formation [17].

The interphase and prophase stages in oocytes include a critical phase and are susceptible to DNA damage caused by various factors, such as free radicals. In addition to DNA damage, these free radicals also cause damage to cell membranes, mitochondria, and microtubules. So that if not handled early, it can cause cell death. During mitosis, a cell mechanism exists to balance free radical formation and antioxidant mechanisms [18].

However, aquatic ecosystems are very susceptible to the entry of chemical compounds that cells cannot tolerate because the antioxidants produced naturally by cells are limited. Celery contains high levels of antioxidants that can help increase antioxidant levels in cells [19]. Celery leaves are rich in phenolics and can make a good source of antioxidants.

The perinucleolar stage, Figure 1B, shows the mean oocyte diameter in the control extract, treatment of 2,000 mg.kg^{-1} and 4,000 mg.kg^{-1} of feed showed results of 104 µm, 82 µm and 98 µm, respectively. Group statistical tests of ANOVA on the 2,000 mg.kg^{-1} and 4,000 mg.kg^{-1} of feed on perinucleolar oocyte diameter showed no significance (P> 0.05). Thus, it is known that the treatment of the administration of celery extract, which is higher, does not have an impact on the increase or decrease in oocyte diameter. On the other hand, the treatment of 2,000 celery extracts and 4,000 mg.kg^{-1} of feed showed that oocyte diameters tended to be lower than controls (Table 2).

Table 2. Average Oocyte Diameter of Perinucleolar Stage

No	Treatment of Celery Extract	Average Oocyte Diameter (µm)
1	0 mg.kg^{-1} of feed (control)	104±11.4 a
2	2,000 mg.kg^{-1} of feed	82±14.8 a
3	4,000 mg.kg^{-1} of feed	98±13.0 a

ISSN. 2087-2852
E-ISSN. 2338-1655

The size of the oocyte in the perinucleolar stage is closely related to the volume of the ooplasm (oocyte cytoplasm). The more ooplasm accumulation, the greater the oocyte diameter in the perinucleolar stage. The ooplasm of tilapia and most sub-class eleostei fish contain various aggregates and cell organelles [20]. As oocytes grow, aggregates and organelles experience an increase in number. The process requires antioxidants to prevent the effects of oxidative stress. Celery with high antioxidant compounds has the potential to help the process. Antioxidants prevent damage from oxidants and free radicals [21].

Interactions between estrogen and estrogen receptors support growing oocytes. Estrogen stimulates estrogen receptor activation, directly triggering the expression of Nppc/Npr2 in the [22]. Nppc/Npr2 functions essential for follicular development, oocyte maturation, and ovulation. The research results by Kiyosu *et al.* [23] prove that NPPC/NPR2 deficiency is known to cause sterility, oocyte chromosomal irregularities, and smaller ovarian size than normal female mice.

Expression of Alfa (Erα) Estrogen Receptors and Estrogen Beta (Erβ) Receptors after Giving Celery Extract

Observations of the effect of supplementation on celery extract on Erα and Erβ have been carried out on the gonads of female tilapia using immunohistochemical methods. The observations show that Erβ is expressed in all treatments, indicated by the brown color, which can be seen in Figures 2. The brown color is generated from the reaction of the DAB chromogen substrate. Whereas the expression Erα was not detected (image not shown).

Estrogen beta (Erβ) was expressed in the control treatment, extract treatment of 4,000 mg.kg^{-1} of feed and 6000 mg.kg^{-1} of feed (Fig. 2). In the control treatment, Erβ was detected in ooplasm and stromal cells (Fig. 2A). The extract treatment of 4,000 mg.kg^{-1} of feed resulted in an Erβ distribution in granulosa cells, theca cells, and in stromal cells (Fig. 2B). The treatment of 6,000 mg.kg^{-1} of feed produced Erβ expression in the area of theca cells, ooplasms, and stromal cells. In the treatment with the highest extract concentration (6,000 mg.kg^{-1} of feed), Erβ expression tends to be more in ooplasm when compared with other cell parts (Fig. 2C).

Alpha and beta estrogen receptors control the body's physiological processes. Among them are the control of the circulatory system, nerves, motion, and reproduction [24]. In the reproductive organs, estrogen receptors can be activated after binding to estrogen. So that the presence of estrogen must always be there at all times so that the reproductive process usually runs. Estrogen receptors have been active and act as activators of transcription [25]. The process of gonad development in female fish requires the presence of estrogen in the cells and tissues that need it.

Expression of β-receptor estrogen has been found in stromal cells in the control and treatment with celery extract. It indicates that the given celery extract can work together with endogenous estrogen in the gonads of fish.

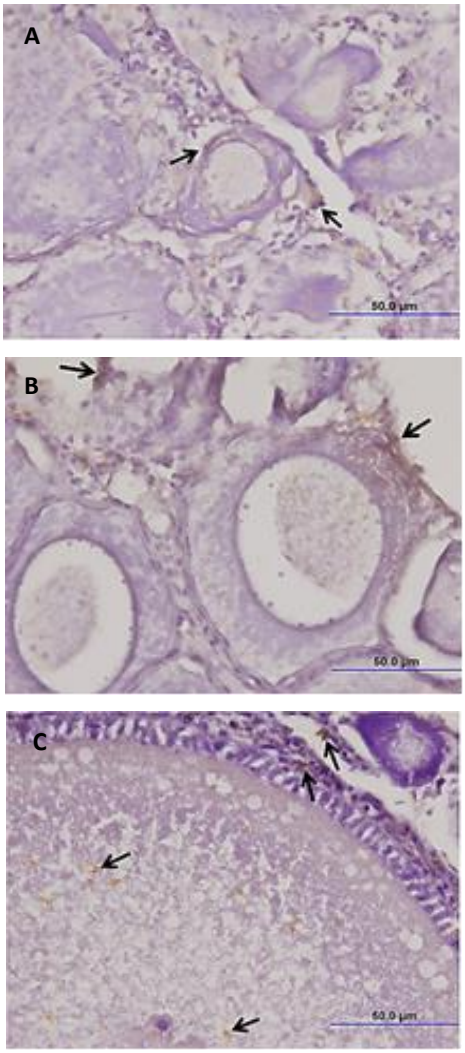

Figure 2. ERβ expression in gonad tissue female tilapia with celery extract, a) 0 mg.kg^{-1} feed (control), b) 4,000 mg.kg^{-1} feed, and c) 6,000 mg.kg^{-1} **Notes:** Black arrows indicate the presence of ERβ

ISSN. 2087-2852
E-ISSN. 2338-1655

In this study, ERβ expression tends to increase in the ooplasm section when given the highest concentration of celery extract. These results indicate celery extract in which the phytoestrogen compounds can circulate into the ooplasm, resulting in ERβ activation in that section. The study by Filby and Tyler [26] shows that the high and low expression of ERβ in the gonad is not the same in every development of gonadal fish. The aquatic environment as a fish habitat will always change in condition. Pollutants that enter the aquatic environment can change water conditions [27]. Unstable water conditions make fish physiology abnormal or even decline, including the synthesis and work of reproductive hormones in fish. Therefore, supplementation of natural hormonal compounds from celery extract can be an alternative solution in helping to stabilize reproductive hormones in fish, one of which is estrogen.

CONCLUSION

The research proves that the supplementation of celery extract (*A. graveolens* L.) with various concentrations has the potential to assist the development process of oocyte Tilapia (*O. niloticus*) nucleolar chromatin stage and help the activation of beta estrogen receptors. On the other hand, the concentration of celery extract used in this study did not affect the perinucleolar oocyte stage and activation of alpha estrogen receptors. With this research, it is hoped that further research will be applied to more comprehensive applications. We recommend using soybeans (*Glycine max*) extracts for further research due to their high phytoestrogen content, which acts as alternative estrogen.

Acknowledgement

The author would like to thank all laboratory staff in the Biochemistry and Biomolecular Laboratory, Faculty of Medicine, and Department of Biology, University of Brawijaya, who provided much assistance and support during the research.

REFERENCES

[1] Bourrachot, S., F. Brion, S. Pereira, M. Floriani, V. Camilleri, I. Cavalié, *et al.* 2014. Effects of depleted uranium on the reproductive success and F1 generation survival of zebrafish (*Danio rerio*). *Aquat. toxicol.* 154. 1-11.

[2] Peng, X., X. Sun, M. Yu, W. Fu, H. Chen, J. Chen. 2019. Chronic exposure to environmental concentrations of phenanthrene impairs zebrafish reproduction. *Ecotoxicol. Environ. Saf.* 182. 109376.

[3] Kooti, W., N. Daraei. 2017. A review of the antioxidant activity of celery (*Apium graveolens* L). *J. Evid. Based Complementary Altern.* Med. 22 (4). 1029-1034.

[4] Patel, D., S. Shukla, S. Gupta. 2007. Apigenin and cancer chemoprevention: progress, potential and promise (review). *Int. J. Oncol.* 30(1). 233-245.

[5] Rice, S., H.D. Mason, S.A. Whitehead. 2006. Phytoestrogens and their low dose combinations inhibit mRNA expression and activity of aromatase in human granulosa-luteal cells. *J. Steroid Biochem. Mol. Biol.* 101(4-5). 216–225.

[6] Lecomte, S., F. Demay, F. Ferrière, F. Pakdel. 2017. Phytochemicals targeting estrogen receptors: beneficial rather than adverse effects?. *Int. J. Mol. Sci.* 18 1381.

[7] Yaron, Z., B. Levavi-Sivan. 2011. Endocrine regulation of fish reproduction. In: Farrell, A.P., (Ed). Encyclopedia of Fish Physiology: From Genome to Environment 2. 1500-1508.

[8] Menuet, A., E. Pellegrini, I. Anglade, O. Blaise, V. Laudet, O. Kah, F. Pakdel. 2002. Molecular characterization of three estrogen receptor forms in zebrafish: binding characteristics, transactivation properties, and tissue distributions. *Biol. Reprod.* 66(6). 1881–1892.

[9] Kagawa, H. 2013. Oogenesis in teleost fish. *Aqua-BioSci. Monogr.* 6(4). 99–127.

[10] Amri, K., Khairuman. 2003. budidaya ikan nila secara intensif. Agromedia Pustaka. Tangerang.

[11] Akmal, M., Aulanni'am, W. Riawan. 2007. Cyclooxygenase-2 (COX-2) expression on testis connective tissue of *Rattus norvegicus* after treatment with betel nut extract (*Areca catechu*). *Jurnal Kedokteran Brawijaya.* 23(3). 121-124.

[12] Srijunngam, J., K. Wattanasirmkit. 2001. Histological structures of nile tilapia *Oreochromis niloticus* Linn. Ovary. *Nat. Hist. J. Chulalongkorn Univ.* 1(1). 53-59.

[13] Le Menn, F., J. Cerdà, P.J. Babin. 2007. Ultrastructural aspects of the ontogeny and differentiation of ray-finned fish ovarian follicles. In: Babin, P.J., J. Cerdà, E. Lubzens

(Eds). The Fish Oocyte: From Basic Studies to Biotechnological Application. 1–37.

[14] Arianti, N. D., M.F. Rahardjo, A. Zahid. 2017. Perkembangan sel telur ikan seriding, Ambassis nalua (Hamilton 1822). *Jurnal Iktiologi Indonesia.* 17(1). 115-123.

[15] Uribe, M.C., H.J. Grier, L.R. Parenti. 2012. Ovarian Structure and oogenesis of the oviparous goodeids *Crenichthys baileyi* (Gilbert, 1893) and *Empetrichthys latos* Miller, 1948 (Teleostei, Cyprino-dontiformes). *J. Morphol.* 273(4). 371–387.

[16] Zulfahmi, I., M. Muliari, Y. Akmal, A.S. Batubara. 2018. reproductive performance and gonad histopathology of female nile tilapia (*Oreochromis niloticus* Linnaeus 1758) exposed to palm oil mill effluent. *Egypt. J. Aquat. Res.* 44(4). 327-332.

[17] Urry, L.A., M.L. Chain, S.A. Wasserman, P.V. Minorsky, J.B. Reece. 2017. Campbell Biology 11th Ed. Pearson Education, Inc. New York.

[18] Hemnani, T., M.S. Parihar. 1998. Reactive Oxygen Species and Oxidative DNA Damage. *Indian J. Physiol. Pharmacol.* 42(4). 440-452.

[19] Jung, W.S., I.M. Chung, S.H. Kim, M.Y. Kim, A. Ahmad, N. Praveen. 2011. In vitro antioxidant activity, total phenolics and flavonoids from celery (*Apium graveolens*) leaves. J. Med. Plants Res. 5. 7022-7030

[20] Wallace, R.A., K. Selman. 1981. Cellular and dynamic aspects of oocyte growth in teleosts. *Am. Zool.* 21(2). 325-343.

[21] Poznyak, A.V., V. Grechko, V.A. Orekhova, S.Y. Chegodaev, W. Wu, A.N. Orekhov. 2020. Oxidative stress and antioxidants in atherosclerosis development and treatment. *Biology.* 9. 60.

[22] Liu, W., Q. Xin, X. Wang, S. Wang, H. Wang, W. Zhang, *et al.* 2017. Estrogen receptors in granulosa cells govern meiotic resumption of pre-ovulatory oocytes in mammals. *Cell Death Dis.* 8(3). 1-11.

[23] Kiyosu, C., T. Tsuji, K. Yamada, S. Kajita, T. Kunieda. 2012. NPPC/NPR2 signaling is essential for oocyte meiotic arrest and cumulus oophorus formation during follicular development in the mouse ovary. *Reproduction.* 144(2). 187-193.

[24] Paterni, I., C. Granchi, J.A. Katzenellenbogen, F. Minutolo. 2014. Estrogen receptors alpha (ERα) and beta (ERβ): Subtype-selective Ligands and Clinical Potential. *Steroids.* 90. 13-29.

[25] Prossnitz, E.R., M. Barton. 2011. The G-Protein-Coupled estrogen receptor GPER in health and disease. *Nat. Rev. Endocrinol.* 7(12). 715–726.

[26] Filby, A.L., C.R. Tyler. 2005. Molecular characterization of estrogen receptors 1, 2a, and 2b and their tissue and ontogenic expression profiles in fathead minnow (*Pimephales promelas*). *Biol. Reprod.* 73(4). 648–662.

[27] Authman, M.M.N., M.S. Zaki, E.A. Khallaf, H.H. Abbas. 2015. Use of fish as bio-indicator of the effects of heavy metals pollution. J. Aquac. Res. Dev. 6(4). 328.

ISSN. 2087-2852
E-ISSN. 2338-1655

Influence of *Marsilea crenata* and *Alpinia purpurata* Ethanol Extract on MDA and SOD Testicular Cells of Hyperglycemia Mice

Febriane Eka Damayanti[1], Sri Rahayu[2*], Sri Widyarti[2]

[1]Master Program of Biology, Department of Biology, Faculty of Mathematics and Natural Sciences, University of Brawijaya, Malang, Indonesia

[2]Department of Biology, Faculty of Mathematics and Natural Sciences, University of Brawijaya, Malang, Indonesia

Abstract

Hyperglycemia can induce testicular damage that leads to male infertility. Herbal plants, such as *Marsilea crenata* and *Alpinia purpurata,* are used for antioxidant defense systems to repair reproductive disorders due to hyperglycemia. This study aims to evaluate the effect of *M. crenata* and *A. purpurata* ethanol extracts on MDA and SOD testes of hyperglycemia mice. This study used a completely randomized design with seven treatment groups (n=4), namely N (control group), H (hyperglycemia mice), Met (hyperglycemia mice given metformin), D1 (0. 09 $mg.g^{-1}$ *M. crenata*), D2 (0.2 $mg.g^{-1}$ *A. purpurata*), D3 (0.09 $mg.g^{-1}$ *M. crenata* + 0.2 $mg.g^{-1}$ *A. purpurata*), and D4 (0.09 $mg.g^{-1}$ *M. crenata* + 0.4 $mg.g^{-1}$ *A. purpurata*). The extracts were administered orally for 17 days. Analysis of testicular MDA and SOD levels was performed by flow cytometry. Data analysis was performed with a one-way ANOVA test and continued with the Tukey test. The results showed that the D4 treatment group, compared to D3, D2, D1, Met, H, and N, showed a better decrease in MDA levels (4.47%) and an increase in SOD levels in the D4 group (4.77%). The research concludes that the combination of 0.09 $mg.g^{-1}$ *M. crenata* and 0.4 $mg.g^{-1}$ *A. purpurata* was an optimal dose to decrease MDA levels and increase SOD levels in the testes of hyperglycemic mice.

Keywords: *Alpinia purpurata*, *Marsilea crenata*, MDA, SOD, testes.

INTRODUCTION

The testes, as the primary male reproductive organ, have the main function of producing sperm and testosterone [1]. This function is supported by a long process of spermatogenesis and steroidogenesis, which underlies the testes as an organ with dense physiological activity [2]. Consequently, it becomes an organ with high mitochondrial oxygen demand, which causes reactive oxygen species (ROS) to accumulate through mitochondrial electron leakage [3]. Although ROS is vital in physiologically tolerable levels for spermatozoa, ROS abundance can initiate oxidative stress (OS), leading to reproductive system disorders [4].

Hyperglycemia is one of the factors that can exacerbate reproductive disorders due to OS. Hyperglycemia is a condition of blood sugar levels exceeding the normal range [5]. Based on reported cases, it was found that hyperglycemia can reduce the birth rate in productive age [6,7]. In this case, 40-50% of them are caused by male infertility [5,8]. In hyperglycemia conditions, ROS can accumulate through several pathways, including activating RAGE by forming advanced glycation end-products (AGEs) [9]. In this condition, antioxidant protection cannot stabilize ROS, which leads to testicular damage [10].

*Correspondence address:
Sri Rahayu
E-mail : srahayu@ub.ac.id
Address : Dept. Biology, University of Brawijaya, Veteran Malang, 65145

Testicular cells comprise long-chain ω-6 and ω-3 polyunsaturated fatty acids (PUFAs) [11]. These structures play a role in testes metabolism and may be associated with OS. ROS caused by hyperglycemia can attack PUFAs and induce lipid peroxidation [12,13]. Lipid peroxidation is a chain reaction due to an imbalance of prooxidants and antioxidants [14,15]. Lipid peroxidation can initiate cell, tissue, and organ damage, particularly in the testes. As a result, malondialdehyde (MDA) can be formed as a secondary product of lipid peroxidation. It underlies the evaluation of MDA levels widely used as a biomarker of lipid peroxidation [16].

The human body already has protection to neutralize excess ROS with endogenous antioxidants. Superoxide Dismutase (SOD) is a part of endogenous antioxidants that catalyze superoxide into oxygen and hydrogen peroxide [17]. However, an increase in ROS due to hyperglycemia can initiate a decrease in SOD [18]. It requires preventive approaches by administering exogenous antioxidants. Previous studies have mentioned that administering exogenous antioxidants based on herbs can inhibit spermatozoa and testicular damage due to ROS [19].

Marsilea crenata is a semi-aquatic plant often found in rice fields and considered a weed [20]. It has been reported that *M. crenata* contains phytochemical components such as flavonoids, terpenoids, and saponins [21,22]. These components can potentially be used as a source

of nutrients supporting spermatogenesis [23]. In addition, *Alpinia purpurata*, which is a member of the Zingiberaceae family, has also been reported to contain flavonoids [24]. Both herbal plants are widespread in Indonesia and widely used for food. However, their effect on the antioxidant system in testicular cells with hyperglycemia has not been studied. This study aims to determine the impact of a combination of *M. crenata* and *A. purpurata* ethanol extracts on MDA and SOD testes of hyperglycemia mice.

MATERIAL AND METHOD

Extract Preparation

The dried leaves of *M. crenata* were collected from *Selendang Semanggi*, Surabaya, Indonesia. The sample was converted into powder at UPT Laboratorium Herbal Materia Medica, Batu, Malang, Indonesia (specimen number: 074/ 497/ 102.20-A/2022). *Alpinia purpurata* rhizome powder was purchased from UPT Laboratorium Herbal Materia Medica, Batu, Malang, Indonesia (specimen number: 074/ 496/ 102.20-A/2022).

The powder of each sample was extracted by maceration using a 70% ethanol solvent. Maceration was carried out for 24 hours with a ratio of 1:10 (w:v). The ethanol extracts of *M. Crenata* leaves, and *A. Purpurata* rhizomes were filtered and evaporated using a rotary evaporator [25].

Experimental Design

The protocol of this research was approved by the Animal Care and Use Committee, University of Brawijaya (No. 114-KEP-UB-2022). 28 male BALB/c mice (*Mus musculus*) were obtained from the Faculty of Veterinary Medicine, Airlangga University, Surabaya, East Java, Indonesia. The criteria for experimental animals were 6-7 weeks old with a minimum body weight of 25 g. Mice were kept at room temperature with a 12-hour light-dark cycle and separated from each tail. Mice were fed standard pellets and water *ad libitum*. Acclimatization was carried out seven days before treatment. This study used a completely randomized design with seven treatment groups (n=4) (Table 1). The ethanol extracts of *M. Crenata* and *A. Purpurata* were administered orally for 17 days.

Metformin is a biguanide derivative frequently used in treating hyperglycemia. Metformin can reduce blood sugar levels through the mechanism of insulin sensitivity [26]. In this study, metformin was used as a comparison to represent synthetic drugs commonly used in hyperglycemia conditions.

Table 1. Treatment groups

	Group Description	Extract combination (mg.g^{-1})	
		M. crenata	*A. purpurata*
N	Normal	-	-
H	Hyperglycemia	-	-
Met	Hyperglycemia + Metformin	-	-
D1	Hyperglycemia	0.09	-
D2	Hyperglycemia	-	0.2
D3	Hyperglycemia	0.09	0.2
D4	Hyperglycemia	0.09	0.4

Induction of Hyperglycemia in Experimental Animals

The diabetic agent streptozotocin (STZ) induces hyperglycemia in experimental animals. STZ induction was performed at a dose of 145 mg.kg^{-1} (single high-dose) intraperitoneally after the mice were fasted for 4 hours. STZ was injected in citrate buffer solvent pH 4.5. This solution is recommended for up to 10 minutes to avoid toxicity [25]. Confirmation of blood sugar levels was performed using the glucometer Easy Touch®GCU (Bioptik Technology, Taiwan). Blood sugar ≥ 200 mg.dL-1 is categorized as hyperglycemia mice.

Immunostaining and Flow cytometry

Testicular organs were isolated and homogenized in 3 mL phosphate buffer saline (PBS). Centrifugation was performed at 2500 rpm at 10°C for 5 minutes. The pellet was resuspended and homogenized with 1 mL PBS. Each 100 µL sample was transferred into a microtube and added with 50 µL of CytofixTM to incubate at 4°C for 20 min. The sample was added with 500 µL permeabilization buffer and resuspended. The pellet formed was added with 50 µL FITC anti-MDA and PerCP anti-SOD (BioLegend, USA). Afterward, samples were incubated at 4°C for 20 min. Samples were added 400 µL PBS for running flow cytometry (BD FACSCali-bur, USA) [25].

Statistical Analysis

Statistical analysis was performed using the one-way ANOVA test with a significance value of $p<0.05$ and a confidence level of 95%. If the ANOVA test results show a significant difference, data analysis is continued with the Tukey test. Data analysis was carried out using SPSS 25.0.

RESULT AND DISCUSSION

Confirmation of STZ-induced Hyperglycemia

Mice are confirmed as hyperglycemia if the random plasma glucose ≥200 mg.dL^{-1} [27]. Figure 1 shows the mean blood sugar levels of mice after STZ injection. The N group refers to mice

ISSN. 2087-2852
E-ISSN. 2338-1655

not injected by STZ, while the group of H, Met, D1, D2, D3, and D4 refers to mice with induction of STZ. The N group had an average blood sugar level of 108 mg.dL^{-1}. The mean blood sugar levels in H, Met, D1, D2, D3, and D4 were 203 mg.dL^{-1}, 369 mg.dL^{-1}, 225 mg.dL^{-1}, 239 mg.dL^{-1}, 248 mg. dL^{-1}, and 285 mg.dL^{-1}, respectively. The results of this study indicate that treated mice meet the requirements for hyperglycemic experimental animals.

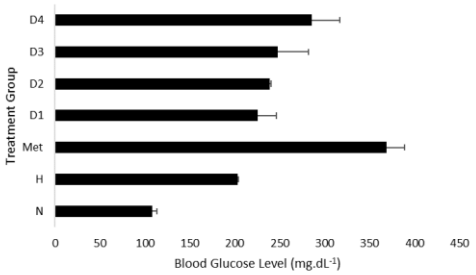

Figure 1. Blood sugar levels post STZ injection. Data are mean ± SD in each group (n=4) with P>0.05.

STZ is a common diabetogenic agent in hyperglycemia model research [28]. STZ induction in experimental animals can selectively damage pancreatic β-cells and increase blood sugar levels [29]. Indeed, STZ can induce Hyperglycemia through processes such as polyol and hexoxamine pathways and glucose autooxidation that causes excess ROS production [30]. Hyperglycemia due to STZ induction can be different in each experimental animal. The use of a single high-dose STZ (145 mg.kg^{-1}) may lead to a rapid increase in blood sugar levels to more than 500 mg.dL^{-1} [29]. It underlies the high blood sugar levels in the Met group (Fig. 1). Hyperglycemia in male primary reproductive organs can initiate ROS accumulation from somatic cells and germ cells. As a result, oxidative stress occurs due to the inability of antioxidant defenses to neutralize ROS, which leads to DNA damage, protein changes, and lipid peroxidation in the testes [31].

The effect of *M. crenata* and *A. purpurata* on MDA Level in Hyperglycemia Testes

MDA is an aldehyde group classified as a secondary product of the lipid peroxidation process [16]. This study showed an increase in the relative number of testicular MDA in mice induced by hyperglycemia characterized by the higher testicular MDA in the H group, with a total of 6.13% compared to the N group, with a total of 5.11%. In sample groups treated with ethanol extract of *M. crenata* and *A. purpurata*, there was a decrease in the relative number of testicular MDA, especially in D2, D3, and D4 when compared to H and Met groups. D2, D3, and D4 groups had testicular MDA levels of 5.65%, 4,62%, and 4.05%. In addition, the amount of testicular MDA in group D4 was found to be significantly different (P<0.05) from that of the H group (Fig. 2).

The increased production of ROS can degrade PUFA and form malondialdehyde (MDA) [32]. ROS represents a reactive free radical that can generate a harmful reduction reaction. ROS is generated in several sources, such as mitochondria, NADPH, cytochrome P450, monocytes, neutrophils, lipoxygenase, and nitric oxide synthase [33]. In the male reproductive system, ROS abundance plays a role in infertility [34]. ROS production in male reproductive organs is classified as internal and external sources.

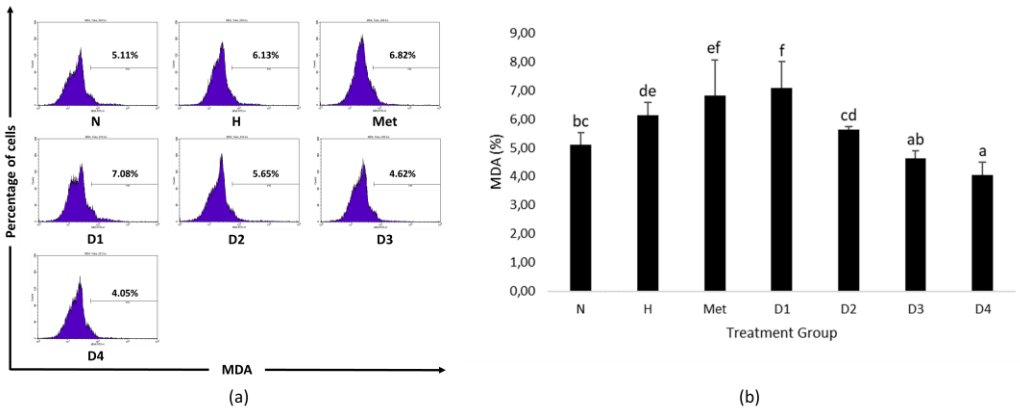

Figure 2. The administration of *M. crenata* and *A. purpurata* extracts reduced testicular MDA levels in hyperglycemia models. (a) Plot of flow cytometry analysis, (b) Histogram of mean statistical results.

ISSN. 2087-2852
E-ISSN. 2338-1655

Internal sources of ROS consist of immature spermatozoa, abnormal spermatozoa, neutrophils, and macrophages, which are part of leukocytes. External sources include endocrine-disrupting chemicals (EDCs), smoking, alcohol and drug consumption, and environmental factors such as radiation [35,36]. In addition, degenerative diseases such as diabetes mellitus also contribute to increased ROS in testicular cells [20].

Excessive ROS accumulation is a crucial issue. Testes and their components are considered to be composed of PUFA, which is very susceptible to lipid peroxidation. As a result, impaired testicular cell function, loss of membrane integrity, decreased sperm quality, and induced apoptosis [37]. It is consistent with the increase in testicular MDA levels in hyperglycemia mice as a biomarker of lipid peroxidation. The antioxidant therapy strategy provided in this study was the decrease in MDA levels after treatment with ethanol extracts of *M. crenata* leaves and *A. purpurata* rhizomes. These results align with previous research that showed a decrease in testicular MDA levels in MSG-induced mice after treatment with ethanol extract of *M. crenata* [38]. *M. crenata* is reported to contain genistein, daidzein, and quercetin to reduce MDA levels in the testes [38-40]. In addition, *A. purpurata* is reported to have several active compounds, such as kaempferol, carbohydrates, terpenoids, glycosides, saponins, and flavonoids, that indicate its high antioxidant activity [41].

The Effect of *M. crenata* and *A. purpurata* on Testicular SOD Activity

Testes with PUFA-rich structures have a distinct strategy for protecting themselves from oxidative stress. Under hyperglycemia conditions, moderate autophagy is required to preserve testicular damage by maintaining homeostasis [12,42]. In addition, antioxidant enzymes provide defense for testicular cells in overcoming excess ROS due to hyperglycemia. SOD, as one of the enzymatic antioxidants, plays a role in protecting testicular cells, especially spermatozoa, from oxidative stress and lipid peroxidation [37]. In addition, endogenous antioxidants in spermatozoa are limited compared to other organs [43]. It underlies the importance of providing exogenous sources of antioxidants as a preventive measure to prevent testicular damage due to ROS accumulation [37].

The results (Fig. 3) showed that the administration of the extract improved in relative number of testicular SOD of mice induced by hyperglycemia. The H group had a total SOD of 5.66%, while group N was 3.43%. The increased SOD in the H group compared to the N group occurred as a result of testicular cells' response to maintain their homeostasis. Although it was unable to exceed Met groups, the administration of ethanol extracts of *M. crenata* and *A. purpurata* at all four doses showed an increase in SOD percentage when compared to the normal group.

The results SOD from the four D-groups were 5.46% (D1), 4.70% (D2), 4.70% (D3), and 4.86% (D4), which significantly different from the normal group ($P<0.05$) (Fig. 3b). These results indicate that D4 is the optimal dose for improving SOD activity in hyperglycemia testes. The calculation of the MDA : SOD ratio used to determine the optimal dose of *M. crenata* and *A. purpurata* ethanol extracts on testicular antioxidant molecules in hyperglycemia mice.

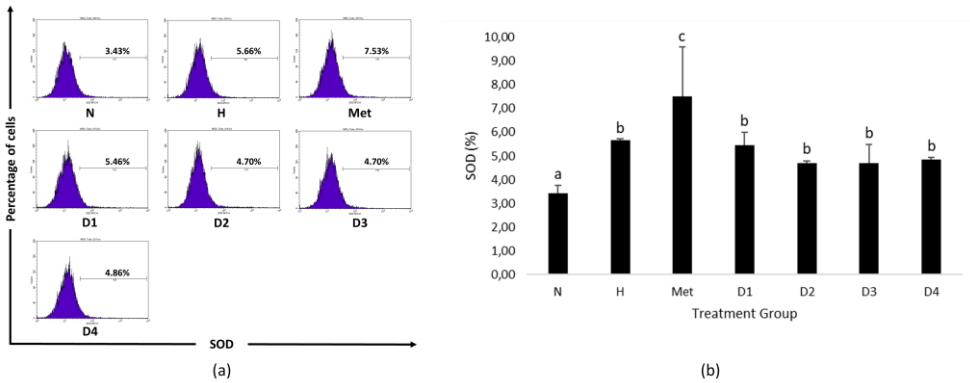

Figure 3. Administration of *M. crenata* and *A. purpurata* extracts increased testicular SOD levels of hyperglycemia models. (a) Plot of flow cytometry analysis, (b) Histogram of mean statistical results.

ISSN. 2087-2852
E-ISSN. 2338-1655

The lowest MDA : SOD ratio can indicate the most optimal dose in improving testicular antioxidants in hyperglycemia mice. Through the ratio calculation of the relative number of testicular MDA : SOD, the lowest ratio was obtained in the D4 group.

Marsilea crenata contained phytochemicals in alkaloid, flavonoid, and terpenoid groups. Besides, *A. purpurata* has been reported to contain glycosides, saponins, terpenoids, resins, tannins, and flavonoids. Kaempferol is identified as one of the flavonoids found in *M. Crenata* and *A. purpurata* [41,44,45]. Kaempferol contains anti-inflammatory, anticancer, and antioxidant activities. As an antioxidant agent, kaempferol suppresses the production of superoxide ions and acts as a scavenges in conditions of excessive ROS. Kaempferol is reported to be a therapeutic agent in diabetes mellitus [46,47]. Previous studies showed that kaempferol can increase SOD activity by increasing SOD1 and SOD2 gene expression [48]. Therefore, this study's results align with previous research.

CONCLUSION

This study demonstrated that ethanol extracts of *M. crenata* leaves and *A. purpurata* rhizomes significantly reduced the percentage of testicular MDA in hyperglycemia-induced mice. In addition, the flavonoid content, especially kaempferol, in both herbs enhanced the activity of the SOD antioxidant enzyme. Thus, *M. crenata* and *A. purpurata* are candidates for antioxidant therapy to prevent male infertility in hyperglycemia. Further research related to in silico antioxidant activity mechanisms is needed to strengthen and confirm the results of this study.

ACKNOWLEDGEMENT

This study was financially supported by University of Brawijaya, Malang, Indonesia, with grant number ID: 3084.9/UN10.F09/PN/2022.

REFERENCES

[1] Foster, R.A. 2017. Chapter 19 - male reproductive system1. In: Zachary, J.F. (Ed). Pathologic basis of veterinary disease, 6th Ed. Mosby. United States. 1194-1222.

[2] Illacqua, A., D. Francomano, A. Aversa. 2018. The physiology of the testes. In: Belfiore, A., D. LeRoith, (Eds). Principles of endocrinology and hormone action. Springer. New York. 455-491.

[3] Guerriero, G., S. Trocchia, F.K. Abdel-Gawad, G. Ciarcia. 2014. Roles of Reactive Oxygen Species in the spermatogenesis regulation. *Front Endocrinol (Lausanne).* 5. 56.

[4] Dutta, S., R. Henkel, P. Sengupta, A. Agarwal. 2020. Physiological role of ROS in sperm function. In: Parekattil, S.J., S.C. Esteves, A. Agarwal (Eds). Male infertility. Springer Cham. Switzerland. 337-345.

[5] Tang, Y., J. Long, J. Liu. 2014. Hyperglycemia-associated oxidative stress induces autophagy: involvement of the ROS-ERK/JNK-p53 pathway. In: Hayat, M.A. (Eds). Autophagy: cancer, other pathologies, inflammation, immunity, infection, and aging. Academic Press. New York. 105-115.

[6] Agbaje, I. M., D.A. Rogers, C.M. McVicar, N. McClure, A.B. Atkinson, C. Mallidis, S.E.M. Lewis. 2007. Insulin dependant diabetes mellitus: implications for male reproductive function. *Hum. Reprod*. 22(7). 1871-1877.

[7] Alves, M.G., A.D. Martins, L. Rato, P.I. Moreira, S. Socorro, P.F. Oliveira. 2013. Molecular mechanisms beyond glucose transport in diabetes-related male infertility. *Biochem. Biophys. Acta*. 1832(5). 626-635.

[8] Temidayo, O., S.S.D. Plessis. 2018. Diabetes mellitus and male infertility. *Asian Pac. J. Reprod.* 7(1). 6-14.

[9] Mahjoub, S., J.M. Roudsari. 2012. Role of oxidative stress in pathogenesis of metabolic syndrome. *Caspian J. Intern. Med*. 3(1). 386-396.

[10] Brand, M.D. 2010. The sites and topology of mitochondrial superoxide production. *Exp. Gerontol.* 45(7-8). 466-472.

[11] AliReza, A., V. Esmaeili, A. Shahverdi, L. Rashidi. 2014. Dietary fish oil can change sperm parameters and fatty acid profiles of ram sperm during oil consumption period and after removal of oil source. *Cell J*. 16(3). 289-298.

[12] Sarıözkan, S., G. Türk, A. Eken, L.Ç. Bayram, A. Baldemir, G. Doğan. 2017. Gilaburu (*Viburnum opulus* L.) fruit extract alleviates testes and sperm damages induced by taxane-based chemotherapeutics. *Biomed. Pharmacother*. 95. 1284-1294.

[13] Li, W.H., X.X. Weng, L.F. Yuan. F. Li, X.P. Yue, F.D. Li. 2021. Effect of feeding linseed diet on testes development, antioxidant capacity, and epididymal cauda sperm concentration in Chinese Hu lamb. *Theriogenology*. 159. 69-76.

ISSN. 2087-2852
E-ISSN. 2338-1655

[14] Singh, Z., I.P. Karthigesu, P. Singh, R. Kaur. 2014. Use of malondialdehyde as a biomarker for assessing oxidative stress in different disease pathologies: a review. *Iranian J. Publ. Health*. 4(3). 7-16.

[15] Yin, H., L. Xu, N.A. Porter. 2011. Free radical lipid peroxidation: mechanisms and analysis*. Chem. Rev*. 111(10). 5944-5972.

[16] Ayala, A., M.F. Muñoz, S. Argüelles. 2014. Lipid peroxidation: production, metabolism, and signaling mechanisms of malondialdehyde and 4-Hydroxy-2-nonenal. *Oxid. Med. Cell. Longev*. 360438.

[17] Wang, Y., R. Branicky, A. Noë, S. Hekimi. 2018. Superoxide dismutases: Dual roles in controlling ROS damage and regulating ROS signaling. *J Cell. Biol*. 217(6). 1915-1928.

[18] Hou, Y., M. Lin. X. Qiu, M. He, Y. Zhang, F. Guo. 2021. Effect of Type-2 diabetes mellitus in retinopathy patients on MDA, SOD activity and its correlation with HbA1c. *Braz. Arch. Biol Technol*. 64(e21200075). 1-8.

[19] Kumar, P., P. Singh. 2018. Delayed response of epididymal sperm characteristics and testicular oxidative stress following EGME exposure: Ameliorating potential of Withania somnifera root extract. *J. Appl. Pharm. Sci*. 8(1). 122-128.

[20] Lall, N. 2020. Aquatic plants: Pharmaceutical and cosmetic applications. CRC Press. UK.

[21] Jacoeb, A.M., Nurjanah, M. Arifin, W. Sulistiono, S.S. Kristiono. 2010. Deskripsi histologi dan perubahan komposisi kimia daun dan tangkai semanggi (*Marsilea crenata* Presl., marsileaceace) akibat perebusan. *Jurnal Pengolahan Hasil Perikanan Indonesia*. 13(2). 81-95.

[22] Gopalakrishnan, K., R. Udayakumar. 2017. Phytochemical content of leaf and stem of *Marsilea quadrifolia* (L.). *J Plant Sci. Phytopathol*. 1. 26-37.

[23] Cheah, Y., W. Yang. 2011. Functions of essential nutrition for high quality spermatogenesis. *Adv. Biosci. Biotechnol*. 2(4). 182-197.

[24] Rajendiran, V., V. Natarajan, S.N. Devaraj. 2018. Anti-inflammatory activity of Alpinia officinarum hance on rat colon inflammation and tissue damage in DSS induced acute and chronic colitis models. *Food Sci. Hum. Wellness*. 7(4). 273-281.

[25] Sari, F.K., R.S. Samoedra, S.K. Pratama, S. Rahayu, A. Soewondo, M.H. Natsir, M. Rifa'i. 2023. Antioxidant activity of unripe sapodilla fruit extract (*Manilkara zapota* L.) through Nrf2 and SOD expression in type 1 diabetic mice. *J. Trop. Life sci.* 13(1). 123-130.

[26] Kirpichnikov, D., S.I. McFarlane, J.R. Sowers. 2002. Metformin: an update. *Ann. Intern. Med*. 137(1). 25-33.

[27] American Diabetes Association. 2021. 2. Classification and diagnosis of diabetes: Standards of Medical Care in Diabetes. *Diabetes Care*. 44(1) 15-33.

[28] Goud, B.J., V. Dwarakanath, B.K. Chikka swamy. 2015. Streptozotocin – A diabetogenic agent in animal models. *Int. J. Pharm. Pharmaceut. Res*. 3(1). 253-269.

[29] Goyal, S.N., N.M. Reddy, K.R. Patil, K.T. Nakhate, S. Ojha, C.R. Patil, Y.O. Agrawal. 2016. Challenges and issues with streptozotocin-induced diabetes e A clinically relevant animal model to understand the diabetes pathogenesis and evaluate therapeutics. *Chemico-Biological Interactions*. 244: 49-63.

[30] Bajaj, S., A. Khan. 2012. Antioxidant and diabetes. *Indian J. Endrocrinol. Metab*. 16(2). 267-271.

[31] Tian, Y., W. Song, D. Xu, X. Chen, X. Li, Y. Zhao. 2020. Autophagy induced by ros aggravates testes oxidative damage in diabetes via breaking the feedforward loop linking p62 and Nrf2. *Oxid. Med. Cell Longev*. 7156579. 1-9.

[32] Umarudin, S. Widyarti, Warsito, S. Rahayu. 2022. Effect of *Lissachatina fulica* chitosan on the antioxidant and lipid profile of hypercholesterolemic male Wistar rats. *J. Pharm. Pharmacogn. Res*. 10(6). 995-1005.

[33] Bardaweel, S.K., M. Gul, M. Alzweiri, A. Ishaqat, H.A. ALSalamat, R.M. Bashatwah. 2018. Reactive Oxygen Species: the dual role in physiological and pathological conditions of the human body. *Eurasian J. Med*. 50(3). 193-201.

[34] Agarwal, A., G. Virk, C. Ong, S.S. du Plesss. 2014. Effect of oxidative stress on male reproduction. *World J. Mens Health*. 33(1). 1-17.

[35] Gharagozloo, P., R.J. Aitken. 2011. The role of sperm oxidative stress in male infertility and the significance of oral antioxidant therapy. *Hum. Reprod*. 26(7). 1628-1640.

[36] Petricca, S., G. Celenza, C. Luzi, B. Cinque, A.R. Lizzi, N. Franceschini, C. Festuccia, R. Iorio. 2022. Synergistic activity of

ISSN. 2087-2852
E-ISSN. 2338-1655

ketoconazole and miconazole with prochloraz in inducing oxidative stress, GSH depletion, mitochondrial dysfunction, and apoptosis in mouse sertoli TM4 Cells. *Int. J. Mol. Sci.* 23(10). 5429.

[37] Bansal, A.K., G.S. Bilaspuri. 2011. Impacts of oxidative stress and antioxidants on semen functions. *Vet. Med. Int*. 686137. 1-7.

[38] Rahayu, S., R. Annisa, I. Anzila, Y.I. Christina, A. Soewondo, A.P.W. Marhendra, M.S. Djati. 2021. *Marsilea crenata* ethanol extract prevents monosodium glutamate adverse effects on the serum level of reproductive hormones, sperm quality, and testes histology in male rats. *Vet. World*. 14(6). 1529-1536.

[39] Astuti, S., D. Muchtadi, M. Astawan, B. Purwantara, T. Wresdiyati. 2009. Pengaruh pemberian tepung kedelai kaya isoflavon terhadap kadar malonaldehid (MDA), aktivitas superoksida dismutase (SOD) testis dan profil Cu,Zn-SOD tubuli seminiferi testis tikus jantan. *Jurnal Teknologi dan Industri Pangan*. 20(2). 129-134.

[40] Titisari, N., A. Fauzi, A. Adyana, P. Trisunuwati. 2016. The effects of water clover (*Marsilea crenata*) extract against estrogen, progesterone and uterine histology on rat (*Rattus Norvegicus*). *Int. J. PharmTech Res*. 9(6). 165-171.

[41] Jovitta, C.J., S. Aswathi, S. Suja. 2012. In-vitro antioxidant and phytochemical screening of ethanolic extract of *Alpinia purpurata. Int. J. Pharm. Sci. Res.* 3(7). 2071-2074.

[42] Sato, S., S. Kataoka, A. Kimura, Y. Mukai. 2016. Azuki bean (*Vigna angularis*) extract reduces oxidative stress and stimulates autophagy in the kidneys of streptozotocin-induced early diabetic rats. *Can. J. Physiol. Pharmacol*. 94(12). 1298-1303.

[43] Saleh, R.A., A. Agarwal. 2002. Oxidative stress and male infertility: from research bench to clinical practice. *J. Androl*. 23. 737-752.

[44] Ma'arif, B., A.A. Elpasha, A. Suryadinata, T.J.D. Dewi, N. Maulina, M. Agil. 2023. Standardization of semanggi (*Marsilea crenata* C. Presl.) leaves from Benowo District, Surabaya for standardized herbal raw material. *FITOFARMAKA: Jurnal Ilmiah Farmasi.* 13(1). 20-30.

[45] Chan, E.W.C., S.K. Wong. 2015. Phytochemistry and pharmacology of ornamental gingers, *Hedychium coronarium* and *Alpinia purpurata*: a review. *J. Integr. Med*. 13(6). 368-379.

[46] Wang, L., Y.C. Tu, T.W. Lian, J.T. Hung, J.H. yen, M.J. Wu. 2006. Distinctive antioxidant and antiinflammatory effects of flavonols. *J. Agric. Food Chem*. 54(26). 9798-9804.

[47] Imran, M., A. rauf, Z.A. Shah, F. Saeed, A. Imran, M.U. Arshad, B. Ahmad, S. Bawazeer, M. Atif, D.G. Peters, M.S. Mubarak. 2018. Chemo-preventive and therapeutic effect of the dietary flavonoid kaempferol: A comprehensive review. *Phytother. Res*. 33(2). 263-275.

[48] Kluska, M., M. Juszczak, J. Zuchowski, A. Stochmal, K, Wozniak. 2022. Effect of kaempferol and its glycoside derivatives on antioxidant status of HL-60 cells treated with etoposide. *Molecules*. 27(333). 1-14.

ISSN. 2087-2852
E-ISSN. 2338-1655

Effect of Stirring Speed and Solid to Solvent Ratio on Fucoidan Yield from *Sargassum sp*.

Naili Uswatun Hasah[1], Dewi Purnama Wati[2], Sugiono Sugiono[3*],

[1]Department of Pharmacy, Faculty of Health, Universitas Islam Madura, Pamekasan, Indonesia
[2]Program of Fisheries Agrobusiness, Faculty of Agriculture, Universitas Islam Madura, Pamekasan, Indonesia
[3]Department of Fisheries Agrobusiness, Faculty of Agriculture, Universitas Islam Madura, Pamekasan, Indonesia

Abstract

Brown alga *Sargassum* sp. has bioactive alginate and fucoidan, which have the potential for raw materials in the biorefinery industry with core processing of fucoidan and alginate extraction. Fucoidan is a polysaccharide found in the cell wall matrix of brown alga *Sargassum* sp. and functions as an anti-cancer, immunomodulatory, and anti-inflammatory. This research aims to determine the effect of stirring speed and solid-to-solvent ratio on fucoidan yield. A 2^K factorial experimental design was used to determine the effect of process conditions, stirring speed, and solid-to-solvent ratio on fucoidan yield. Analysis of yield response data and model accuracy was carried out by regression analysis using the Design Expert program. The results showed that the stirring speed and solid-to-solvent ratio affected the yield of fucoidan. The highest fucoidan yield of 3.77% occurred at a stirring speed of 750 rpm and a solid-to-solvent ratio of 1:20 ($g.mL^{-1}$). The first-order experimental model is quadratic. The model test shows that the curvature is significant at the confidence level $\alpha = 0.05$.

Keywords: Fucoidan, *Sargassum* sp, stirring speed, solid to solvent ratio.

INTRODUCTION

Brown algae have several important polysaccharide components, fucoidan, alginate, and cellulose, with different characteristics [1]. Fucoidan is a polysaccharide found in the cell wall matrix of brown algae. Its structure is composed of fucose, sulfate, and, in small amounts, xylose, galactose, mannose, and glucose [2-4]. Fucoidan functions as an anti-cancer, immunomodulatory, and anti-inflammatory compound [5-7]. Fucoidan is an expensive imported product. Indonesia has an enormous potential for brown algae resources. However, there is no domestic fucoidan industry. This is because currently developed fucoidan extraction methods still need to be improved.

Fucoidan extraction methodology generally involves extraction with hot water, acid solution, alkali solution, and adding $CaCl_2$ to precipitate alginate [1,5]. A previous study [6] extracted *Sargassum horneri* fucoidan at a temperature of 60°C with 0.1 M HCl for 4 hours, two extraction stages, and precipitation with 4 volumes of 96% ethanol. Meanwhile, Li et al. [8] performed *Hizikia fusiforme* fucoidan extraction in 3 stages at 70°C for 6 hours, precipitation with $CaCl_2$ and ethanol. Ale *et al.* [3] performed fucoidan extraction from *Sargassum henslowianum* at 90°C for 5 hours. The conventional fucoidan extraction method using water batch heating has the advantage of not requiring high technology and being accessible to industrial applications [9,10]. Stirring speed and the solid-to-solvent ratio in fucoidan extraction influence the yield of fucoidan.

The *Sargassum* species is the most abundant brown algae on the Poteran Island of Madura. With minimal use of brown algae and the low price, research reports on *Sargassum* fucoidan extraction could be more extensive, especially on the stirring speed and the solid-to-solvent ratio. Therefore, it is essential to assess the effect of stirring speed and solid-to-solvent ratio on the yield of fucoidan from *Sargassum* sp.

MATERIAL AND METHOD

Materials

The raw material used in this research is brown alga *Sargassum* sp origin, Sumenep district, Madura. Chemicals such as chloroform, methanol, distilled water, hydrochloric acid (HCl) 37%, and ethanol 96% have a pro-analytical purity degree (p.a) obtained from local markets.

Research Design

The experimental design used in this research was a two-level factorial design (2^k) with five center points for a first-order experiment. The two variables studied in this research are stirring speed and solid-to-solvent ratio coded as -1 and +1. The center point of the research was coded 0 with five repetitions [11]. The experimental

*Correspondence address:
Sugiono Sugiono
Email : sugiono@uim.ac.id
Address : Department of Agrobusiness Fisheries, Faculty of Agriculture, Universitas Islam Madura Pamekasan 6931, Indonesia

design is shown in Table 1. The center point is a stirring speed of 750 rpm, and a solid-to-solvent ratio of 1:20 (g.mL^{-1}) results from a previous study.

Table 1. The factorial design 2^2 and fucoidan yield

No	Variable actual		Variable code		Fucoidan yield (%)
	Speed (rpm)	Alga/water ratio (g.mL^{-1})	x_1	x_2	
1	500	1/15	-1	-1	2.18
2	500	1/25	-1	1	2.47
3	1000	1/15	1	-1	2.86
4	1000	1/25	1	1	3.19
5	750	1/20	0	0	3.06
6	750	1/20	0	0	3.47
7	750	1/20	0	0	3.77
8	750	1/20	0	0	3.16
9	750	1/20	0	0	3.42

Analysis of the yield data and the accuracy of the center point carried out regression analysis and the accuracy of the model using equations:

$$Y = \beta_0 + \beta_1 X_1 + \beta_2 X_2 + \beta_1 X_2 \quad \text{..... (1)}$$

Description:
Y = the response variable
β_0 = the intercept coefficient
βi, βii, βij = linear regression coefficients respectively.
X_{12} = the code for two independent variables, namely stirring speed and solvent ratio

Sample Preparation

Samples of brown algae, The *Sargassum* sp., used in this research were taken from the coastal waters of Poteran Island at a depth of 10 m at the lowest tide at 5 points. The length of the *Sargassum* sp. was 40–50 cm. Fresh *Sargassum* sp. were washed with tap water to remove dirt, sand, and mud. The cleaned *Sargassum* sp. was put in a cool box, brought to the laboratory, dried in the sun, and then dried in a 60°C oven. Dried sample of *Sargassum* sp. was ground by milling using a 100-watt OBH Nordia mill, then sieved with a 500 µm sieve and pretreated with MeOH-CHCl3-H2O (4:2:1) overnight (12 hours) at room temperature to remove color, phenol, and fat components. It was then dried in a 60°C oven and stored in the refrigerator at a temperature of 4°C until further analysis [3].

Fucoidan Extraction

A number of grams of *Sargassum* sp. in a solution of 0.03 M HCl was extracted by heating to a temperature of 80°C and for 4 hours with a stirring speed of 500-1000 rpm and a solid to solvent ratio of 1:15 to 1:25 (g.mL^{-1}). The filtrate was filtered using a 150-mesh filter cloth to obtain supernatant 1, the precipitate was washed with distilled water at a ratio of 1:5 (w/v) and filtered to obtain supernatant 2, and supernatant 1 and supernatant 2 were combined (extract A). Filtrate A was added with 1 M $CaCl_2$ (w/v) and left overnight at 4°C to precipitate the alginate. Then, the alginate precipitate was separated by filtering. The supernatant was added to 3 volumes of 96% ethanol and kept for 8 hours at 4°C to precipitate the fucoidan. The precipitated fucoidan was centrifuged (speed 5000 rpm, 15 minutes), and the pellet (crude fucoidan extract) was collected and transferred to a petri dish. The pellets obtained were dried in an oven overnight at 50°C [4].

Data Analysis

The data of fucoidan yield were analyzed for regression. The accuracy polynomial model used Design Expert version 7.

RESULT AND DISCUSSION

Fucoidan yield

Research on the effect of stirring speed and solid-to-solvent ratio on the fucoidan yield response of *Sargassum* sp. In the first-order experiment, the extraction process was carried out at a stirring speed of 500–1000 rpm and a solid-to-solvent ratio of 1:15–1:25 g.mL^{-1}. The results of the first-order experimental research showed that the fucoidan yield response ranged from 2.18% to 3.77%. The effect of stirring speed and solid-to-solvent ratio on the yield of fucoidan is presented in Figure 1.

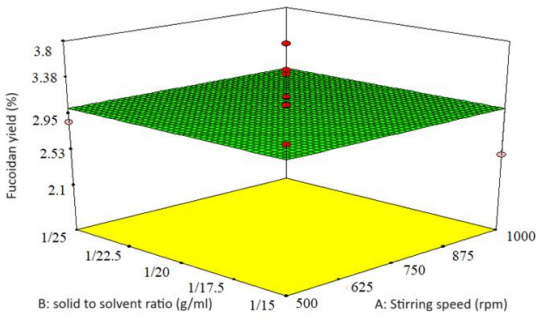

Figure 1. Effect of stirring speed and solid to solvent ratio on the yield of fucoidan from *Sargassum* sp.

The results showed that the yield of fucoidan increased at a stirring speed of 500–750 rpm and a solid-to-solvent ratio of 1:15–1:25 g.mL^{-1}. The results of this study are in accordance with the statement of Lorbeer *et al.* [12] that the more solvent used, the more fucoidan will be extracted. Fucoidan yield of *Sargassum* sp. at a stirring speed of 500 rpm and a solid-to-solvent ratio of 1:15 g.mL^{-1} of 2.18%; the highest fucoidan yield of 3.58 ± 0.35% occurred at a

ISSN. 2087-2852
E-ISSN. 2338-1655

stirring speed of 750 rpm and a solid to solvent ratio of 1:20 $g.mL^{-1}$.

Several phenomena can explain this. First, the increased stirring speed leads to increased frictional forces, effective collisions between algae particles, and collisions between algae particles and acid solvents. The cell walls of algae are porous and soft. Fucoidan is easily soluble in acid solvents [13,14]. In the results of polysaccharide extraction from the brown algae *Hyriopsis cumingii*, it was found that the polysaccharide yield increased with increasing stirring speed. Second, increasing the solid-to-solvent ratio from 1:15 to 1:20 $g.mL^{-1}$ causes the difference in concentration between the solvent and the fucoidan compound in algae to be greater; the solvent diffuses into the algae cell wall, and the fucoidan compound dissolves and is extracted so that the yield increases [12]. Third, the increasing volume of acid solvent causes the surface area of contact between the acid solvent and the fucoidan compound to be larger so that the fucoidan is easily dissolved and the yield is greater.

Meanwhile, at an extraction stirring speed of 1000 rpm and a solid-to-solvent ratio of 1:25 $g.mL^{-1}$, the yield of fucoidan decreased by 3.19%. The stirring speed of 1000 rpm causes the fucoidan polymer to be degraded, decreasing its solubility in acidic solutions. When centrifuged, the fucoidan precipitates, so the yield is low. Rodriquez-Jasso *et al.* [15] reported that the yield of fucoidan from *Fucus vesiculosus* tended to increase with increasing power and solvent ratios and then decreased after reaching the optimal point. There were decreases in this fucoidan yield because the degraded fucoidan polymer and its solubility in acid solution were reduced. Noviyanti *et al.* [16] explained that the increased amount of solvent used will cause the yield to decrease because the equilibrium state between solid and liquid has been reached. The levels of compounds in the solvent became lower, making it difficult to separate and precipitate, so the yield was low.

Model Accuracy

A two-level factorial design was used to evaluate the effect of extraction parameters, i.e., stirring speed and solid-to-solvent ratio, on fucoidan yield. The first-order model of the fucoidan yield response was obtained below:

$$y = 3.1756 + 0.35X_1 + 0.155X_2 \quad R^2 = 0.9587$$

Results of the analysis of various responses to fucoidan yield of *Sargassum* sp. show that the linear regression model has a calculated F value of 0.77, which is smaller than the F table value (α = 0.05), which is 5.14. This indicates that the linear regression model is not significant for the yield response at the confidence level (α = 0.05). According to Gaspersz [17], if the calculated F of the regression model is smaller than the F table of 0.05, it means that the model is not significant for the response at a confidence level of α = 5%, so the model is not appropriate for predicting the optimal response. A regression parameter test, which simultaneously obtained that the calculated F was smaller than the F table with α = 5%, means that the independent variables X_i do not represent the model [18]. The deviation parameter test from the model (curvature) has an F value of 7.51, which is greater than the F table value (α = 0.05) of 6.94, which means the curvature is significant at the 0.05 confidence level. The curvature test has a calculated F value greater than the F table of 0.05, meaning that the curvature is significant at the 0.05 confidence level [19].

Kadam *et al.* [20] explained that the accuracy and acceptable model are based on parameters, i.e., the significance of $P<0.05$, $R^2 \geq 0.8$, and lack of fit>0.1 [11]. It shows that the optimal response in the quadratic polynomial model is around a stirring speed of 750 rpm and a solid-to-solvent ratio of 1:20 $g.mL^{-1}$. It can be concluded that the center point of the research planning for the stirring speed of 750 rpm and the solid-to-solvent ratio of 1:20 $g.mL^{-1}$ is correct.

CONCLUSION

Fucoidan extraction, stirring speed, and solid-to-solvent ratio affect the yield of fucoidan. The highest fucoidan (3.77%) yield was obtained from a processing condition at 750 rpm and a solid-to-solvent ratio of 1:20 $g.mL^{-1}$. The analysis regression model obtained for that linear model was insignificant. At the same time, curvature analysis was found to be significant as a first-order quadratic model.

Acknowledgement

The author would like to thank DRPM DIKTI for funding this research through the 2023 Beginner Lecturer Research Grant contract number 041/SP2H/PT/LL7/2023.

REFERENCES

[1] Rioux, L. E., S.L. Turgeon, M. Beaulieu. 2007. Characterization of polysaccharides

ISSN. 2087-2852
E-ISSN. 2338-1655

extracted from brown seaweeds. *J. Carbohydr. Polym*. 69. 530-537.

[2] Li, B., L. Fei, X. Wei, R. Zhao. 2008. Review: Fucoidan structure and bioactivity. *Molecules.* 13(8). 1671-1695.

[3] Ale, M.T., J.D. Mikkelsen, A.S. Meyer. 2011. Designed optimization of a single-step extraction of fucose-containing sulfated polysaccharides from Sargassum sp. *J. Appl. Phycol.* 24. 715-723. DOI: 10.1007/s10811-011-9690-3.

[4] Sugiono, S.B. Widjanarko, L.A. Soehono. 2014. Extraction optimization by response surface methodology and characterization of fucoidan from brown seaweed *Sargassum polycystum*. *Int. J. ChemTech Res.* 6(1). 195–205.

[5] Cumashi, A., N.A. Ushakova, M.E. Preobrazhenskaya, A. D'Incecco, A. Piccoli, L. Totani, *et al.* 2007. A comparative study of the anti-inflammatory, anticoagulant, antiangiogenic, and antiadhesive activities of nine different fucoidans from brown seaweeds. *Glycobiology*. 17(5). 541–552.

[6] Ermakova, S., R. Sokolova, S.M. Kim, B. Um, V. Isavakov, T. Zvyaginseva. 2011. Fucoidans from brown seaweeds *Sargassum hornery*, *Eclonia cava*, *Costaria costata*: Structural characteristics and anticancer activity. *Appl. Biochem. Biotechnol*. 164(6). 841–850.

[7] Lakshmanan, A., B. Balasubramanian, V. Maluventhen, A. Malaisamy, R. Baskaran, W.C. Liu, M. Arumugam. 2022. Extraction and characterization of fucoidan derived from *Sargassum ilicifolium* and its biomedical potential with in silico molecular docking. *Appl. Sci*. 12. 13010. DOI: 10.3390/app122413010.

[8] Li. J., S. Ding, X. Ding. 2006. Optimization of the ultrasonically assisted extraction of polysaccharides from Zizyphus jujuba cv. Jinsixiaozao. *J. Food Eng.* 80(1). 176-184.

[9] Wang, J., J. Zhang, B. Zhao, X. Wang, Y. Wu, J. Yao. 2010. A comparison study on microwave-assisted extraction of *Potentilla anserina* L. polysaccharides with conventional method: Molecule weight and antioxidant activities evaluation. *Carbohydr. Polym*. 80(1). 84–93. DOI: 10.1016/j.carbpol.2009.10.07.

[10] Hernandez-Carmona G., Y. Freile-Pelegrín, E. Hernández-Garibay. 2013. Conventional and alternative technologies for the extraction of algal polysaccharides. In: Functional ingredients from algae for foods and nutraceuticals. 475–516. DOI: 10.1533/9780857098689.3.475.

[11] Montgomery D.C. 2017. Design and analysis of experiments. In Wiley, 9th Ed. Wiley, NewYork. Available at: https://lccn.loc.gov/2017002355.

[12] Lorbeer, A.J., J. Lahnstein, V. Bulone, T. Nguyen, W. Zhang. 2015. Multiple-response optimization of the acidic treatment of the brown alga *Ecklonia radiata* for the sequential extraction of fucoidan and alginate. *Bioresour. Technol.* 197. 302–309. DOI: 10.1016/j.biortech.2015.08.103.

[13] Sugiono, S., D. Ferdiansyah. 2020. Biorefinery for sequential extraction of fucoidan and alginate from brown alga Sargassum cristaefolium. *Carpathian J. Food Sci. Technol.* 12(2). 88–99.

[14] Qiao D., B. Hu, D. Gan, Y. Sun, X. Zeng. 2009. Extraction optimized by using response surface methodology, purification and preliminary characterzation of polysaccharide from *Hyriopsis cumingi*. *Carbohydr. Polym*. 76(3). 422-429.

[15] Rodriguez-Jasso, R.M., S.I. Mussatto, L. Pastrana, C.N. Aguilar, J.A. Teixeira. 2011. Microwave-assisted extraction of sulfated polysaccharides (fucoidan) from brown seaweed. *Carbohydr. Polym*. 86(3). 1137-1144. DOI: 10.1016/j.carbpol.06.006.

[16] Noviyanty, A., C.A. Salingkat, Syamsiar. 2019. The effect of solvent ratio to the quality of extracts from the red dragon fruit peel (*Hylocereus polyrhizus*). *J. Kovalen*. 5(3). 280-289.

[17] Gaspersz. 1991. Metode perancangan percobaan. Armico. Bandung.

[18] Nuryanti., D.H. Salimy. 2008. Metode permukaan respon dan aplikasinya pada optimasi eksperimen kimia. *Jurnal Risalah Lokakarya Komputasi dalam Sains dan Teknologi Nuklir*. 373-391.

[19] Montgomery, D.C. 2005. Response surface methods and designs. John Willy and Sons. Inc.

[20] Kadam, S.U., B.K. Tiwari, T.J. Smyth, C.P.O. Donnell. 2015. Ultrasonics sonochemistry optimization of ultrasound assisted extraction of bioactive components from brown seaweed *Ascophyllum nodosum* using response surface methodology. *Ultrason. Sonochem.* 23. DOI: 10.1016/j.ultsonch.2014.10.007.

ISSN. 2087-2852
E-ISSN. 2338-1655

Effect of Combination between the Extract of *Marsilea crenata* and *Alpinia purpurata* K.Schum Rhizome on Sperm Quality of Hyperglycemia Mice

Shofi Nur Aliyah[1], Sri Rahayu[2*], Agung Pramana Warih Marhendra[3]

[1]Master Program of Biology, Faculty of Mathematics and Natural Sciences, Brawijaya University, Malang, Indonesia
[2]Department of Biology, Faculty of Mathematics and Natural Sciences, Brawijaya University, Malang, Indonesia

Abstract

This study aims to analyze the effect of the combination between water clover (*Marsilea crenata*) and red galangal rhizome (*Alpinia purpurata*) on sperm quality of hyperglycemia model mice. *Mus musculus* were randomly divided into eight groups: non-hyperglycemia (P_0), hyperglycemia (P_1), metformin 0.375 mg.kg^{-1} (P_2), hyperglycemia with *M. crenata* extract dose 0.09 mg.g^{-1} (P_3), *A. purpurata* dose 0.20 mg.g^{-1} (P_4), combination of *M. crenata* (0.09 mg.g^{-1}) - *A. purpurata* (0.20 mg.g^{-1}) (P_5), combination of *M. crenata* (0.09 mg.g^{-1}) - *A. purpurata* (0.40 mg.g^{-1}) (P_6), and combination of *M. crenata* (0.18 mg.g^{-1}) - *A. purpurata* (0.20 mg.g^{-1}) (P_7). Hyperglycemia mice were induced by streptozotocin 145 mg.kg^{-1}. STZ induction and oral extract addition were carried out for 20 days. Sperm quality parameters observed in this study included motility, viability, and concentration. Sperm quality data were statistically analyzed with One-Way ANOVA followed by the Tukey HSD test using the SPSS 23 for Windows program ($p<0.05$). This research demonstrates that adding *M. crenata*, *A. purpurata*, and their combination for 20 days can significantly increase motility, viability, and sperm concentration in hyperglycemia-model mice. The combination of *M. crenata* and *A. purpurata* in the ratio of 1:1 was considered effective in improving the sperm quality of hyperglycemia model mice.

Keywords: *A. purpurata*, hyperglycemia, *M. crenata*, oxidative stress, sperm quality.

INTRODUCTION

Diabetes mellitus (DM) is a metabolic disease caused by abnormalities in insulin secretion and action, or even both [1]. Hyperglycemia is one of the characteristics of diabetes mellitus caused by decreased insulin secretion by pancreatic β cells [2]. Based on data from the International Diabetes Federation (IDF), in 2021, the global prevalence of diabetes mellitus will reach 536 million people (20-70 years old) and will increase to 783 million [3]. The data also shows that Indonesia ranks 5th with a hight number of DM sufferers reaching 19.5 million, and it is expected to continue to increase in 2045 with a prevalence of 28.6 million [4].

Diabetes mellitus could affect several organs, including the liver, pancreas, kidneys, and testicles. Previous research shows that DM also causes a decrease in genes that play a role in steroidogenesis, such as steroidogenic acute regulatory protein (StAR), cytochrome P450 enzyme (CYP11A1), and 17β-hydroxysteroid dehydrogenase (HSD). Thus, these conditions trigger impaired spermatogenesis and decreased sperm quality [5]. Hyperglycemia occurs due to increased production of Reactive Oxygen Species (ROS) and decreased antioxidant activity in the body. The imbalance between ROS and endogenous antioxidants in the body can cause oxidative stress elevation [6].

Diabetes mellitus is also widely known to cause Hypothalamus-Pituitary-Gonadal (HPG) Axis dysfunction. The dysfunction causes a decrease in the secretion of Gonadotropin Realizing Hormone (GnRH), Follicle-Stimulating Hormone (FSH), Luteinizing Hormone (LH), and Testosterone [7]. Furthermore, it also affects the damage of spermatogenic cells, stromal cells, seminiferous tubules, and various other structures that play a role in the male reproductive system [8,9]. Previous studies have shown that diabetes mellitus can reduce sperm quality, causing decreased sperm count, motility, viability, maturity, and chromatin quality in Wistar rats [10].

Several antidiabetic agents are available in the market to help reduce the effect of DM, including metformin. Metformin is one of the commonly consumed antidiabetic agents [11]. However, its long-term use risks the organ system in the body. Thus, there is a need for alternative antidiabetic agents with minimal side effects. Biodiversity, especially plants, is a potential source of developing these antidiabetic agents. Phytochemicals such as flavonoids, vitamin C, and vitamin A found in plants play an important role in stimulating endogenous antioxidant activity to minimize the impact of oxidative stress due to hyperglycemia [12].

*Correspondence address:
Sri Rahayu
Email : srahayu@ub.ac.id
Address : Dept. Biology, University of Brawijaya, Veteran Malang, 65145.

ISSN. 2087-2852
E-ISSN. 2338-1655

It is known that the water clover plant (*Marsilea crenata*) has anti-cholesterol and anti-inflammatory activity. Bioactive compounds such as flavonoids, vitamin A, vitamin C, and zinc can act as antioxidants [13]. Previous research showed that the extract of *M.* crenata increased LH and testosterone hormones in rats which were given MSG. Furthermore, *M. crenata* can also reduce MDA levels and increase spermatogonia cells, spermatocytes, spermatids, and Leydig cells [7].

One of the native Indonesian plants that is often used as medicine is the Red galangal (*Alpinia purpurata*). The rhizome part *of A. purpurata* is widely used as a prevention of antioxidants [14]. Active compounds found in *A. purpurata* include flavonoids, saponins, tannins, terpenoids, glycosides, carbohydrates, and proteins [15]. Previous research stated that *A. purpurata* rhizomes have a DPPH value of (IC_{50} 50 $\mu g.mL^{-1}$), meaning that the antioxidant activity in *A. purpurata* rhizomes is classified as very strong [16].

Apart from that, *M. crenata* and *A. purpurata* are plants with antioxidant activity. The combination of *M. crenata* and *A. purpurata* is expected to increase the effectiveness of the active substances contained in the two plants, especially in improving sperm quality due to hyperglycemia. Thus, this study aims to analyze the effect of the combination of *M. crenata* and *A. purpurata* on the sperm quality of hyperglycemia model mice.

MATERIAL AND METHOD

Study Design

This research was conducted in January – March 2023 at Laboratory of Biology, Animal Physiological Structure and Development, Department of Biology, University of Brawijaya, Malang, East Java, Indonesia. This research used male mice (*Mus musculus*) BALB/C (n=24, eight weeks old), for which the procedure was reviewed and approved by the Ethics Commission (Approval No. 157-KEP-UB).

Mice were randomly divided into eight groups. The treatment details are in Table 1. The Hyperglycemia mice model was induced by a streptozotocin (STZ) dose of 145 $mg.kg^{-1}$ [17]. The STZ was dissolved with buffer citrate with pH 4.5. The mice were confirmed to have hyperglycemia, with the glucose concentration > 200 $mg.dL^{-1}$. The P_1 group has hyperglycemia without extract treatment, and other hyperglycemia rats were orally added daily by extract for 20 days. Besides, a group of hyperglycemia mice was treated with metformin as a positive control (P_2).

Table 1. Groups of Mice

Code	Dose (mg. kg^{-1})		Dose ($mg.g^{-1}$)		Ratio*
	STZ	Met-formin	*M. crenata*	*A. purpurata*	
P_0	0	-	-	-	-
P_1	145	-	-	-	-
P_2	145	0.375	-	-	-
P_3	145	-	0.09	-	-
P_4	145	-	-	0.20	-
P_5	145	-	0.09	0.20	1:1
P_6	145	-	0.09	0.40	1:2
P_7	145	-	0.18	0.20	2:1

Notes: *ratio of the extract combination of *M. crenata* and *A. purpurata.*

Preparation for the Combination of *M. crenata* and *A. purpurata* Extract

The *M. crenata* was obtained from local farmers in Sememi Street, Jaya Baru VII, Benowo, Surabaya. Meanwhile, the *A. purpurata* was obtained from Materia Medica, Batu, Malang, Indonesia. Each powdered sample of as much as 1 kg was extracted with 5 L of 70% ethanol solvent at room temperature for 24 hours. Samples were filtered and evaporated using a rotary evaporator after 24 hours of maceration. The *M. crenata* and *A. purpurata* ethanolic extract were obtained and stored at 4°C for further analysis [7].

Sperm Motility

Semen fluid was taken as much as 10 µL and placed on a glass object. Sperm motility analysis is carried out by observing spermatozoa that move progressively using a light microscope with 100X magnification in 5 fields of view [7]. The progressivity of spermatozoa is categorized into several groups, as seen in Table 2.

Table 2. Sperm Motility Category

Score	Category	Progressive Motility (%)
1	Very poor	0-20
2	Poor	20-40
3	Good	40-60
4	Very Good	60-80
5	Excellent	80-100

Sperm Viability

A total of 10 µL of semen liquid was dripped on a glass object, and stained with 1% eosin and 5% nigrosin. The percentage of spermatozoa viability was observed with a 400X magnification light microscope and calculated using the formula below [7] :

$$Viability\ (\%) = \frac{live\ sperm\ count}{total\ count\ of\ sperm} \times 100$$

ISSN. 2087-2852
E-ISSN. 2338-1655

Sperm Concentration

A total of 10 µL of semen was diluted with 100 µL of fixative solution (physiological NaCl). The suspension was taken as much as 10 µL, inserted into the Hemocytometer chamber, and observed with a 400X magnification light microscope in triplicate. The concentration of spermatozoa was calculated using the following formula [7].

$$Sperm\ concentration = n \times k \times FP \times 10^4$$

Description:

n = counted number of spermatozoa
k = number of counted small squares (5)
FP = dilution factor (10)
10^4 = volume of hemocytometer

Statistical Analysis

All values were given as mean ± standard deviation of the mean (SD). All statistical analyses were done by the SPSS 23 program. In addition, One-Way ANOVA was used to asseses the overall differences between groups, followed by the Tukey HSD test to identify significant differences ($p<0.05$) between the groups.

RESULT AND DISCUSSION

The sperm quality data is displayed in Table 3. The sperm quality parameters observed include motility, viability, and sperm concentration.

Sperm Motility

The results of this study showed that the mice that were only induced with Streptozotocin (STZ) without treatment (P_1) resulted in a significant decrease in sperm motility compared to the control group (P_0). The percentage of sperm motility in the hyperglycemia group (P_1) was 39.22 ± 4.868% (Table 3). The data also reveal that the hyperglycemia group (P_1) has the lowest percentage of sperm motility compared to other treatment groups. This result aligns with previous research, which explains that sperm motility is significantly reduced by 18.16% in streptozotocin-induced diabetic groups [18].

Furthermore, streptozotocin (STZ) induction for 20 days can increase Reactive Oxygen Species (ROS) due to lipid peroxidation. Previous studies have shown that sperm membranes contain many polyunsaturated fatty acids (PUFA), making spermatozoa sensitive to ROS [18]. The imbalance between ROS and antioxidants can trigger mitochondrial damage due to oxidative stress. Mitochondrial damage can inhibit ATP production as a source of energy needed by spermatozoa so that sperm motility decreases [20].

The result also showed that the combination of *M. crenata* and *A. purpurata* can increase the percentage of spermatozoa motility significantly ($p<0.05$) when compared to the hyperglycemia group (P_1). The combination of *M. crenata* and *A. purpurata* in the P_5 group produced the highest sperm motility of 78.89 ± 6.509% compared to other treatment groups.

Besides that, the antioxidant content contained in *M. crenata* and *A. Purpurata* can increase sperm motility. This study also aligns with previous research, showing that combining *M. crenata* and *C. xanthorriza* extracts can significantly increase sperm motility [21]. *Marsilea crenata* contains bioactive compounds such as quercetin, vitamin A, zinc, and vitamin C, the factors that can increase motility [7]. Quercetin plays a role in preventing lipid peroxidation caused by ROS in sperm cell membranes [22]. Thus, mitochondrial function is able to produce ATP optimally. The availability of sufficient ATP can increase sperm motility [23].

Table 3. Effect of STZ, metformin, and combination of *M. crenata* and *A. purpurata* extracts on sperm quality of mice

Group	Sperm Quality ± SD		
	Sperm Motility (%)	Sperm Viability (%)	Sperm Concentration (x 10^6 cell.mL^{-1})
P_0	73.44 ± 3.844^{bc}	71.56 ± 7.683^{bc}	37.86 ± 8.385^{cd}
P_1	39.22 ± 4.868^{a}	42.22 ± 6.360^{a}	17.73 ± 6.833^{a}
P_2	65.11 ± 13.138^{b}	60.67 ± 13.883^{b}	25.49 ± 6.336^{ab}
P_3	71.44 ± 9.632^{bc}	71.44 ± 9.554^{bc}	33.56 ± 11.387^{bcd}
P_4	70.22 ± 13.507^{bc}	70.89 ± 14.650^{bc}	30.71 ± 7.843^{bc}
P_5	78.89 ± 6.509^{c}	79.44 ± 7.333^{c}	50.06 ± 5.474^{e}
P_6	75.11 ± 8.162^{bc}	74.56 ± 7.844^{bc}	43.58 ± 9.724^{de}
P_7	73.33 ± 3.391^{bc}	73.22 ± 6.534^{bc}	45.36 ± 8.758^{de}

Notes : The values with different superscript letters in the same row represent significant difference ($p<0.05$).

P_0 = non-hyperglycemia
P_1 = hyperglycemia
P_2 = metformin
P_3 = hyperglycemia mice + *M. crenata* 0.09 mg.g^{-1}
P_4 = hyperglycemia mice + *A. purpurata* 0.20 mg.g^{-1}
P_5 = hyperglycemia mice + combination (1:1)
P_6 = hyperglycemia mice + combination (1:2)
P_7 = hyperglycemia mice + combination (2:1)

ISSN. 2087-2852
E-ISSN. 2338-1655

Meanwhile, *A. purpurata* contains flavonoid compounds, which act as antioxidants. Previous studies show that *A. purpurata* has an IC50 of 38.004 µg.mL^{-1}, indicating that red galangal rhizome's antioxidant activity is very strong [16]. Flavonoids can reduce the effects of free radicals as they have an aromatic ring structure containing hydroxyl groups, so they can bind with free radicals to form more stable molecules [22]. Stabilization of these molecules results in mitochondria being able to produce ATP as an energy source for spermatozoa [19].

Sperm Viability

Sperm viability is indicated by stained sperm (Fig. 1). Streptozotocin (STZ) induction for 20 days caused a decrease in spermatozoa viability in the group (P1) with an average value of 42.22 ± 6.360% compared to the control group (P0). Furthermore, streptozotocin (STZ) induction can increase oxidative stress biomarkers such as superoxide anion (O2-), nitric oxide (NO), and malondialdehyde (MDA) in spermatozoa. [25]. Superoxide anion (O2-) is one of the ROS types associated with diabetes pathology due to its ability to damage cells and insulin resistance. The high level of ROS also impacts the mitochondrial function and induction of spermatozoa apoptosis [26].

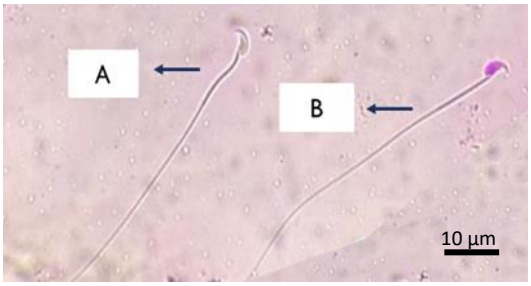

Figure 1. Live and Dead Spermatozoa Stained With Eosin Negrosin in 400X magnification, A. dead sperm and B. live sperm.

Spermatozoa membranes contain many polyunsaturated fatty acids (PUFAs), which are highly susceptible to ROS. The accumulation of ROS due to hyperglycemia leads to lipid peroxidation in spermatogonia, spermatosids, and spermatids. Thus, the integrity of the spermatozoa membrane is lost [19]. Previous studies have shown that streptozotocin (STZ) induction can reduce sperm viability in mice [27].

Besides that, the combination of *M. crenata* and *A. purpurata* extracts increased spermatozoa viability significantly ($p<0.05$). The zinc compound in *M. crenata* can increase spermatozoa viability. Zinc acts as an exogenous antioxidant that can protect the spermatozoa membrane from free radical reactivity through a scavenging mechanism so that the fluidity and integrity of the spermatozoa phospholipid membrane are maintained [28,29]. Previous research showed that adding *M.crenata* extract at a dose of 0.09 mg.g^{-1} resulted in increased spermatozoa viability [22].

Meanwhile, *A. purpurata* contains bioactive compounds such as flavonoids, which act as antioxidants. One of them is quercetin, a bioflavonoid with phenolic rings that serve as scavengers against free radicals [28]. Previous studies have shown that quercetin can increase motility, viability, and the number of spermatozoa in diabetic model rats [31].

Sperm Concentration

This research found that hyperglycemia can reduce the sperm concentration of mice by 17.89 x 106 ± 6,833 cells.mL^{-1} compared to the control group (P_0) (Table 1). This study aligns with previous studies that explain diabetic rats induced Streptozotocin (STZ) have a decreased sperm count [17].

The spermatozoa membrane contains high amounts of polyunsaturated fatty acids (PUFA). Additionally, high amounts of glycolytic products can interact with specific proteins and lipids in spermatozoa, leading to increased ROS production [32]. High accumulation of ROS can cause lipid peroxidation in spermatogonia, spermatid, and spermatozoa cells [33]. In turn, lipid peroxidation causes alteration of phospholipid conformation that leads to decreased spermatozoa membrane fluidity and increased membrane permeability [34]. The decreased spermatozoa membrane fluidity and increased membrane permeability spermatozoa lead to necrotic death. The death cell that occurs in spermatogenic cells can alter the sperm concentration to decrease [35].

Meanwhile, adding the combination of *M. crenata* and *A. purpurata* extracts for 20 days increase the sperm concentration significantly ($p<0.05$). The group P_5 produced the highest sperm concentration, 50.06 ± 5.474 x 106 cells.mL^{-1} (Table 3). Bioactive compounds contained in *M. crenata* include flavonoids, vitamin C, zinc, and other phenolic compounds [36]. These bioactive compounds act as antioxidants, which can absorb free radical ions or atoms, making them inactive and preventing damage to spermatozoa DNA and lipid membranes [37].

ISSN. 2087-2852
E-ISSN. 2338-1655

Besides that, *A. purpurata* contains antioxidant compounds, one of which is flavonoids [38]. Flavonoid compounds act as antioxidants, bind to free radicals by hydrogen donor atoms, and form more stable molecules [39]. Flavonoids from *A. purpurata* are one of the phytochemicals that can inhibit the activity of the aromatase enzyme. The aromatase enzyme plays a role in converting androgens (testosterone) into estrogen. The inhibition by flavonoids can increase the production of testosterone [40]. The increased testosterone production is correlated with the increased spermatogenesis production [4].

CONCLUSION

The addition of *M. crenata, A. pupurata*, and their combination for 20 days can significantly increase motility, viability, and sperm concentration in hyperglycemia model mice. The combination of *M. crenata* and *A. purpurata* with a 1:1 ratio was considered effective in improving the the sperm quality of hyperglycemia model mice.

REFERENCES

[1] Von Scholten, F.F. Kreiner, S.C.L. Gough, M. von Herrath. 2021. Current and future therapies for type 1 diabetes. *Diabetologia*. 64(5). 1037–1048. DOI: 10.1007/s00125-021-05398-3.

[2] Amrulloh H., N. Bella, S. Intan, W. Sri, R. Muhaimin. 2020. The Study of combination ethanol extract of *Averrhoa bilimbi* L. and *Momordica charantia* L. on CD4+CD25+TGF-β+ spleenocytes of hyperglycemia mice. *J. Exp. Life Sci.* 10(3). 171–176. DOI: 10.21776/ub.jels.2020.010.03.05.

[3] Magliano, D., E.J. Boyko. 2021. *IDF diabetes atlas*, 10th ed. International Diabetes Federation. Brussels.

[4] Sun, H, P. Saeedi, S. Karuranga, M. Pinkepank, K. Ogurtsova, B.B. Duncan, *et al.* 2021. IDF diabetes atlas: Global, regional and country-level diabetes prevalence estimates for 2021 and projections for 2045. *Diabetes Res. Clin. Pract.* 183. 109-119. DOI: 10.1016/j.diabres.2021.109-119.

[5] Mao. C.F, S. Sudirman, C.C. Lee, D. Tsou, Z.L. Kong. 2021. *Echinacea purpurea* Ethanol extract improves male reproductive dysfunction with streptozotocin–nicotinamide-induced diabetic rats. *Front. Vet. Sci.* 8. 651-286. DOI: 10.3389/fvets. 2021.651286.

[6] Jannah, R, N.L.E. Setiasih, P. Suastika. 2018. Histopathological of diabetes mellitus white rat testicle after given moringa leaf extract. *Bul. Vet. Udayana*. 176. DOI: 10.24843/ bulvet.2018.v10.i02.p11.

[7] Rahayu, S., R. Annisa, I. Anzila, Y.I. Christina, A. Soewondo, A.P.W. Marhendra, M.S. Djati. 2021. *Marsilea crenata* ethanol extract prevents monosodium glutamate adverse effects on the serum levels of reproductive hormones, sperm quality, and testis histology in male rats. *Vet. World*. 14. 1529–1536. DOI: 10.14202/vetworld.2021. 1529-1536.

[8] Oduwole. O.O., H. Peltoketo, I.T. Huhtaniemi. 2018. Role of follicle-stimulating hormone in spermatogenesis. *Front. Endocrinol.* 9. 763. DOI: 10.3389/ fendo.2018.00763.

[9] Andlib, N., M. Sajad, R. Kumar, S.C. Thakur. 2023. Abnormalities in sex hormones and sexual dysfunction in males with diabetes mellitus: A mechanistic insight. *Acta Histochem.* 125(1). 151-974. DOI: 10.1016/ j.acthis.2022.151974.

[10] Barsiah, S., M. Behnam-Rassouli, F. Shahabipour, S. Rostami, M.A. Sabbaghi, Z. Momeni, A. Tavassoli, A. Sahebkar. 2019. Evaluation of testis hormonal and histopathological alterations in type I and type II diabetic rats. *J. Cell. Biochem.* 120(10). 16775–16785. DOI: 10.1002/jcb. 28936.

[11] Shokri, A, B. Pourheydar, G.H. Farjah, M. Krimipour, M. Pourheydar. 2023. Effects of glibenclamide and troxerutin on the sperm parameters and histopathological changes of testis in streptozotocin-induced diabetic male rats: An experimental study. *Int. J. Reprod. Biomed. IJRM*. 21(2). 123-138. DOI: 10.18502/ijrm.v21i2.12803.

[12] A-Ishaq, R.K, M. Abotaleb, P. Kubatka, K. Kajo., D. Büsselberg, 2019. Flavonoids and their anti-diabetic effects: cellular mechanisms and effects to improve blood sugar levels. *Biomolecules*. 9(9). 430. DOI: 10.3390/biom9090430.

[13] Nurjanah., A. Azka, A. Abdullah. 2012. Aktivitas antioksidan dan komponen bioaktif semanggi air (*Marsilea crenata*). *Asian J. Innov. Entrepreneur.* 1(3). 152-158.

[14] Khairullah, A.R, T.I. Solikhah, A.N.M. Ansori, A. Fadholly, S. C. Ramandinianto, R. Ansharieta, *et al.* 2011. A review of an

ISSN. 2087-2852
E-ISSN. 2338-1655

important medicinal plant: *Alpina galanga* (L.) Willd. *Sys. Rev. Pharm*. 11(10). 387-395.

[15] Jovitta. J.C., S. Aswathi, S. Suja. 2012. In-vitro antioxidant and phytochemical screening of ethanolic extract of *Alpinia purpurata. Int. J. Pharm. Sci. Res.* 3(7). 2071-2074.

[16] Putri, F.L., S. Rahayu, A.P.W. Marhendra. The effect of *Alpinia purpurata* K. Schum rhizome extract supplementation in tris-egg yolk extender on the quality of cryopreserved Bali Bull sperm. *J. Exp. Life Sci.*, 13(2). 84–93. DOI: 10.21776/ub.jels. 2023.013.02.03.

[17] Furman, B.L. 2021 Streptozotocin-induced diabetic models in mice and rats. *Curr. Protoc. Pharmacol.* 70(1). 78. DOI: 10.1002/ 0471141755.ph0547s70.

[18] Akondi, R.B., P. Kumar, A. Annapurna., M. Pujari. 2011. Protective effect of rutin and naringin on sperm quality in streptozotocin (STZ) induced type 1 diabetic rats. *Iran. J. Pharm. Res.* 10(3). 585-596.

[19] Agarwal, A., G. Virk, C. Ong, S.S. du Plessis. 2014. Effect of oxidative stress on male reproduction. *World J. Mens. Health*. 32(1). 1-17. DOI: 10.5534/wjmh.2014.32.1.1.

[20] Turner, T.T., J.J. Lysiak. 2008. Oxidative stress: A common factor in testicular dysfunction. *J. Androl*. 29(5). 488–498.

[21] Firstiantono, A., S. Rahayu, A.P.W. Marhendra, A. Soewondo. 2022. Potential of combination *Marsilea crenata* and *Curcuma xanthorriza* to improve sperm quality of male mice exposed by monosodium glutamate. *Biotropika J. Trop. Biol.* 10(1). 33–39. DOI: 10.21776/ub. biotropika.2022.010.01.04.

[22] Bouayed, J., T. Bohn. 2010. Exogenous antioxidants—double-edged swords in cellular redox state: health beneficial effects at physiologic doses versus deleterious effects at high doses. *Oxid. Med. Cell. Longev.* 3(4). 228–237. DOI: 10.4161/oxim.3.4.12858.

[23] Tomar, R.A., K. Jain, N.K. Mohanty, B. Bastia, S.N. Kumar. 2008. Role of oxidative stress and antioxidants in male infertility. *Toxicol. Lett.* 180. 32-46. DOI: 10.1016/ j.toxlet.2008.06.240.

[24] Purdy, P.H., S.A. Ericsson, R.E. Dodson, K.L. Sternes, D.L. Garner. 2004. Effects of the flavonoids, silibinin and catechin, on the motility of extended cooled caprine sperm. *Small Rumin. Res.* 55(1–3). 239–243. DOI: 10.1016/j.smallrumres.2004.02.005.

[25] Kaneto, H., N. Katakami, M. Matsuhisa., T. Matsuoka. 2010. Role of reactive oxygen species in the progression of type 2 diabetes and atherosclerosis. *Mediators Inflamm.* 1–11. DOI: 10.1155/2010/453892.

[26] Kandemir, Y.B., V. Tosum, U. Guntekin. 2019. Melatonin protects against streptozotocin-induceddiabetic cardiomyo-pathy through themammalian targetof rapamycin (mTOR) signaling pathway. *Adv. Clin. Exp. Med.* 28(9). 1171–1177. DOI: 10.17219/acem/103799.

[27] Baszary, C.D.U. B., P. Kakisina, L. Linda. 2021. Peningkatan motilitas dan viabilitas spermatozoa mencit (*Mus muscullus*) diabetes mellitus tipe-ii setelah di beri diet tepung sagu (*Metroxylon sagu* Rottb.). *Biofaal J.* 2(1). 42–46. DOI: 10.30598/ biofaal.v2i1pp42-46.

[28] Nimse, S.B., D. Pal. 2015. Free radicals, natural antioxidants, and their reaction mechanisms. *RSC Adv.* 35.27986–28006. DOI: 10.1039/C4RA13315C.

[29] Hamza, R.Z., N.S. El-Shenawy, H.A.A. Ismail. 2015. Protective effects of blackberry and quercetin on sodium fluoride-induced oxidative stress and histological changes in the hepatic, renal, testis and brain tissue of male rat. *J. Basic Clin. Physiol. Pharmacol.* 26(3). 237-251. DOI: 10.1515/jbcpp-2014-0065.

[30] Yelumalai, S., N. Giribabu, K. Karim, S.Z. Omar, N.B. Salleh. 2019. In vivo administration of quercetin ameliorates sperm oxidative stress, inflammation, preserves sperm morphology and functions in streptozotocin-nicotinamide induced adult male diabetic rats. *Arch. Med. Sci.* 15(1). 240–249. DOI: 10.5114/aoms.2018. 81038.

[31] Lesmana, R. 2019. Combination formulated herbals (*Pimpinella alpina*, *Eurycoma longifolia*, and *Curcuma xanthorrhiza*) increases number and improves the quality of sperm in male rat. *Int. J. Pharma Med. Biol. Sci.* 8(3). 106–109. DOI: 10.18178/ ijpmbs.8.3.106-109.

[32] Gill, S.S., O.M. Pulido. 2001. Review article: glutamate receptors in peripheral tissues: current knowledge, future research, and implications for toxicology. *Toxicol. Pathol.* 29(2). 208–223. DOI: 10.1080/ 019262301317052486.

ISSN. 2087-2852
E-ISSN. 2338-1655

[33] Gaschler, M.M., B.R. Stockwell. 2017. Lipid peroxidation in cell death. *Biochem. Biophys. Res. Commun*. 482(3). 419–425. DOI: 10.1016/j.bbrc.2016.10.086.
[34] El-Demerdash, F.M., M.I. Yousef, F.S. Kedwany, H.H. Baghdadi. 2004. Cadmium-induced changes in lipid peroxidation, blood hematology, biochemical parameters and semen quality of male rats: protective role of vitamin E and β-carotene. *Food Chem. Toxicol.* 42(10). 1563–1571. DOI: 10.1016/ j.fct.2004.05.001.
[35] Anzila. I. 2019. Potensi semanggi air (*Marsilea crenata*) dalam memperbaiki spermatogenesis dan kualitas sperma tikus (*Rattus norvegicus*) setelah pemberian *monosodium glutamat* (MSG). Master Thesis. Master Program of Biology, Universitas Brawijaya. Malang.
[36] Choudhary, R., Vk. Chawala, N.D. Sony, J. Kumar, Rk. Vyas. 2010. Oxidative stress and role of antioxidants in male infertility. *J. Physiol.* 6(2). 54-59.
[37] Mardhiyyah, K., Y.I. Ryandini, Y. Hermawan. 2021. Red and white galangal puree antioxidant activity and phytochemistry screening. *Jurnal Jamu Indonesia.* 6(1). 23–31. DOI: 10.29244/jji.v6i1.174.
[38] Oloyede, G.K., P.A. Onocha, B.B. Olaniran, 2011. Phytochemical, toxicity, antimicrobial and antioxidant screening of leaf extracts of *Peperomia pellucida* from Nigeria. *J. Adv. Environ. Biol.* 5(12). 3700-3709.
[39] Anas, Y., I. Faozi, Suharjono. 2015. Potensi fraksi N-heksan ekstrak etanol rimpang lengkuas [*Alpina GalangaI* (L) Swartz.] dalam meningkatkan kualitas sperma dan spermatogenesis. *Prosiding Seminar Nasional Peluang Herbal sebagai Alternatif Medicine*. 7-19.
[40] Hong, Y., S. Chen. 2006. Aromatase Inhibitors: structural features and biochemical characterization. *Ann. N.Y. Acad. Sci.* 1089(1). 237–251. DOI: 10.1196/ annals.1386.022.

ISSN. 2087-2852
E-ISSN. 2338-1655

Reduction of Remazol Brilliant Blue-R Dye Levels Through Electrocoagulation Process at Laboratory Scale to Reduce Pollution Levels of Textile Industrial Waste in River Streams

Moh. Sholichin[1*], Bambang Ismuyanto[2], A. S. Dwi Saptati N. H.[2], H. Susilo[3]

[1]Department of Water Resources Engineering, Faculty of Engineering, Universitas Brawijaya, Malang, Indonesia
[2]Department of Chemical Engineering, Faculty of Engineering, Universitas Brawijaya, Malang, Indonesia
[3]Department of Civil Engineering, Faculty of Engineering, Universitas Brawijaya, Malang, Indonesia

Abstract

The textile industry produces liquid waste, which is the main cause of pollution in rivers. Textile industry wastewater has a dye content of about 40%. Electrocoagulation is one method that is able to reduce waste by using electrolysis reactions. This study aims to analyze the level of the electrode plan's capability to reduce the level of dye waste pollution from the industry on a laboratory scale. The submerged electrode material was 7 cm x 8 cm, 7 cm x 10 cm, and 7 cm x 12 cm in dimensions. The electrocoagulation process was run for 120 minutes with a voltage of 30 volts and stirring at 200 rpm. Samples were taken at 0, 5, 15, 30, 45, 60, and 120 minutes for the electrocoagulation process. Determination of the maximum wavelength of Remazol Brilliant Blue-R was carried out by measuring 60 ppm of Remazol Brilliant Blue solution at various wavelengths in the range of 400 - 800 nm with 1 nm intervals. Measurements were carried out using a UV-Vis spectrophotometer. First-order and second-order reaction kinetics models were used to study the reaction kinetics of the Remazol Brilliant Blue-R electrocoagulation process. The highest efficiency in the Remazol Brilliant Blue-R reduction process was obtained at 86% at 120 minutes. The kinetics of the Remazol Brilliant Blue-R electrocoagulation process using aluminum-based electrodes was under the first order with an R^2 value > 0.96.

Keywords: Electrocoagulation, Industrial Wastewater, Remazol Brilliant Blue-R, UV-Vis Spectrophotometer.

INTRODUCTION

Liquid waste from the textile industry is one of the main causes of pollution in water areas. The textile industry liquid waste has a dye content of 40% [1]. One of the textile dyes in use is Remazol Brilliant Blue-R, which results in a blue color to liquid waste dye textiles used is Remazol Brilliant. Remazol Brilliant Blue-R is an azo dye derivative of azobenzene. The dye is hard to degrade naturally due to the presence of a double bond (-N=N-), which should be broken down first for the dye to become degradable faster [2]. The dye contains benzene compounds at 60% - 70%, making it difficult to degrade naturally [3]. The benzene content in the dye can cause cancer [4]. Therefore, it becomes imperative to conduct pre-treatment on liquid waste from the textile industry before it is disposed of in a body of water [5].

Electrocoagulation is a method of waste removal with the use of electrolysis [6]. Electrocoagulation uses a pair of metal plates, which act as electrodes consisting of an anode and a cathode using the principle of electrochemistry, where the anode will experience oxidation. At the same time, the water will be reduced and form a coagulant after the process is complete. Liquid waste that has been processed becomes more apparent than before the process [7]. Aluminum plate is a commonly used electrode as it is naturally a suitable coagulant. An aluminum electrode is a source of Al^{3+} - ions in the anode and a coagulant in the coagulation-flocculation process that occurs [8]. Besides, aluminum is affordable, easy to obtain, highly effective, and nontoxic [9].

An electrocoagulation process is influenced by several factors, such as temperature, current density, voltage, pH, time, the thickness of the electrodes, and the distance between electrode plates [9]. To obtain an effective process, it is necessary to learn the reaction kinetics that occur besides considering factors that influence it. The reaction kinetics of an electrocoagulation process to reduce Remazol Brilliant Blue-R levels is concerned with the rate of the chemical reaction that takes place and the factors that influence it. The number of moles of the reactants and the unit volume at a given time influence the rate of a chemical reaction. As the concentration of a reactant decreases with time, the curve that is generated will have a negative gradient. Therefore, the rate of a reaction at one point along the curve is given by -dC/dt from the experiment result and is independent of the equation stoichiometry [10].

*Correspondence address:
Moh Sholichin
Email: mochsholichin@ub.ac.id
Address: Department of Water Resources Engineering, Faculty of Engineering, University of Brawijaya, Malang, Indonesia

ISSN. 2087-2852
E-ISSN. 2338-1655

In determining the rate of a chemical reaction, it is important to know the reaction order. Reaction order is the relationship between the chemical reaction rate and species concentration. Theoretically, a reaction order is a small round number, but it can be a fraction or zero in several cases. In general, reaction order differs from the equation stoichiometry coefficient. By order, there are zero-order, first-order, and second-order reactions. A zero-order reaction can occur if the rate of reaction is not affected by the concentrations of the reactants [10]. A first-order reaction can occur if the rate of reaction is dependent on the concentration of one of the reactants. A second-order reaction can occur if the rate of reaction is dependent on the squared concentration of one reactant or the concentration of two reactants involved in the reaction [11]. In determining the order of a reaction, the k value or constant is obtained from the slope of the line on the graph. The zero-order constant from [A] is obtained from the intercept on the graph to the coordinate on the y-axis, and the suitability of the linear regression chart with the graph of the experimental data set with the coefficient [12].

The determination of reaction kinetics in an electrocoagulation process is very important for an easier industry-scale application. In addition, reaction kinetics is also used for predicting the product of a reaction at a certain time and under a certain condition, as well as for controlling the reaction condition [13]. Reaction kinetics can also be used to find out the influence of the concentrations of reactants to the rate of reaction [14]. Reaction kinetics is very important for considering the size and design of more economical, larger-scale tools. The current research aims to figure out the first-order and second-order reaction kinetics involved in the process of reducing the Remazol Brilliant Blue-R dye levels in industrial textile liquid waste by electrocoagulation using aluminum-based electrodes. The research aims to analyze the reaction kinetics involved in the electrocoagulation process and the effects of variations of the electrode surface area submerged in the solution on the electrocoagulation process efficiency and the final concentration of Remazol Brilliant Blue-R dye produced.

MATERIAL AND METHOD

The equipment used included UV-VIS spectrophotometer, magnetic stirrer, electrocoagulation device, power supply, Beaker glass, volumetric pipette, dropper pipette, funnel glass, suction ball, stopwatch, analytical balance, measuring spoon, vial, and glass watch (Fig. 1). Meanwhile, the main ingredients used were demineralized water, Remazol Brilliant Blue-R dye, universal pH paper, and strain paper.

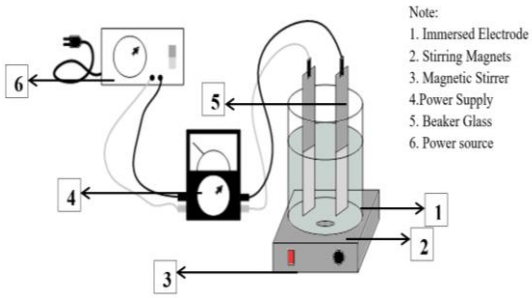

Figure 1. The equipment used in the research

Liquid Remazol Brilliant Blue-R dye was made by weighing solid Remazol Brilliant Blue-R dye at 0.1 g and dissolving it with 50 mL of water in a Beaker glass. The Remazol Brilliant Blue-R dye was then diluted in a laboratory flask to a measure of 1000 mL by adding water to the limit sign so that a Remazol Brilliant Blue-R solution was obtained at a concentration of 100 ppm. Then, the pH of the liquid was measured.

The next step was to measure the electrocoagulation process variable submerged electrode surface area within the Remazol Brilliant Blue-R solution. It was conducted by first filling Beaker glasses with 1000 mL of Remazol Brilliant Blue-R solution each. Then, electrodes with dimensions 7 cm x 8 cm, 7 cm x 10 cm, and 7 cm x 12 cm were each submerged into the solution for 120 minutes with an electrical voltage of 30 volts applied, accompanied by stirring at 200 rpm. Test samples were taken at 0, 5, 15, 30, 45, 60, and 120 minutes (Fig. 2).

Determination of the maximum wavelength of Remazol Brilliant Blue-R dye was conducted by measuring the wavelengths of 0 ppm of Remazol Brilliant Blue-R solution in the range of 400–800 nm with 1 nm intervals using a UV-Vis spectrophotometer. A calibration curve of Remazol Brilliant Blue-R solution at concentrations of 20, 40, 60, 80, and 100 ppm against the Remazol Brilliant Blue-R dye absorbance at maximum wavelength that was measured using a UV-Vis spectrophotometer was created.

The UV-Vis spectrophotometer was applied to samples of Remazol Brilliant Blue-R solution that had gone through an electrocoagulation process. A filtration process was carried out using paper strain to separate coagulants from cleared water.

ISSN. 2087-2852
E-ISSN. 2338-1655

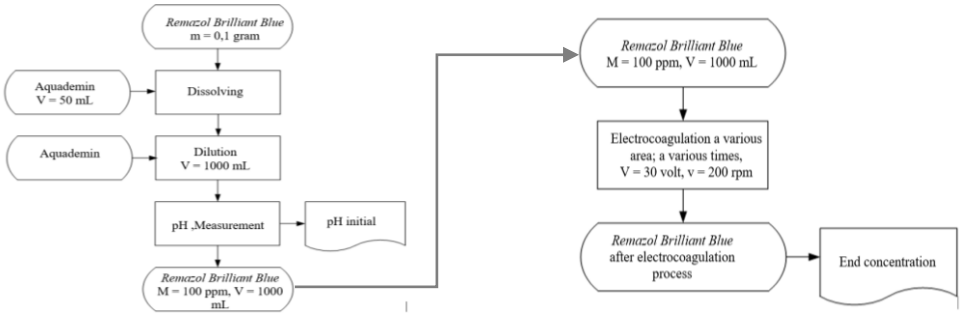

Figure 2. Flowchart of Remazol Brilliant Blue-R solution preparation and electrocoagulation process

Efficiency of the Electrocoagulation Process

The electrocoagulation process efficiency can be influenced by the submerged electrode surface area. The efficiency of the electrocoagulation process in reducing Remazol Brilliant Blue-R contained in the liquid samples used was calculated using the equation below:

$$\%\ allowance = \frac{(C_{A0} - C_{At})}{C_{At}} \times 100 \quad (1)$$

Description:

C_{A0} = initial concentration of Remazol Brilliant Blue-R solution in units of mg.L^{-1},

C_{At} = final concentration of Remazol Brilliant Blue-R at time *t* (minutes)

Electrocoagulation Kinetics

An analysis of the reaction kinetics that occurred in the electrocoagulation process was carried out. The analysis used first-order and second-order reaction kinetics models. The reaction kinetics involved in the electrocoagulation process is generally given in the equation below:

$$-r_A = -\frac{d_{CA}}{d_t} = kC_A \quad (2)$$

Description:

k = Reaction constant

C_A = Final concentration

From the equation reaction base conducted integral method and get equation kinetics reaction orde 1 (one), i.e.:

$$-ln\frac{C_A}{C_{A0}} = kt \quad (3)$$

Description:

k = First-order reaction rate constant

t = Time (minutes)

From the basic reaction equation above, an equation for the second-order reaction kinetics was also obtained by substitution method as follows:

$$\frac{1}{C_A} = \frac{1}{C_{A0}} + kt \quad (4)$$

Description:

k = Second-order reaction rate constant

t = time (minutes)

C_{A0} = Initial concentration

The final pH of the solution, as well as the absorbance of the filtered solution using a UV-Vis spectrophotometer at maximum wavelength, was conducted. The curve calibration was used to determine the final concentration of the filtered solution based on the absorbance input.

The reaction kinetics were determined using the initial and final solution concentrations, and the data obtained were processed using Microsoft Excel. The k and R^2 values were computed with first-order and second-order reaction equation data. The values obtained were plotted on a graph for comparison to determine the optimum reaction kinetics.

RESULT AND DISCUSSION

An electrocoagulation process on Remazol Brilliant Blue-R dye was carried out at an initial concentration of 100 ppm using a voltage of 30 volts with a surface contact area between the electrodes and the fluid varied (Table 1). Samples were taken at varied time in minutes.

Tabel 1. The electrocoagulation process on Remazol Brilliant Blue-R with electrodes set 2 cm apart

Submerged Surface Area	Time (Minutes)	Initial Concentration (mg.L^{-1})	Final Concentration (Mmg.L^{-1})
7 cm X 8 cm	0	100	98.64
	5		89,11
	15		78.74
	30		59.65
	45		50.29
	60		45.27
	120		27.95
7 cm X 10 cm	0	100	99.55
	5		93.27
	15		76.88
	30		57.89
	45		49.77
	60		38.41
	120		17.11
7 cm X 12 cm	0	100	99.07
	5		87.77
	15		72.74
	30		55.76
	45		47.16
	60		33.90
	120		14.08

ISSN. 2087-2852
E-ISSN. 2338-1655

The Effect of Submerged Electrode Surface Area on the Final Concentration of Remazol Brilliant Blue-R Solution

Electrodes hold an important role in an electrocoagulation process as they are used for delivering electricity. The variations of submerged electrode surface area can naturally affect the electrocoagulation process. The larger the electrode surface submerged, the larger the electrode contact area with liquid Remazol Brilliant Blue-R. The influence of the submerged electrode surface area and processing time on the Remazol Brilliant Blue-R solution concentration is indicated by the change in the concentration of Remazol Brilliant Blue-R solution with the variations in the submerged electrode surface area. Based on the research data in Table 1, a plot of data was created (Fig. 2).

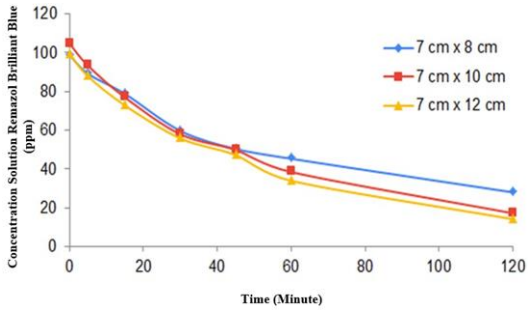

Figure 3. The influence of the submerged electrode surface area on the Remazol Brilliant Blue-R solution concentration with time

Based on Figure 3, the electrode with a submerged area of 7 cm x 12 cm produced a greater reduction in concentration than the electrodes with submerged areas of 7 cm x 8 cm and 7 cm x 10 cm. It shows that the electrode with the largest submerged surface area performed the best in the electrocoagulation process. The larger submerged surface area will allow for a larger contact area of the electrodes with the Remazol Brilliant Blue-R solution. The wider the contact area of the electrodes with the Remazol Brilliant Blue-R solution, the greater the electric current produced [15]. This, of course, affects the electrocoagulation process because the electrons become more reactive and move more easily so that more electrons are channeled [16].

Apart from that, more and more Al3+ ions are formed [17]. When more electrons are distributed, more binding occurs between electrons and H+, which causes the H_2 produced to become more abundant [18]. The more Al^{3+} ions are produced, the more binding there will be between Al^{3+} and OH-, which will cause more flocs to form [15].

The electrocoagulation process results also proved that there is an influence on this process, where the concentration of the Remazol Brilliant Blue-R solution decreased from minute 0 to minute 120 in all variations of submerged electrode surface area. The longer the time that passes in the electrocoagulation process, the more the accumulation of electron movement occurs, which results in more aluminum hydroxide binding to the dye [16,19].

The Effect of Time on the Efficiency of the Electrocoagulation Process in Reducing Remazol Brilliant Blue-R

Many factors, including the submerged electrode surface area, can influence the electrocoagulation process efficiency. In the current research, the electrocoagulation process was conducted with several variations in the submerged electrode surface area, namely 7 cm x 8 cm, 7 cm x 10 cm, and 7 cm x 12 cm. The results of the calculation are provided in Table 2.

Table 2. Electrocoagulation Process Efficiency in Reducing Remazol Brilliant Blue-R Levels

Submerged Surface Area	Time (Mintutes)	Remazol Brilliant Blue Reduction Efficiency (%)
7 cm X 8 cm	0	0.00
	5	9.67
	15	20.18
	30	39.53
	45	49.02
	60	54.11
	120	71.66
7 cm X 10 cm	0	0.00
	5	10.78
	15	26.47
	30	44.62
	45	52.39
	60	63.26
	120	83.63
7 cm X 12 cm	0	0.00
	5	11.40
	15	26.57
	30	43.71
	45	52.39
	60	65.78
	120	85.78

Table 2 shows that the larger the submerged electrode surface area, the greater the percent efficiency of the electrocoagulation process in reducing Remazol Brilliant Blue-R in the samples. The final efficiency rates at 120 minutes of the electrocoagulation process with submerged electrode surface areas of 7 cm x 8 cm, 7 x 10 cm, and 7 cm x 12 cm were 71.66%, 83.63%, and 85.78%, respectively. It was figured out that a larger submerged electrode surface area will increase the efficiency of the electrocoagulation process (Fig. 4).

ISSN. 2087-2852
E-ISSN. 2338-1655

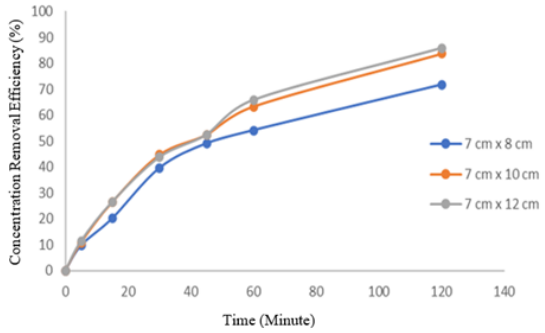

Figure 4. The Efficiency of the Electrocoagulation Process in Reducing Remazol Brilliant Blue-R with time

Figure 4 shows that the percent efficiency of the electrocoagulation process in reducing Remazol Brilliant Blue-R increased significantly until minute 120. As the graph does not show an equilibrium point, it is assumed that an equilibrium point of electrocoagulation process efficiency will be encountered if the electrocoagulation process is extended beyond 120 minutes.

Electrocoagulation Kinetics to Electrocoagulation Process Time in Remazol Brilliant Blue-R Reduction

Figures 5 and 6 show the first-order and second-order reaction rate constants calculated. It is shown that the electrocoagulation process in reducing Remazol Brilliant Blue-R with variations in submerged electrode surface area could happen at the first-order and second-order of reaction [17].

Table 3. Comparison of first-order and second-order reaction rate constants in the electrocoagulation process on Remazol Brilliant Blue-R

Surface Area (cm)	First Order		
	K_1 (L/mg.min^{-1})	R^2	equation
7 x 8	0.0104	0.962	y = 0.0104x + 0.0967
7 x 10	0.0149	0.993	y = 0.0149x + 0.0681
7 x 15	0.0161	0.996	y = 0.0161x + 0.0492
Surface Area (cm)	**Second Order**		
	K_2 (L/mg.min^{-1})	R^2	equation
7 x 8	0.0002	0.997	y = 0.0002x + 0.01
7 x 10	0.0004	0.959	y = 0.0004x + 0.0064
7 x 15	0.0005	0.944	y = 0.0005x + 0.0054

The study results in Table 3 show increases in k_1 and k_2 values with the increased area of the submerged electrode surface. It has been proven that the submerged electrode surface area could affect the electrocoagulation process. The larger the submerged electrode surface area, the higher the electric current supplied, resulting in more Al^{3+} ions produced. Therefore, the bond between Al^{3+} and OH- ions will also increase, causing more flocs on the plate surface [20].

The first-order reaction rate constant (k_1)

Excellent R^2 values were obtained from the calculation with the formula (3), which were then plotted in a chart (Fig. 5). The calculation results are shown in Table 3. From the table, it is known that k_1 was proportional to the submerged electrode surface area. The value of k_1 can be increased by increasing the submerged electrode surface area. The largest $k1$ value of 0.0161 L/mg.min^{-1} was obtained when the submerged electrode surface area variation 7 cm x 12 cm was used [21].

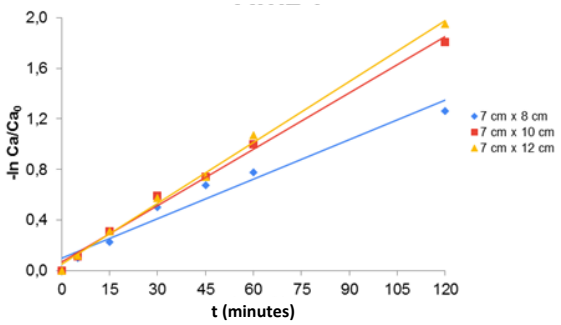

Figure 5. The First-order Reaction Kinetics in the Electrocoagulation Process

The second-order reaction rate constant (k_2)

k_2 values were obtained using the formula (4) and plotted in a chart (Fig. 6). The calculation results are presented in Table 3. From the table, it is known that k_2 was proportional to the submerged electrode surface area. The larger the submerged electrode surface area, the higher the k_2 value. The largest k_2 value of 0.0005 L/mg.min^{-1} was obtained when the submerged electrode surface area variation 7 cm x 12 cm was used.

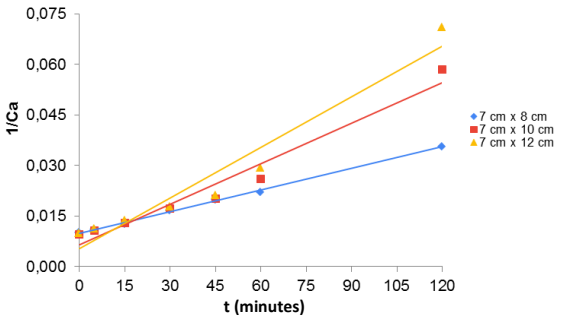

Figure 6. The Second-order Reaction Kinetics in the Electrocoagulation Process

ISSN. 2087-2852
E-ISSN. 2338-1655

CONCLUSION

The larger the submerged electrode surface area, the higher the efficiency (%) of the coagulation process in reducing Remazol Brilliant Blue-R levels. The electrocoagulation process efficiency rates in reducing Remazol Brilliant Blue-R at 120 minutes with submerged electrode surface areas of 7 cm x 8 cm, 7 cm x 10 cm, and 7 cm x 12 cm were 72%, 84%, and 86%, respectively. The first-order reaction kinetics in the electrocoagulation process in reducing Remazol Brilliant Blue-R with aluminum-based electrodes had an R^2 value > 0.96. The first-order reaction rate constant increased with time proportional to the submerged electrode surface area, with a value of 0.0161 min^{-1}.

REFERENCES

[1] Sastrawidana, I.D.K., D. O. Rachmawati. 2016. Efficiency of color change of artificial textile wastewater treated by electrooxidation at variations in pH, salt concentration and potential difference. *Proceedings of the National Seminar, MIPA*, 356–362.

[2] Harisha, S., J. Keshavayya, B.E. Kumara Swamy, C.C. Viswanath. 2017. Synthesis, characterization, and electrochemical studies of azo dyes derived from barbituric acid. *Dyes Pigm*. 136. 742–753. DOI: 10.1016/ j.dyepig.2016.09.004.

[3] Wijaya, K., E. Sugiharto, I. Fatimah, S. Sudiono, D. Kurniaysih. 2006. Utilization of TiO_2-Zeolite and UV-Light for photodegradation of Congo red dyes. *Berkala MIPA*. 3. 27-35.

[4] Christina M., S. Mu'nisatun, R. Saptaaji, D. Marjanto. 2007. Preliminary study on the degradation of Azo dyes (methyl orange) in water solvents using a 350 keV/10 mA electron beam machine. *Jurnal Forum Nuklir.* 1 (1). 31–44.

[5] Naimah, S., S. Ardhanie, B.N. Jati, N.N. Aidha, A.A. Cahyaningtyas. 2014. Degradasi zat warna pada limbah cair industri tekstil dengan metode fotokatalitik menggunakan nanokomposit TiO_2 – Zeolit. *Jurnal Kimia dan Kemasan.* 36. 225-236. DOI: 10.24817/jkk. v36i2.1889

[6] Fatimah, N., Alimuddin, R. Gunawan. 2018. Determination of Rhemazol RED RB 133 color intensity in Batik waste by electrocoagulation using NaCl. *Jurnal Atomik*. 3(1). 39–46.

[7] Pratika, A.R., B. Widiono. 2020. Studi literatur pengolahan limbah cair elektroplating untuk mengurangi kadar logam nikel dan TSS (Total Suspended Solid) menggunakan elektro-koagulator. Distilat. 6(2). 346-353. DOI: 10.33795/distilat.v6i2.120.

[8] Hanum, F., R. Tambun, M.Y. Ritonga, W.W. Kasim. 2015. Aplikasi elektrokoagulasi dalam pengolahan limbah cair pabrik kelapa sawit. *Jurnal Teknik Kimia USU*. 4(4). 13-17. DOI: 10.32734/jtk.v4i4.1508.

[9] Hernaningsih, T. 2016. Tinjauan teknologi pengolahan air limbah industri dengan proses elektrokoagulasi. *Jurnal Rekayasa Lingungan.* 9(1). 31-46. DOI: 10.29122/jrl. v9i1.1988.

[10] Prayitno. 2007. Kajian kinetika kimia model matematik reduksi kadmium melalui laju reaksi, konstante dan orde reaksi dalam proses elektrokimia. *Ganendra*. 10(1). 27-34. DOI: 10.17146/gnd.2007.10.1.159.

[11] Kurniawati, P. B. Wiyantoko, A. Kurniawan, T.E. Purbaningtias. 2013. Kinetic study of Cr(VI) adsorption on hydrotalcite Mg/Al with molar ratio 2:1. *EKSAKTA: Journal of Science and Data Analysis.* 13(1). 11-21. DOI: 10.20885/eksakta.vol13.iss1-2.art2.

[12] Siahaan, P. 2000. Analisa data kinetika dengan Mathcad: Reaksi dekomposisi Etilen oksida asumsi Orde-1, Orde-2, dan Orde-3. *Jurnal Kimia Sains dan Aplikasi*. 3(3). 197-202. DOI: 10.14710/jksa.3.3.197-202.

[13] Haryanto, A., O. Yozana, S. Triyono. 2017. Aplikasi kinetika reaksi pembuatan biodiesel dari minyak jelantah melalui reaksi transesterifikasi basa. *Jurnal Keteknikan Pertanian*. 5(3). 261-266. DOI: 10.19028/jtep. 05.3.261-266.

[14] Rahmadyo, A.N., D. Cahayandari, S. Rahardjo. 2017. Comparative Analysis of the kinetics of the $CaCO_3$-$CaSO_4$ scale formation reaction using the Arrhenius equation and the Scanning Calorimeter (DSC) differential analysis. Thesis. Muhammadiyah University of Semarang. Semarang.

[15] Sutanto., A. Iryani, Sarahwati. 2018. Efisiensi dan efektifitas serta kinetika elektrokoagulasi pengolahan limbah sagu aren. *Ekologia*. 18(1). 10-16. DOI: 10.33751/ekol.v18i1.802.

[16] Topayung, D. 2011. Pengaruh arus listrik dan waktu proses terhadap ketebalan dan massa lapisan yang terbentuk pada proses elektroplating pelat baja. *Jurnal Ilmiah Sains.* 11(1). 97-101. DOI: 10.35799/jis.11.1.2011. 50.

[17] Nur, A., A. J. Effendi. 2014. Aplikasi elektrokoagulasi pasangan elektroda

aluminium pada proses daur ulang grey water hotel. *Jurnal Teknik Lingkungan*. 20(1). 58-67. DOI: 10.5614/jtl.2014.20.1.7.

[18] Wahyu, D.S. 2021. Reducing the levels of Remazol Brilliant Blue R dye using the adsorption method using chitosan. Chemical Engineering, Samarinda State Polytechnic. Samarinda.

[19] Dwijayanti, U., Gunawan, D.S. Widodo, A. Haris, L. Suyati, R.A. Lusiana. 2020. Adsorpsi Methylene Blue (MB) menggunakan abu layang batubara teraktivasi larutan NaOH. *Analit: Anal. Environ. Chem.* 5(1). 1-14. DOI: 10.23960/aec. v5.i1.2020.p01-14.

[20] Sukarta, I.N., N.K.S. Lusiani. 2016. Adsorpsi zat warna azo jenis remazol brilliant blue oleh limbah daun ketapang (*Terminalia catappa.* L.). Prosiding Seminar Nasional MIPA UNDIKSHA 2016. 311-316.

[21] Oko, S., Harjanto., A. Kurniawan, C. Winanti 2022. Penurunan kadar zat warna Remazol Brilliant Blue R dengan metode adsorpsi menggunakan serbuk $CaCO_3$ dari cangkang telur dan karbon aktif. *METANA.* 18(1). 39-45. DOI: 10.14710/metana.v18i1.45766.

ISSN. 2087-2852
E-ISSN. 2338-1655

Potency of Coconut Shell Biochar to Remediate Ion Chromium in Contaminated Water

Salman Faris[1], Harmin Sulistiyaning Titah[1*], Herman Pratikno[2]

[1]Department of Environmental Engineering, Faculty of Civil, Planning and Geo Engineering, Institut Teknologi Sepuluh Nopember, Surabaya, Indonesia
[2]Department of Ocean Engineering, Faculty of Marine Technology, Institut Teknologi Sepuluh Nopember, Surabaya, Indonesia

Abstract

Many heavy metals contaminate our environment, including chromium (Cr(VI) contaminated water. The aim of this study was to determine the removal of ion Cr(VI) using the coconut shell biochar. Biochar activation processes were conducted at 350℃ and 550℃. The characteristic tests of biochar were conducted, such as testing for moisture, ash, volatile, and carbon content. Additionally, a scanning electron microscope was also performed. The remediation test was carried out on a laboratory scale with a batch system. The variables were the mass of coconut shell biochar (0, 8, and 16 r) and the time of process were 0, 30, and 60 min. Based on the results, the characteristics of coconut shell biochar showed a high carbon content, which reaches 80.4% for activation temperature at 500℃ and 73.02% for 350℃. Coconut shell biochar can reduce ion Cr(VI) in water; it reached 73.78% to 88.15%. The percentage of Cr(VI) reduction in water reached 88.15% using biochar that was activated at a temperature of 350℃ and a mass of 16 g at a detention time of 60 min. In conclusion, coconut shell biochar has good potential to reduce chromium in water.

Keywords: Biochar, Chromium, Coconut Shells, Remediation.

INTRODUCTION

The increasing industrial activities have influenced the level of environmental pollution caused by heavy metal-containing waste [1]. One of the heavy metals that can pose environmental and human health problems is chromium [2]. The Cr(VI) ion is a strong oxidizing agent and can cause chronic toxic effects, including skin infections and cancer. Chromium is commonly found in the industrial waste of batteries, paints, cement, coating, dyeing, and photography [3]. One method to reduce the levels of heavy metals in water is the adsorption method. One method to reduce the levels of heavy metals in water is the adsorption method.

Adsorption is a process of precipitating a dissolved substance in a solution onto the surface of an absorbent material, causing the substance to enter and accumulate within the absorbent material [4]. This technique can employ biochar, which has demonstrated considerable effectiveness in absorbing heavy metals in wastewater [5]. Biochar possesses a large surface area and high capacity for adsorbing heavy metals, thus holding the potential for mitigating the bioavailability of heavy metals and organic pollutants through adsorption and other physiochemical reactions.

Biochar is produced when biomass waste is heated without air or with minimal air. This combustion process, typically referred to as pyrolysis, occurs at relatively low temperatures (<700℃) [1]. Raw materials suitable for biochar production include unused biomass residues such as rice husks, corn cobs, coconut shells, and similar materials [6]. Previous research indicates that biochar derived from coconut shells has shown an effectiveness of up to 39.35% with continuous systems [7].

Therefore, a study was conducted on the remediation of Cr(VI)-contaminated water using biochar derived from coconut shells. The variables examined included the influence of pyrolysis temperature during biochar activation, with temperature variations of 350℃ and 500℃, as well as the application of biochar mass with variations of 0 g, 8 g, and 16 g. This research is expected to provide scientific information regarding the ability of coconut shell biochar to remove Cr(VI) heavy metals from polluted water media and can serve as a reference for environmental restoration efforts to mitigate water pollution caused by Cr(VI) heavy metals.

MATERIAL AND METHOD

Biochar Preparation and Characterization

The initial stage involves the production of coconut shell biochar. This process begins with washing the coconut shells thoroughly with water

*Correspondence address:
Salman Faris
Email : salmanfaris032112@gmail.com
Address : Dept. Environmental Engineering, Faculty of Civil, Planning and Geo Engineering, Institut Teknologi Sepuluh Nopember, Keputih, Sukolilo, 60111 Surabaya, Indonesia

and drying them under direct sunlight until they are completely dry. Subsequently, the cleaned coconut shells are pyrolyzed at temperatures of 350°C for 1 hour and 500°C for 30 minutes (as the variables). They are then sieved using a 60-mesh sieve.

Following this, the biochar's characteristics are analyzed and compared to the Indonesian National Standard (SNI) 06-3730-1995 activated charcoal technical requirements [8] for activated charcoal. The biochar characteristics compared include moisture, ash, volatile, and fixed carbon content. The moisture content analysis is conducted using the ASTM D 3173/ D 3173 M – 17A method, the Standard Test Method for Moisture in the Analysis Sample [9]. The ash content analysis is performed using the ASTM D 3174-129 (2018) method to determine the inorganic residue as ash in the analysis sample [10]. The volatile content analysis uses the ISO 562-2010 method to determine the volatile matter of hard coal and coke [11]. A morphology analysis is conducted using Scanning Electron Microscopy (SEM) to determine the size of the formed pores. Biochar characterization tests were conducted at the Energy and Materials Laboratory, DRPM ITS.

Artificial Contaminated Water Preparation

The preparation of a heavy metal Cr(VI) stock solution of 1000 $mg.L^{-1}$ was carried out by dissolving 2.829 g of $K_2Cr_2O_7$ in a 1 L volumetric flask, the addition of distilled water up to the mark and thorough homogenization. Subsequently, a standard solution was prepared by pipetting 10 mL of the 1000 $mg.L^{-1}$ heavy metal Cr(VI) stock solution into a 100 mL volumetric flask. Distilled water was added to the mark, resulting in a 100 $mg.L^{-1}$ Cr(VI) heavy metal-contaminated solution.

Adsorption Test

The Cr(VI) solution was treated with sieved biochar and stirred at a stirring speed of 180 rpm [12]. The next step involved filtering the solution using filter paper. The research was conducted in reactors, each with two replications. Testing of the Cr(VI) levels in the solution samples was performed at detention times of 0 minutes, 30 minutes, and 60 minutes. The Cr(VI) heavy metal levels were analyzed using the Atomic Absorption Spectrophotometer – Flame (AAS-Flame) method. The instrument specifications used for the AAS-Flame in this study were the Hitachi AAS Z-2000 series.

The results and discussion were obtained from the analysis of parameters, which included data on the reduction of Cr(VI) concentration. To determine the percentage of Cr(VI) removal, it can be calculated using the equation:

$$\%\ Removal = \frac{(C_0 - C_e)}{C_0} \times 100\% \quad (1)$$

Description:
C_0 = the initial concentration of the heavy metal ($mg.L^{-1}$)
C_e = the final concentration of the heavy metal ($mg.L^{-1}$)

Calculating the adsorption isotherms was conducted using the Langmuir, Freundlich, and Brunauer, Emmett, and Teller (BET) models. Adsorption isotherms demonstrate the equilibrium relationship between the solution concentration and the amount of adsorbate adsorbed at a constant temperature. In calculating the isotherms, the quantity of adsorbate absorbed per gram of adsorbent ($mg.g^{-1}$) or qe is essential. The value of qe is obtained using the equation:

$$qe = \frac{(C_0 - C_E) \times V}{m} \quad (2)$$

Description:
qe = the amount of adsorbate adsorbed per gram of adsorbent ($mg.g^{-1}$)
C_0 = the initial concentration of the heavy metal ($mg.L^{-1}$)
C_e = the final concentration of the heavy metal ($mg.L^{-1}$)
V = the volume of the contaminated media (L)
m = the mass of the adsorbent (g).

Once qe is obtained, each isotherm model can be calculated. The BET isotherm is constructed by following Formula (3). Figure 1 depicted the adsorption process in this study.

$$\frac{\left({}^{C_e}/_{C_0}\right)}{\left(qe - \left(1 - \left(\frac{C_e}{C_0}\right)\right)\right)} \quad (3)$$

Description:
qe = the amount of adsorbate adsorbed per gram of adsorbent ($mg.g^{-1}$)
C_0 = the initial concentration of the heavy metal ($mg.L^{-1}$)
C_e = the final concentration of the heavy metal ($mg.L^{-1}$)

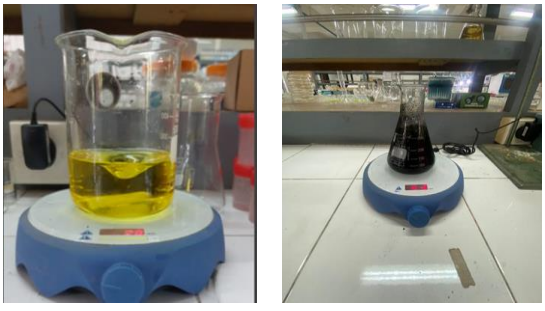

(a) (b)

Figure 1. (a) Adsorption Reactor, (b) Adsorption Process

ISSN. 2087-2852
E-ISSN. 2338-1655

RESULT AND DISCUSSION

The results of the biochar characterization analysis was shown in Table 1. In this study, the characterization results of the coconut shell-derived biochar have complied with the Indonesian National Standard (SNI) 06-3730-1995.

The determination of moisture content serves the purpose of understanding the hygroscopic nature of activated carbon. This highly hygroscopic characteristic of activated carbon renders it effective as an adsorbent. Both the temperature and the duration of carbonization significantly influence the absorbed moisture content. As the temperature and duration of carbonization increase, the moisture content decreases [13]. Ash content is the quantity of metal oxide consisting of minerals in a material that does not vaporize during combustion. The ash content influences the adsorption capacity of activated carbon, where the lower the ash content, the greater the adsorption capacity. Excessive ash in activated carbon can lead to blockages in its pores, thereby reducing its surface area and adsorption capacity [14].

The determination of volatile content aims to identify the presence of compounds that do not evaporate during the carbonization and activation process but do evaporate at 950℃. A high content of volatile substances can reduce the adsorption capacity of the biochar because the metal compounds contained in the sample can clog the pores of the biochar itself [15]. The moisture, ash, and volatile content influence the value of fixed carbon. A lower fixed carbon content can affect the adsorption capacity of activated carbon because organic compounds cover the carbon surface during the adsorption process [16]. Based on the results, the characteristics of coconut shells biochar show a high fixed carbon content that reaches 80.4% when it is activated at 500℃. The SEM test results of coconut shell biochar at activation temperatures of 350℃ and 500℃ described in Figure 2.

The SEM analysis of carbon conducted at a magnification of 3000X showed a porous and cavernous carbon surface structure with diameters ranging from 5.045 µm to 26.34 µm. Higher carbonization temperatures lead to the formation of more pores and an improved yield of carbon. With the temperature increase, impurities initially present within the pores, obstructing them, were released or vaporized, thus expanding the surface area of the activated carbon.

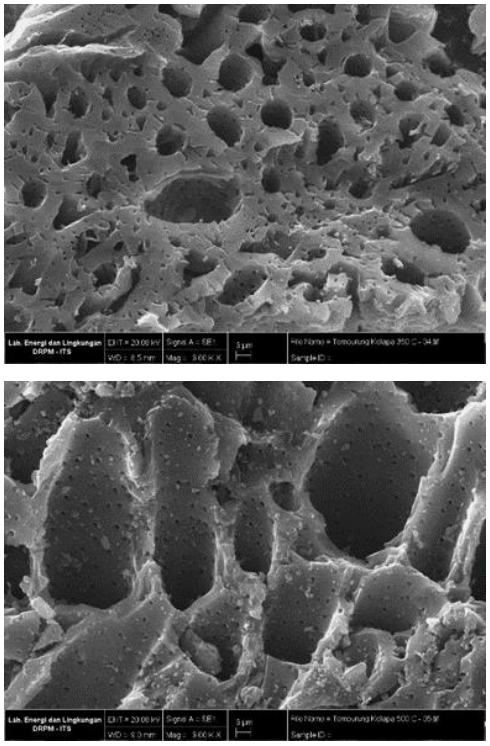

Figure 2. Surface Morphology of Coconut Shell Biochar (a) at 350℃, (b) at 500℃.

This study was conducted by comparing the biochar activation temperatures and the addition of biochar mass (0 g, 8 g, 16 g) as adsorbents at the same adsorbate concentration (±100 $mg.L^{-1}$) with a solution volume of 160 mL. The concentration reduction and percentage removal of ion Cr(VI) metal were recorded at contact times of 0, 30, and 60 min. Table 2 showed the percentage removal of ion Cr(VI).

The percentage removal of ion Cr(VI) without the addition of biochar did not increase at each contact time increment due to there being nothing to bind the ion Cr(VI). The highest removal occurred at 60 min. The percentage removal reached 76.95% with biochar activated at 500℃ in 8g of biochar mass. However, the percentage removal was 88.15% in 16 g of biochar mass that was activated at 350℃. The temperature during the biochar activation process was quite crucial as it can affect the fixed carbon value of a biochar. However, the temperature variable showed any significant difference.

Table 1. Biochar Characterization Test Results

Sample Name	Moisture Content (%)	Ash Content (%)	Volatile Content (%)	Fixed Carbon (%)
Coconut Shells 350℃	4.61	1.11	21.26	73.02
Coconut Shells 500℃	4.64	1.21	13.75	80.4

ISSN. 2087-2852
E-ISSN. 2338-1655

Table 2. Percentage Removal of Cr.

Sample Name	Mass of biochar (g)	0 Min (%)	30 Min (%)	60 Min (%)
Coconut Shells 350°C	0	0	0.01	0
Coconut Shells 500°C	0	0	3.21	2.14
Coconut Shells 350°C	8	0	59.02	73.78
Coconut Shells 500°C	8	0	64.53	76.95
Coconut Shells 350°C	16	0	84.46	88.15
Coconut Shells 500°C	16	0	72.08	83.42

The effect of the addition of adsorbent mass was one of the crucial factors in the adsorption process as it can affect the adsorbent's adsorption capacity. The increase in the percentage of adsorption was caused by the enlargement of the adsorbent's surface area, thereby increasing the sites for the adsorption process. However, excessive addition of the adsorbent weight was not recommended as it can lead to the saturation point of the solution, which would disrupt the adsorption process [17].

Contact time was also crucial in the adsorption process. The adsorption force of molecules from a solute can increase with longer contact time with activated carbon. Longer contact time allowed for a more efficient adsorption process [18]. In this study, the obtained adsorption effectiveness reached 88.15%, which might increase with a longer contact time. However, the effectiveness of the adsorption process may not increase significantly due to the saturation of binding sites on the adsorbent and the attainment of equilibrium.

Adsorption isotherms were typically used to explain the interactions between adsorbent and adsorbate. These isotherms depicted the relationship between the amount of adsorbed substance and the amount of adsorbent at equilibrium [19]. The Freundlich isotherm was constructed by plotting the log values of C_e against log qe. The Freundlich isotherm graph of coconut shell adsorbent is described in Figure 3. In the Freundlich isotherm, it was known that the value of R^2 is 0.8461. Following this, the Langmuir isotherm was constructed by plotting the values of C_e against C_e/qe, described in Figure 4. In the Langmuir isotherm, the value of R^2 was known to be 0.2265. Meanwhile, in the BET isotherm, the value of R^2 was known to be 0.3275 (Fig. 5).

Based on Figures 3 to 5, it was found that the Freundlich isotherm was more linear compared to the Langmuir and BET isotherms. This is indicated by the higher R^2 value of the Freundlich isotherm graph at 60 min. The Freundlich isotherm suggested that the adsorbent attaches to a heterogeneous surface, so the adsorbent adheres to more than one surface layer (multilayer) [20]. This isotherm also suggested that adsorption on each surface had different binding energies.

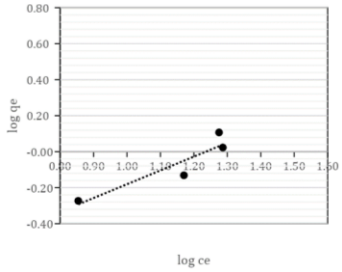

Figure 3. Freundlich isotherm of Coconut Shells Biochar Adsorbent at Contact Time of 60 min.

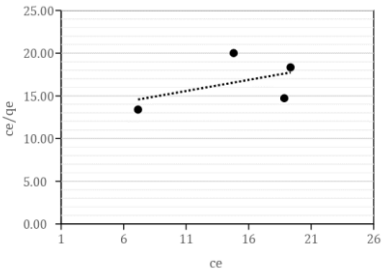

Figure 4. Langmuir isotherm of Coconut Shells Biochar Adsorbent at Contact Time of 60 min.

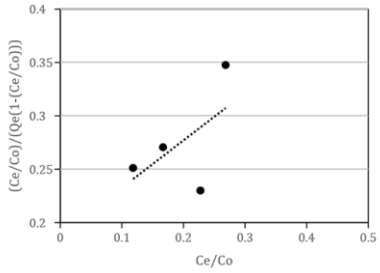

Figure 5. BET isotherm of Coconut Shells Biochar Adsorbent at Contact Time of 60 min

CONCLUSION

The activation of coconut shell biochar at 500°C yields a higher fixed carbon content than at 350°C. It reached 80.4%. The highest removal occurred at 60 min. The percentage removal reached 76.95% with biochar activated at 500°C in 16 g of biochar. However, the highest removal percentage was 88.15% in 16 g of biochar mass activated at 350°C with the Freundlich isotherm pattern.

ISSN. 2087-2852
E-ISSN. 2338-1655

ACKNOWLEDGEMENT

The authors are grateful to the *Direktorat Riset dan Pengabdian Masyarakat* (DRPM) ITS trough the *Keilmuan* Grant for funding this study with Contract No. 1715/PKS/ITS/2023.

REFERENCES

[1] Hidayat, B. 2015. Remediasi tanah tercemar logam berat dengan menggunakan biochar. *Jurnal Pertanian Tropik.* 2(1). 51-61.

[2] Almira, U., A. Sasmita., Isnaini. 2021. Analisis kadar air, kadar abu, volatil dan *fixed carbon* pada biochar cangkang sawit dengan variasi suhu pirolisis. J*OM FTEKNIK.* 8(2).1-5.

[3] Asmadi, E. Sutrisno, W. Oktiawan. 2019. Pengurangan Chrom (Cr) dalam limbah cair industri kulit pada proses tannery menggunakan senyawa alkali $Ca(OH)_2$, NaOH dan $NaHCO_3$ (Studi Kasus PT. Trimulyo Kencana Mas Semarang). *Jurnal Air Indonesia.* 5(1). 41-54. DOI: 10.29122/jai. v5i1.2431.

[4] Giyatmi, Z.K., D. Melati. 2008. Reduction of Cu, Cr, and Ag Levels in silver industry wastewater in Kotagede after adsorption with clay from the Godean Area. The 4th National Seminar on Nuclear Technology HR.

[5] Mutiara, R. 2021. Optimization of biochar synthesis from modified cassava peel (*Manihot exculenta* Crantz) with Fe_3O_4 using mass and time variations as adsorbents for methylene blue waste. Thesis. Chemistry Study Program, Faculty of Mathematics and Natural Sciences, Universitas Islam Indonesia. Yogyakarta.

[6] Widiastuti, M.M.D., B. Lantang. 2017. Pelatihan pembuatan biochar dari limbah sekam padi menggunakan metode Retort Kiln. *Jurnal Ilmiah Pengabdian Kepada Masyarakat.* 3 (2). 129-135.

[7] Nurfitriyani, A., E. Wardhani, M. Dirgawati. 2013. Penentuan efisiensi penyisihan kromium heksavalen (Cr^{6+}) dengan adsorpsi menggunakan tempurung kelapa secara kontinyu. *Reka Lingkungan.* 2(1). 57-68.

[8] Indonesian National Standard (SNI) 06-3730-1995 - Technical Requirements of Activated Carbon.

[9] ASTM D 3173/ D 3173 M – 17A Method - Standard test method for moisture in the analysis sample of coal and coke.

[10] ASTM D 3174-129 (2018) Method - Standard test method for ash in the analysis sample of coal and coke from coal.

[11] ISO 562-2010 Method - Hard coal and coke Determination of volatile matter

[12] Laos, L.E., A. Selan. 2016. Pemanfaatan kulit singkong sebagai bahan baku karbon aktif. *JIPF (Jurnal Ilmu Pendidikan Fisika)*. 1(1). 32-36.

[13] Saputri, C.A. 2020. Kapasitas adsorpsi serbuk nata de coco (bacterial sellulose) terhadap ion Pb^{2+} menggunakan metode batch. Jurnal Kimia. 14(1). 71-76. DOI: 10.24843/JCHEM. 2020.v14.i01.p12.

[14] Ariyanto, E., D.D. Lestari, D. Kharismadewi. 2021. Analysis of the adsorption capacity and kinetics of activated carbon from the shell of ketapang towards methyl orange dye. Master Thesis. Master's Program in Chemical Engineering, Universitas Muhammadiyah Palembang. Palembang.

[15] Widayanti, I. Isa, L.O. Aman. 2012. Study of the activation power of rice husk charcoal in the process of cd metal adsorption. Thesis. Department of Chemistry Education, Faculty of Mathematics and Natural Sciences, Universitas Negeri Gorontalo. Gorontalo.

[16] Sa'diyah. K., C.E. Lusiani. 2022. Kualitas karbon aktif kulit pisang kepok menggunakan aktivator kimia dengan variasi konsentrasi dan waktu aktivasi. *Jurnal Teknik Kimia dan Lingkungan.* 6(1). 9-19. DOI: 10.33795/jtkl. v6i1.259.

[17] Syauqiah. I. M. Amalia., H. A. Kartini. 2011. Analysis of variations in time and stirring speed in the process of heavy metal waste adsorption with activated carbon. *Jurnal Keilmuan dan Aplikasi Teknik.* 12(1). 11-20.

[18] Subarkhah, M.J., H.S. Titah. 2023. Remediasi logam berat Pb dengan menggunakan biochar sekam padi dan tongkol jagung. *Jurnal Sains dan Seni ITS.* 12(1). F48-F53.

[19] Suardana, I.N. 2008. Optimalisasi daya adsorpsi zeolit terhadap ion kromium (III). Jurnal Penelitian dan Pengembangan Sains dan Humaniora. 2(1). 17-33.

[20] Triana, G.Y. 2015. Effect of activation and dosage of rice husk adsorbent for methylene blue from textile industry manufacturing. Thesis. Department of Environmental Engineering, Faculty of Civil, Planning and Geo Engineering, Institut Teknologi Sepuluh Nopember. Surabaya.

ISSN. 2087-2852
E-ISSN. 2338-1655

MANUSCRIPT SUBMISSION

FOCUS AND SCOPE

Journal of Experimental Life Science (JELS) is scientific journal published by Graduate Program of Brawijaya University as distribution media of Indonesian researcher's results in life science to wider community. JELS is published in every four months. JELS published scientific papers in review, short report, and life sciences especially nanobiology, molecular biology and cellular biology. JELS is scientific journal that published compatible qualified articles to academic standard, scientific and all articles reviewed by expert in their field.

Journal of Experimental Life Science (JELS) have vision to become qualified reference media to publish the best and original research results, and become the foundation of science development through invention and innovation on cellular, molecular, and nanobiology rapidly to community.

Journal of Experimental Life Science (JELS) have objectives to published qualified articles on research's results of Indonesian researchers in life science scope. JELS encompasses articles which discuss basic principles on nature phenomenon with cellular, molecular, and nanobiology approach.

PEER REVIEW PROCESS

Publication of articles by JITODE is dependent primarily on their validity and coherence, as judged by peer reviewers, who are also asked whether the writing is comprehensible and how interesting they consider the article to be. All submitted manuscripts are read by the editorial staff and only those articles that seem most likely to meet our editorial criteria are sent for formal review. All forms of published correction may also be peer-reviewed at the discretion of the editors. Reviewer selection is critical to the publication process, and we base our choice on many factors, including expertise, reputation, and specific recommendations. The editors then make a decision based on the reviewers' advice, from among several possibilities:

Accepted, with or without editorial revisions
Invite the authors to revise their manuscript to address specific concerns before a final decision

Rejected, but indicate to the authors that further work might justify a resubmission

Rejected outright, typically on grounds of specialist interest, lack of novelty, insufficient conceptual advance or major technical and/or interpretational problems

PUBLICATION FREQUENCY

JELS publish 2 Issues per year until 2017. JELS started to publish 3 Issues per year since 2018.

OPEN ACCESS POLICY

This journal provides immediate open access to its content on the principle that making research freely available to the public supports a greater global exchange of knowledge.

COPYRIGHT NOTICE

Authors who publish with this journal agree to the following terms:

Authors retain copyright and grant the journal right of first publication with the work simultaneously licensed under a Creative Commons Attribution License that allows others to share the work with an acknowledgement of the work's authorship and initial publication in this journal.

Authors are able to enter into separate, additional contractual arrangements for the non-exclusive distribution of the journal's published version of the work (e.g., post it to an institutional repository or publish it in a book), with an acknowledgement of its initial publication in this journal.

Authors are permitted and encouraged to post their work online (e.g., in institutional repositories or on their website) prior to and during the submission process, as it can lead to productive exchanges, as well as earlier and greater citation of published work (The Effect of Open Access).

PRIVACY STATEMENT

The names and email addresses entered in this journal site will be used exclusively for the stated purposes of this journal and will not be made available for any other purpose or to any other party.

ETHICS PUBLICATION

Research that using animal, human, and clinical testing is should already have ethical clearance certificate from authorized institution.

Title Typed in Bold, Capitalize each First Letter of Each Word, Except Conjunctive, *Scientific name* should not be Abbreviated (Calibri 14 Bold Center, should not exceed 12 words, except conjuctive)

First Author[1]*, Second Author[2], Third Author[3] (Calibri 12 Center, without title)

[1]First Author Affiliation, Correspondence author should be indicated by * symbol (Calibri 9 Center)
[2]Department of Biology, Faculty of Mathematics and Natural Sciences, University of Brawijaya, Malang, Indonesia
[3]Laboratorium of Physiology, Faculty of Medicine, University of Brawijaya, Malang, Indonesia

Abstract (Calibri 9 Bold Center)

This article illustrates preparation of your paper using MS-WORD (.doc or .rtf). Manuscript was numbered consecutively. Main text typed in two columns (67 characters), except title and abstract in one column. The manuscript should be written in English. The length of manuscript should not exceed 10 pages including table and figure in this format using A4 paper single space. The text should be in the margin of 3 cm up, down and left side, 2.5 cm on right side. Abstract includes the research purposes, research method and research results in one paragraph of *essay,* not *enumerative*. No citation in abstract. Abstract should not exceed 200 words. Keywords typed after abstract. (Calibri 9 Justify).

Keywords: manuscript, English, format, 5 words maximum (Calibri 9 Left)

INTRODUCTION* (Calibri 10 Bold, Left, Capslock)

All submitted manuscripts should contain original research which not previously published and not under consideration for publication elsewhere. Articles must be written in ENGLISH and manuscripts may be submitted for consideration as research report articles, short reports or reviews.

The introduction explains the background of the problem, the study of literature and research purposes. Some initial introduction paragraphs explain the problem and background to these problems [1]. The next few paragraphs explain the study of literature that contains recent knowledge development which is directly related to the issues. The last paragraph of the introductory section contains a description of the purposes of the study. (Calibri 10 Justify)

MATERIAL AND METHOD (Calibri 10 Bold, Left, Capslock)

This section describes the types of methods (qualitative, quantitative or mixed-method) with details of methods of data collection and data analysis [2]. This section also describes the perspective that underlying the selection of a particular method. (Calibri 10 Justify)

Correspondence address: (Calibri 8 Bold, Left)
Full name of correspondence author
Email : sapto@jurnal.ub.ac.id
Address : afiliation address include post code

Data Collection (Calibri 10 Bold, Left)

Explain the data collection methods, i.e. surveys, observations or archive, accompanied by details of the use of such methods. This section also describes the population, sampling and sample selection methods. (Calibri 10 Justify)

The use of English language should followed proper grammar and terms. Name of organism shoul be followed by its full scientific name in the first mention, in *italic* [3]. Author of the scientific name and the word of "var." typed regular. Example: *Stellaria saxatillis* Buch. Ham. First abbreviation typed in colon after the abbreviated phrase.

Author must use International Standard Unit (SI). Negative exponent used to show the denominator unit. Example: g l^{-1}, instead of g/l. The unit spaced after the numbers, except percentage [4]. Example: 25 g l^{-1}, instead of 25gl^{-1}; 35% instead of 35 %. Decimal typed in dot (not coma). All tables and figures should be mentioned in the text.

RESULT AND DISCUSSION (Calibri 10 Bold, Left, Capslock)

This section contains the results of the analysis and interpretation or discussion of the results of the analysis. Describe a structured, detailed, complete and concise explanation, so that the reader can follow the flow of analysis and thinking of researchers [5]. Part of the results study should be integrated with the results of the

analysis and the results and discussion are not separated.

Table

Table should be submitted within the manuscript and in separated file of *Microsoft Excel* (xls.). Table whould not exceed 8 cm (one column) and 17 cm (two columns). Table should be embedded in different page after references.

Table should be numbered in sequence. Table title should be brief and clear above the table, with uppercase in initial sentence. Vertical line should not be used. Footnote use number with colon and superscripted. Symbol of (*) or (**) was used to show difference in confidence interval of 95 and 99%.

Table 1. Example of the Table (Calibri 8.5 Left)

No	Point (Calibri 8.5 Justify)	Description
1		
2		
3		
4		
5		

Sources: Journal of PPSUB (Calibri 8.5 Left)

Figures

Figures should be in high resolution and well contrast in JPEG or PDF with the following conditions:

- Monochrome image (line art), figures of black and white diagram (solid/no shades of gray), resolution 1000-1200 dpi (dot per inch).
- Combination Halftone, combine figure and text (image containing text) and coloured graphic or in grayscale format. Resolution 600-900 dpi.
- Halftone, coloured figure or grayscale format without text. Resolution 300 dpi.
- Black and white figure should be in the grayscale mode, while coloured figures should be in RGB mode.
- Figure should not exceed the width of 8 cm (one column), 12.5 cm (1.5 columns) or 17 cm (two columns).
- Figures title typed clearly below the figure.
- Figure with pointing arrow should be grouped (grouping).
- Figures were recommended in black and white.
- Legend or figure description should be clear and complete. If compressed, the figure should be readable.
- Statistic graphic should be supplemented with data sources.
- If the figures come from the third party, it should have the copyright transfer from the sources.

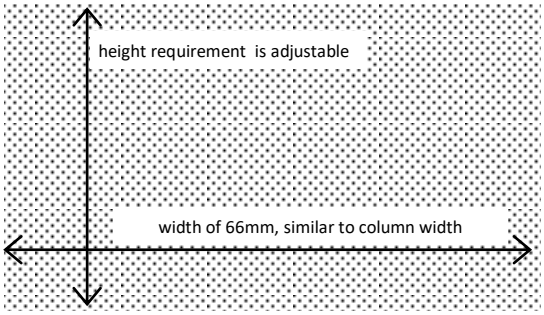

Figure 1. Illustration of Dimensional Figure of one column width. Figure dimension adjusted to the width of one column. Name the figure (diagram) written below the image. (Calibri 8.5 Justify)

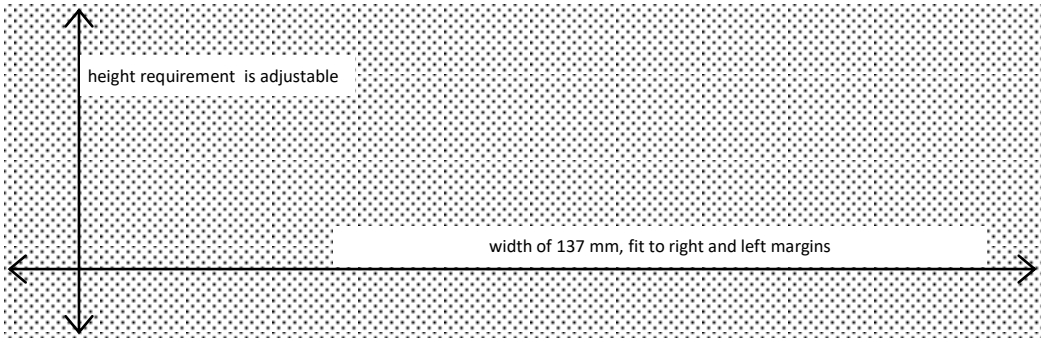

Figure 2. . Illustration of Dimensional Figure of two column width. Figure dimension adjusted to the width of two columns (137 mm). Figure were align top or bottom of the page. (Calibri 8.5 Justify)

References

1. Primary references include journal, patent, dissertation, thesis, paper in proceeding and text book.
2. Avoid self citation.
3. Author should avoid reference in reference, popular book, and internet reference except journal and private ana state institution.
4. Author was not allowed to use abstract as references.
5. References should been published (book, research journal or proceeding). Unpublished references or not displayed data can not be used as references.
6. References typed in numbering list (format number 1,2,3,…), ordered sequentially as they appear in the text (system of Vancouver or author-number style).
7. Citation in the manuscript typed only the references number (not the author and year), example: Obesity is an accumulation of fat in large quantities which would cause excessive body weight (overweight) [1]. Obesity is a risk factor of diabetic, hypertension dan atherosclerosis [2].

CONCLUSION (Calibri 10 Bold, Left, Capslock)

Conclusion of the study's findings are written in brief, concise and solid, without more additional new interpretation. This section can also be written on research novelty, advantages and disadvantages of the research, as well as recommendations for future research.(Calibri 10 Justify)

ACKNOWLEDGEMENT (Calibri 10 Bold, Left, Capslock)

This section describes gratitude to those who have helped in substance as well as financially. (Calibri 10 Justify)

REFERENCES (Calibri 10 Bold, Left, Capslock)

[1]. (Calibri 10 Justify, citation labelling by references numbering)
[2]. Vander, A., J. Sherman., D. Luciano. 2001. Human Physiology: The Mecanisms of Body Function. McGraw-Hill Higher Education. New York. (Book)
[3]. Shi, Z., M. Rifa'i, Y. Lee, K. Isobe, H. Suzuki. 2007. Importance of CD80/CD86-CD28 interaction in the recognation of target cells by $CD8^{+}CD122^{+}$ regulatory T cells. *Journal Immunology.* 124. 1:121-128. (Article in Journal)
[4]. Syafi'i, M., Hakim, L., dan Yanuwiyadi, B. 2010. Potential Analysis of Indigenous Knowledge (IK) in Ngadas Village as Tourism Attraction. pp. 217-234. In: Widodo, Y. Noviantari (eds.) Proceed-ing *Basic Science National Seminar 7* Vol.4. Universitas Brawijaya, Malang. (Article within conference proceeding)
[5]. Dean, R.G. 1990. Freak waves: A possible explanation. p. 1-65. *In* Torum, A., O.T. Gudmestad (eds). Water wave kinetics. CRC Press. New York. (Chapter in a Book)
[6]. Astuti, A.M. 2008. The Effect of Water Fraction of *Stellaria* sp. on the Content of TNF-α in Mice (*Mus musculus* BALB-C). Thesis. Department of Biology. University of Brawijaya. Malang. (Thesis)

Cover Image
3D Structure of EGCG (Epigallocatechin-3-Gallate)
Green Tea Component
Created by ::
Prof. Widodo, S.Si.,M.Si.,Ph.D MED Sc.

Address :
Building B, 1st Floor, Graduate Program Universitas Brawijaya
Jl. Mayor Jenderal Haryono 169, Malang, 65145,
East Java, Indonesia
Tel.: (+62341) 571260; Fax: (+62341) 580801
Email: jels@ub.ac.id
Web: jels.ub.ac.id

9 772087 285007